THE ROLE OF G-DOMAIN ON K-RAS AND Gα DIMERIZATION

A THESIS SUBMITTED TO
THE GRADUATE SCHOOL OF NATURAL AND APPLIED SCIENCES
OF
MIDDLE EAST TECHNICAL UNIVERSITY

BY

İREM AYDIN

IN PARTIAL FULFILLMENT OF THE REQUIREMENTS
FOR
THE DEGREE OF MASTER OF SCIENCE
IN
MOLECULAR BIOLOGY AND GENETICS

JANUARY 2024

Approval of the thesis:

THE ROLE OF G-DOMAIN ON K-RAS AND Gα DIMERIZATION

submitted by **İREM AYDIN** in partial fulfillment of the requirements for the degree of **Master of Science** in **Molecular Biology and Genetics, Middle East Technical University** by,

Prof. Dr. Halil Kalıpçılar

Dean, **Graduate School of Natural and Applied Sciences**

Prof. Dr. Mesut Muyan

Head of the Department, **Biological Sciences, METU**

Assoc. Prof. Dr. Çağdaş Devrim Son

Supervisor, **Biological Sciences, METU**

Examining Committee Members:

Prof. Dr. Mehmet Somel

Biological Sciences, METU

Assoc. Prof. Dr. Çağdaş Devrim Son

Biological Sciences, METU

Prof. Dr. Yeşim Soyer Küçükşenel

Food Engineering, METU

Assoc. Prof. Dr. Salih Özçubukçu

Chemistry, METU

Assoc. Prof. Dr. Gamze Bora Akoğlu

Medical Biology, Hacettepe University

Date: 26.01.2024

I hereby declare that all information in this document has been obtained and presented in accordance with academic rules and ethical conduct. I also declare that, as required by these rules and conduct, I have fully cited and referenced all material and results that are not original to this work.

Name, Surname : İrem Aydın

Signature :

ABSTRACT

THE ROLE OF G-DOMAIN ON K-RAS AND Gα DIMERIZATION

Aydın, İrem
Master of Science, Molecular Biology and Genetics
Supervisor : Assoc. Prof. Dr. Çağdaş Devrim Son

January 2024, 157 pages

K-Ras protein is a member of the Ras superfamily, also known as a small G protein, and plays roles in different signaling pathways via binding and activating various effectors. Most of these pathways enable cellular activities such as cell proliferation, migration, survival, and differentiation. The G-domain, which is common to all G-proteins, is defined as the active site of these proteins. Some of the mutations in this domain affect protein function and protein-protein interactions. These mutations, which cause the K-Ras protein to remain constitutively active, have been detected in many types of cancer by various research groups. Studies in recent years have shown that proteins belonging to the Ras family form dimers, which play essential roles in numerous signaling pathways. In this study, the physical interactions between K-Ras and Gα proteins and the regions that have been identified as hot spots in K-Ras homodimerization, which are also conserved in Gα proteins, has been exposed to site-directed mutagenesis and the impact of these conserved regions on the possible K-Ras - Gα heterodimerization has been investigated using FRET technique.

Keywords: K-Ras, Gα Proteins, Protein Interactions, Dimerization, FRET

ÖZ

K-RAS VE Gα DİMERİZASYONUNDA G-DOMAIN BÖLGESİNİN ROLÜ

Aydın, İrem
Yüksek Lisans, Moleküler Biyoloji ve Genetik
Tez Yöneticisi: Doç. Dr. Çağdaş Devrim Son

Ocak 2024, 157 sayfa

K-Ras proteini küçük G proteini olarak bilinen Ras ailesinin üyesidir ve birçok efektöre bağlanıp, aktif hale gelerek, farklı sinyal yolaklarında rol almaktadır. Bu yolaklar, hücre çoğalması, hücre göçü, hayatta kalma ve farklılaşma gibi önemli hücresel aktivitelerde kontrolü sağlar. Ras proteinlerinde ortak bulunan G-domain bölgesi bu proteinlerin aktif bölgesidir. Bu bölgede gerçekleşen mutasyonlar protein işlevinde veya protein etkileşimlerinde rol oynamaktadır. Birçok kanser çeşidinde K-Ras proteininin sürekli aktif kalmasına sebep olan bu mutasyonlar farklı araştırmalarda gösterilmiştir. Son yıllarda yapılan çalışmalar, Ras ailesine ait proteinlerin dimer oluşturduğunu ve dimerlerin farklı sinyal yolaklarında önemli roller oynadığını göstermiştir. Bu çalışmada K-Ras homodimerizasyonunda önemli olduğu tespit edilen ve Gα proteinlerinde de yüksek benzerlik gösteren bölgeler mutasyona uğratılarak bu bölgelerin olası K-Ras ve Gα proteinleri heterodimerizasyonu üzerindeki etkileri FRET yöntemi ile araştırılmıştır.

Anahtar Kelimeler: K-Ras, Gα Proteinleri, Protein Etkileşimleri, Dimerizasyon, FRET

To my precious family and loved ones.

ACKNOWLEDGMENTS

I would like to express my deepest gratitude for the guidance and unwavering support provided by my advisor Assoc. Prof. Dr. Çağdaş Devrim Son. His expertise and encouragement have been invaluable throughout my entire journey. I feel lucky and grateful to have been a part of his research team.

I would like to thank my thesis examining committee; Prof. Dr. Mehmet Somel, Prof. Dr. Yeşim Soyer Küçükşenel, Assoc. Prof. Dr. Salih Özçubukçu and Assoc. Prof. Dr. Gamze Bora Akoğlu.

I wish to express my sincere appreciation to the Scientific and Technological Research Council of Turkey (TÜBİTAK) for its 2210-A National Graduate Scholarship program, which helped cover my expenses during my master's studies. I wish to extend my profound gratitude to TÜBİTAK for supporting this study with project number 121Z907. I am thankful to the Office of Scientific Research Projects Coordination in METU for the partial funding for this study under the designated Graduate Thesis Project-11091.

I am deeply grateful to Dr. Tuğba Dursun Usal and Dr. Fatma Küçük Baloğlu for their both academic contributions and emotional support. I want to thank to all past and recent Son Lab members, Ali Akyol, Tolgahan Suat Sezen, Şeyda Culfa, Enise Nallı Sezer, Seyda Balkan Durhan, Zeynep Eda Karaboğa, Ahmet Zübeyir Nursoy, Bengü Çakır, Mert Coşgun, Soha Wasim, Pardis Safarnezhad, Betül Yiyen, Sait Şeyhanlı and all undergraduate special project students for their support, fellowship and inspiring collaboration. I am forever grateful for everything they have done for me. I also thank Naz Özoğul for her emotional support and encouragement. Her presence in my life has brought immense joy and comfort for years. She has been by my side whenever I needed her the most, providing emotionally and academically unwavering support.

I want to express my heartfelt gratitude to Göksel Üstündağ for his incredible support throughout my thesis journey. His guidance and emotional encouragement have been indispensable. His willingness to share his expertise and stand by me during both challenges and successes has made a significant impact on my life. I am truly fortunate to have someone like him.

I would like to thank from the bottom of my soul, my mother, Nurten Aydın, my father, Alp Aydın, and my brother, İlker Aydın, for being the unwavering foundation of love, support, and understanding in my life. Their presence has been my constant source of strength, and their sacrifices, unconditional love, and boundless encouragement have shaped the person I am today. I am forever blessed with the warmth of our shared moments and the resilience they have instilled in me, enduring and priceless treasures I hold close to my heart.

Most importantly, I am forever grateful and blessed to have my love, Berker Acır, in my life. I was overwhelmed with emotion at the depth of his love and the unwavering endless support during my studies. He has been my anchor, his encouragement my guiding star, and his belief in me my greatest strength. I thank him for being my love, my friend, and my everything. I am profoundly blessed to share my life with him. I look forward to a future filled with continued love, laughter, endless joy, and many more shared moments of growth as we continue to navigate life hand in hand.

Finally, s*paw*cial thanks to my furball cats, Dardanel and Pirinç, for their unconditional love. Whether curled up by my side or playfully exploring their surroundings, they made every day brighter and more meaningful. They were my *purr*-fect companions, and I have cherished every charming moment with them.

TABLE OF CONTENTS

CHAPTERS

LIST OF TABLES

TABLES

LIST OF FIGURES

FIGURES

LIST OF ABBREVIATIONS

ABBREVIATIONS

AC	Adenylyl Cyclase
ATP	Adenosine Triphosphate
bp	Base Pair
BSA	Bovine Serum Albumin
cAMP	Cyclic Adenosine Monophosphate
DAG	Diacylglycerol
DMEM	Dulbecco's Modified Eagle Medium
DNA	Deoxyribonucleic Acid
EDTA	Ethylenediamine Tetraacetic Acid
EGFP	Enhanced Green Fluorescent Protein
ERK	Extracellular Signal-Regulated Kinase
FBS	Fetal Bovine Serum
FRET	Förster Resonance Energy Transfer
GAP	GTPase-Activating Protein
GDP	Guanosine Diphosphate
GEF	Guanine Nucleotide Exchange Factors
GPCR	G-Protein Coupled Receptor
GTP	Guanosine Triphosphate
HVR	Hyper Variable Region
IP3	Inositol Trisphosphate
K-Ras *onc*	K-Ras oncogenic
K-Ras *wt*	K-Ras wild-type
kDa	Kilodalton
LB	Lysogeny Broth
MAPK	Mitogen-Activated Protein Kinase

mCherry	Monomeric Mcherry
N2-a	Neuro2-A
PBS	Phosphate Buffered Saline
PCR	Polymerase Chain Reaction
PDB	Protein Data Bank
PI3K	Phosphoinositide 3-Kinases
PIP2	Phosphatidylinositol 4,5-Bisphosphate
PIP3	Phosphatidylinositol 3,4,5-Triphosphate
PKC	Protein Kinase C
PPi	Protein-Protein Interaction
RalGEF	Ral Guanin Nucleotide Exchange Factor
ROCK	Rho-Associated Protein Kinase
SDM	Site-Directed Mutagenesis
TAE	Tris Acetate EDTA
TBS-T	Tris Buffered Saline Tween-20

CHAPTER 1

INTRODUCTION

1.1 GTP-Binding Proteins

Guanosine triphosphate (GTP) binding proteins are one of the crucial components in multicellular systems for signal transduction, where they can transmit signals from the extracellular environment to the inside of the cells (Spiegel, 1987). With the help of this signal transduction, they can control metabolic regulation, growth, proliferation, differentiation, and cellular communications.

They can bind both guanosine triphosphate (GTP) and guanosine diphosphate (GDP) and hydrolyze GTP, thus acting as GTPases. When they are bound to GDP, they are inactive and referred to as "Off-State"; however, when they are bound to GTP, they are active and called "On-State" (Lacal, 2001). The GTP-bound form of the GTP binding proteins can transduce signals to their downstream pathways to regulate cellular responses. The activation of GTP binding proteins is also regulated by Guanin Exchange Factors (GEFs), which facilitate GDP to GTP exchange, and the termination of the signal transduction is depended on GTPase Activating Proteins (GAPs), which can help to catalyze GTP to GDP and switching to "Off-State" (Ligeti *et al*., 2012; Quilliam *et al*., 2002).

There are two types of GTP Binding proteins: Monomeric Small GTP Binding Proteins and Heterotrimeric GTP Binding Proteins. Monomeric Small G proteins are in monomeric form and are homologous to the Gα-subunit of the heterotrimeric G proteins. They include Ras, Rho, Rab, etc., proteins and are also called Ras superfamily (Takai *et al*., 2001). Heterotrimeric G proteins have three subunits, which are α, β, and γ- subunit. Each Gα subunit has a variety of different isoforms such as Gα11, Gα12, Gα13, Gαi, Gαs, etc. proteins (Milligan & Kostenis, 2006).

1.1.1 Monomeric Small GTP-Binding Proteins

Small G proteins have essential roles in proper cellular functioning. They play roles in proliferation, growth, cellular migration, differentiation, and cellular trafficking via signal transduction (Song *et al.*, 2019). They act as molecular switches in which GDP/GTP transitions between states. In the inactive state, GDP is bound to the α subunit of the proteins, and they do not transduce any signal. When a ligand such as epidermal or fibroblast growth factors bind Receptor Tyrosine Kinase, they active monomeric G proteins. With the help of GEFs, GTP is bound to the α subunit with replacing GDP, and it turns the protein to the on state and starts signal transduction to downstream effectors. Once they relay the signals to downstream effectors, they hydrolyze the GTP to GDP via intrinsic GTPase activity with the help of GAPs and turn back to the off-state *(*Simanshu *et al.*, 2017). They play a role in numerous signaling pathways where they can change gene expression in different ways. They include several protein families such as Ras, which is the most prominent family in the group that plays crucial roles in cell viability; Rho is another important family that helps cell migration and cytoskeleton formation; Rab family facilitates vesicle trafficking in the cell (Wennerberg *et al.*, 2005).

1.1.2 Heterotrimeric GTP-Binding Proteins

Similar to small GTP-binding proteins, they have crucial roles in cellular functioning and signal transduction. They are also known as G proteins and consist of three different subunits called G alpha (α), G beta (β), and G gamma (γ) (Hurowitz *et al.*, 2000). They also work as molecular switches that can exchange GDP/GTP. In the GDP bound inactive state of G proteins can be stimulated after ligand binding to the G Protein Coupled Receptors (GPCRs), and with the aid of these receptors, which act as GEFs, GTP can bind to Gα subunit, turn them into an active state and cause disassociation of them from Gβγ dimeric subunits (Oldham & Hamm, 2008). Then, these subunits can start conveying signals separately from extracellular stimulants to different effectors. Once the signals are transmitted, GTP is hydrolyzed back to GDP form with the help of GAPs and intrinsic GTPase activity, terminates activation, and reassociates all subunits back to inactive state formation. Gα proteins have four different families called $G\alpha_{o/11}$, $G\alpha_{12}$, $G\alpha_{i}$, and Gαs, where they involve different signaling pathways and regulate many cellular metabolic activities and gene expressions (Kamato *et al*., 2015).

1.2 K-Ras Protein

K-Ras protein, also called Kirsten rat sarcoma viral oncogene, belongs to the Ras family of small GTP-binding proteins and is expressed from the KRAS gene (Zhu *et al*., 2019). K-Ras protein and other Ras proteins H-Ras and N-Ras are different in their Hyper Variable Region (HVR) at the C-terminus of the proteins, which covers 20 different amino acids in the regions (Henis *et al*., 2009). In the genome, the K-Ras protein is coded by the KRAS gene that is found on chromosome 12 in the short arm (12p11.1–12p12.1) with two different isoforms called K-Ras4A and K-Ras4B (Nussinov *et al*., 2016). K-Ras4B is the most abundant one, and it has 189 amino acids with 21 kDa molecular weight (Aran, 2021). As a GTP-binding protein, it depends on the conversion of GDP to GTP for activation and relaying signals in essential signaling pathways. To terminate this activation, they use their GTPase activity and hydrolyze GTP that is bound to the α subunit and turn it into GDP. K-Ras protein plays crucial roles in cellular mechanisms such as proliferation and survival. Figure 1.1 shows a schematical representation of the activation of the K-Ras protein during the GDP to GTP transition with GEP and GAP complexes.

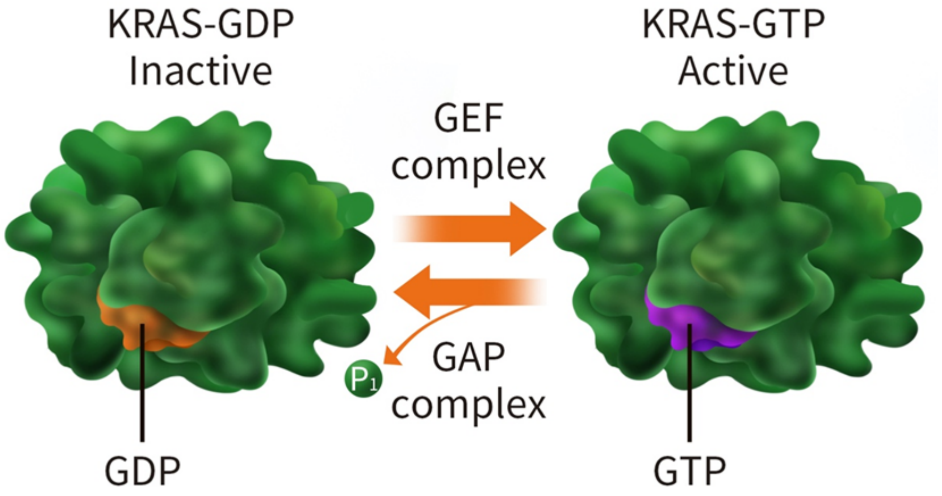

Figure 1.1: K-Ras protein GDP/GTP transition. Off-state GDP-bound form to on-state GTP-bound form. Adapted from Origene, 2024.

1.2.1 Structure of K-Ras Protein

As a member of GTP-binding proteins, K-Ras has a central G-domain. This domain is responsible for nucleotide binding, where GTP or GDP binds to protein. These bindings cause a conformational change in the protein, turning it into an active or inactive state. This domain contains 6 α-helices and 5 β-sheets (Pantsar, 2020). In the G-domain, there are phosphate binding groups, also called P loops, and they are conserved motifs that are responsible for interacting and stabilizing GDP or GTP (Shi *et al.*, 2023). Also, K-Ras has two different switch regions called Switch I and Switch II (Gasper & Wittinghofer, 2020). During the transition of GDP-GTP, protein goes under conformational changes and switch regions toggles between each state when these conformations change. They play a role during the interaction of effector proteins from downstream pathways when K-Ras is in its active GTP-bound form. In addition to switch regions, effector binding sites are also able to bind downstream proteins in the pathways, such as Raf or Phosphoinositide 3- Kinase PI3K (Ternet *et al.*, 2022). Another important region of the K-Ras protein is the C-terminus of the protein. In this region, there is a motif called CAAX motif, which refers to Cysteine-

Alanine-Alanine-Leucine residues that undergo post-translational modifications such as farnesylation and palmitoylation that can play a vital role in functioning and membrane localization (Michaelson *et al*., 2005). In this way, protein can be bound to the membrane and continue properly conducting signal transduction in its active state. Figure 1.2 shows detailed properties of the K-Ras structure and its elements.

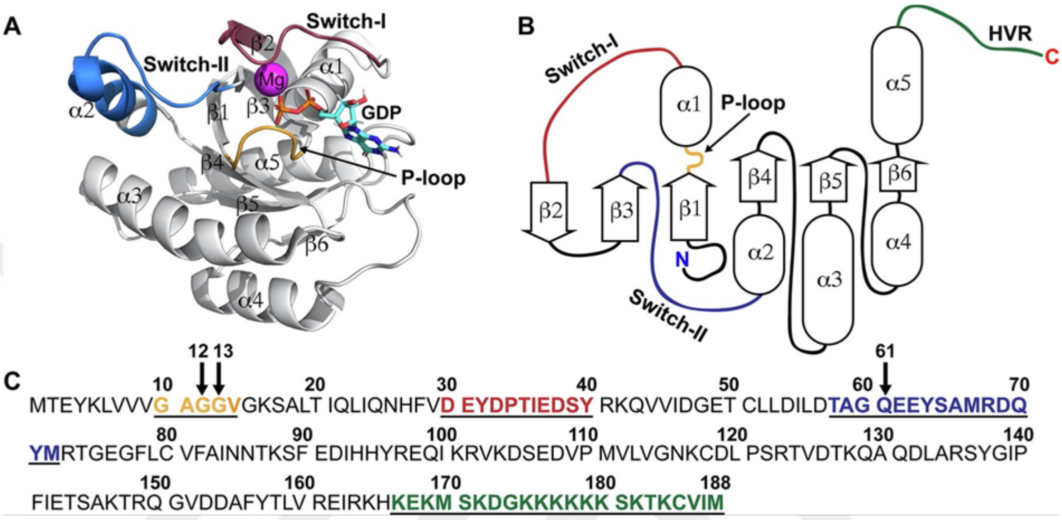

Figure 1.2: K-Ras protein structure and mRNA sequence with properties. (A) K-Ras 3D structure shows alpha-helices and beta-sheets, Switch regions, P-loop, and nucleotide binding region. (B) Schematic representation of elements of secondary structure of K-Ras protein. (C) mRNA coding sequence of K-Ras protein with color highlighted properties with corresponding regions in 3D structure in (A). Adapted from Pantsar, 2020.

1.2.2 Localization and Trafficking of K-Ras Protein

For the proper functioning of the K-Ras protein in the cell, its trafficking and localization play an important role. It should be targeted to the inner cell membrane to initiate signaling pathways with the interaction of its signaling partners (Schmick *et al*., 2014). For its localization, once the KRAS gene is translated into protein, its CAAX motif in the C-terminus is recognized for farnesylation, and the farnesyl group is added to Cysteine residue that initiates interaction with the membrane

(Blanden *et al.*, 2017). After farnesylation, palmitoylation occurs and it causes a strong anchoring to the membrane (Busquets-Hernández & Triola, 2021). These lipid modifications are vital for the trafficking of K-Ras protein to the cellular membrane. During this trafficking, K-Ras can be transported to the membrane through vesicles such as endosomes or Golgi apparatus-derived vesicles (Fivaz & Meyer, 2005). According to cell needs or stimuli location, this trafficking process is dynamically controlled for the proper regulation in the cell for external stimuli. When the external signaling occur, this trafficking is processed to different specific membrane regions. For the termination of this mechanism, with the help of depalmitoylation, K-Ras proteins are removed from the cellular membrane, which prevents association with the membrane and stops signaling (Wang *et al.*, 2020). During all these processes, K-Ras is tightly regulated for proper functioning. In the case of activation or inactivation of proteins, GAPs for the GTPase activities and GEFs for the nucleotide exchanges play crucial roles in the regulation.

1.2.3 Signaling and Effectors of K-Ras Protein

Once a ligand such as growth factors binds to its receptor such as receptor tyrosine kinase, K-Ras activation is triggered, and GDP is replaced with GTP, which initiates signal transduction through K-Ras to its effectors, shown in Figure 1.3. K-Ras interacts with different types of effectors in different signaling pathways for conveying various signal cascades. It can interact with Raf, Phosphatidylinositol 3-kinase (PI3K), Ral Guanin Nucleotide Exchange Factor (RalGEFs), and T-lymphoma invasion and metastasis-inducing protein-1 (Tiam1) to initiate signaling pathways (Yuan *et al.*, 2018).

When K-Ras interacts with Raf kinase after its activation, it initiates phosphorylation cascades to downstream proteins called Mitogen-Activated Protein Kinase Pathway (MAPK) (Terrell & Morrison, 2019). Once Raf phosphorylates MEK, MEK continues to phosphorylate ERK, and ERK translocates to the nucleus to interact with different transcription factors (Morrison, 2012). This situation regulates gene expression and causes cell growth, survival, and proliferation.

Another pathway that K-Ras can activate is the PI3K pathway (Castellano & Downward, 2011). Once K-Ras is activated, it can interact with Phosphatidylinositol 3-kinase (PI3K), and activated PI3K can turn (4,5)-bisphosphate (PIP2) to phosphatidylinositol (3,4,5)-trisphosphate (PIP3) (Yang *et al*., 2019). Then, PIP3 can bind and phosphorylate downstream protein Akt (Protein kinase B), promoting cell survival, cell growth, and proliferation by facilitating entry to the cell cycle (Song *et al*., 2005). Also, Akt can further interact with NF-κB, Bcl-2, mTOR, and Mdm2, which can cause metabolism changes, apoptosis inhibition, and other oncogenic transcription (Liu *et al*., 2020).

The third downstream effector group for K-Ras protein includes the Ral Guanin Nucleotide Exchange Factor family (RalGEFs), which includes RGL, RGL2, and RalGDS (Cooper *et al*., 2013). When K-Ras interact with these effectors, they can promote metastasis and tumorigenesis by affecting cytoskeletal elements and cell migration (Soriano *et al*., 2021).

K-Ras could also interact and activate the Tiam1 protein (Menyhárd *et al*., 2020). Tiam1 further activates Rac1 protein that interacts with Rho downstream (Lambert *et al*., 2002). Then, Rho interacts with ROCK, which is an essential regulator of cytoskeleton formation and, thus, affects cell shape, cell motility, and cellular invasion by reshaping actin and microtubule formation and their distribution in the cell (Guan *et al*., 2023).

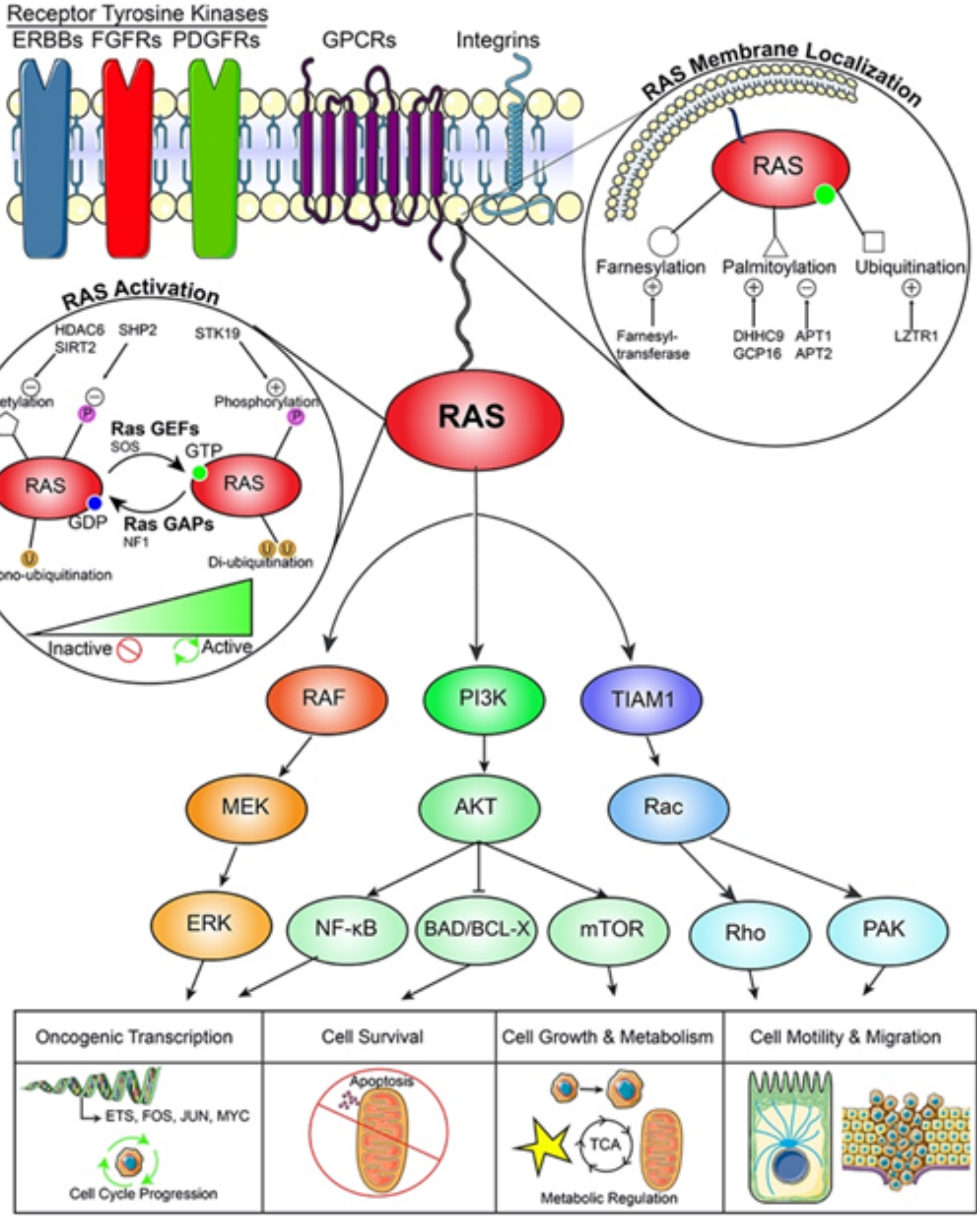

Figure 1.3: Ras protein downstream signaling pathway. Peripheral cell membrane-bound K-Ras protein and its downstream signaling pathways that include RAF-MEK-ERK, PI3K-AKT, TIAM1-RHO transductions, and their corresponding cellular responses. Adapted from Gimple & Wang, 2019

1.2.4 K-Ras Dimerization

After the discovery of Ras proteins, it was thought that this protein functions as a monomer directly binding to different effectors during signal transduction. However, it has recently been shown that in vitro Raf1 activation in liposomes is facilitated by Ras dimerization, one of the first studies that mentions Ras protein operating as a dimer (Inouye *et al.*, 2000). Following studies establish that Ras proteins form nanoclusters on the plasma membrane in a similar manner to receptor oligomerizations, which shows their dimerization has physiological and functional importance (Güldenhaupt *et al.*, 2012). Then, photoactivated localization microscopy (PALM) shows that GTP-bound K-Ras4B forms dimer on the plasma membrane to activate the downstream MAPK signaling pathway (Nan *et al.*, 2015). Moreover, in recent years, it has been revealed that the increased activation of K-Ras protein in its dimeric form has been reported to play a significant role in enhancing oncogenic activity in the MAPK pathway (Muratcioglu *et al.*, 2020). Their predicted dimerization interfaces are shown in Figure 1.4.

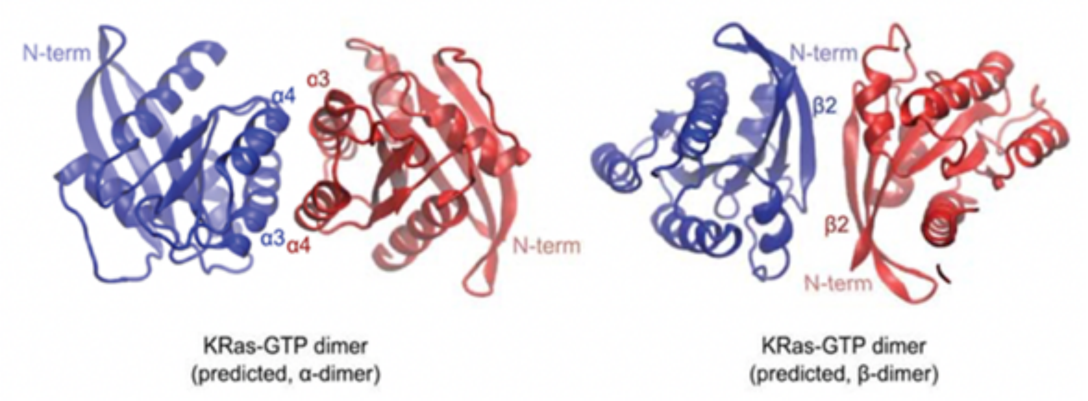

Figure 1.4: K-Ras protein dimerization interfaces. On the peripheral plasma membrane, K-Ras is predicted to be dimerized in its alpha helices or beta sheets interfaces, which are α3-α4 interfaces and β2-β2 interface. Adapted from Chen *et al.*, 2016.

1.2.5 K-Ras Protein in Diseases

K-Ras protein has many effects on different proteins, including their expression levels in the cell, as mentioned above. It facilitates proliferation and cell survival, which are prone to disease progression after any problem with its expression. As with other proteins, K-Ras is open to mutations that cause various cancer progressions in the human body such as colorectal or lung cancer (Waters & Der, 2018). K-Ras protein has some hot spots that get point mutations and interfere with its function. These hot spots are mainly 12. amino acid Glycine, 13. amino acid and 61. amino acid Glutamine (Stolze *et al.*, 2015). Some of these amino acid sequences get point mutation, such as glycine to valine, aspartic acid, cysteine or glutamine to lysine and K-Ras loses its functional properties in its structure. Especially, codon 12 hot spot is found at the p-loop that is responsible for phosphate binding to GTP, and when it is mutated to aspartic acid, the newly introduced negative charge and bulkier structure of aspartic acid prevent GTP hydrolysis (Zeissig *et al.*, 2023). These changes cause a malfunction in intrinsic GTPase activity and gain resistance to GAPs, resulting in GTP-bound stably active K-Ras form. This constitutively active form of K-Ras continues to signal transduction in the MAPK pathway, PI3K pathway, Rho/ROCK pathway, and so on without any termination; in the end, cells uncontrollably grow, proliferate and gain resistance to apoptosis, which are defined as hallmarks of the cancer (Hanahan & Weinberg, 2011). Therefore, K-Ras is classified as a proto-oncogene in normal cells, but once it is mutated, it turns into an oncogene and triggers neoplasm formation and metastasis. Moreover, K-Ras mutations are responsible for ~30% of all cancer types in the human body (Liu *et al.*, 2019). Codon 12 mutations are the most common, with 82%, and codon 13 mutations follow it with 17% (Yoon *et al.*, 2014). In addition, in the codon 12 mutations, aspartic acid codon mutations are 36%, valine codon mutations 23%, and cysteine codon mutations are 14% in the population (Vatansever *et al.*, 2017). These different mutations in K-Ras cause broad types of cancer. These mutations are commonly accountable for colorectal, pancreatic, and lung cancer (Prior *et al.*, 2012).

There are many studies to treat tumorigenesis caused by K-Ras. Many drug development studies aimed to solve the constitutive binding of GTP to K-Ras, but not having a binding pocket in the mutated regions of K-Ras prevents targeted drugs from functioning (Issahaku *et al*., 2022). Therefore, there are different approaches to drug development. Firstly, drugs are developed either aimed to inhibit upstream signaling pathway proteins of K-Ras such as SHP2, RTKs, or SOS that play a role in K-Ras activation or inhibit downstream signaling pathways such as Raf, MEK, ERK, PI3K, Akt that carry signals through K-Ras and their combined usage (Moore & Malek, 2021). Secondly, some RNAi studies interfere with the RNA expression of KRAS to decrease the number of KRAS transcription (Golan *et al*., 2015). Thirdly, there are direct targeted drugs such as antibodies bind and inhibit protein expression (Wang *et al*., 2022). Lastly, the most common drugs have been discovered to inhibit post-translational modifications on K-Ras that prevent trafficking and membrane localization, such as targeting farnesyl transferase (Kazi *et al*., 2019). Moreover, in recent years, some drugs such as AMG510 can bind and lock K-Ras in its GDP-bound form in some mutated versions, such as G12C in some cancer types, and prevent tumor progression (Canon *et al*., 2019).

1.3 Gα Proteins

As a member of heterotrimeric G-proteins, Gα proteins are separated into four different families called Gαq/11, Gα12/13, Gαi, and Gαs (Kamato *et al*., 2015). All of them are membrane-associated and able to bind GTP to get activated and convey signals to downstream pathways when ligand binds to GPCRs and cause various cellular responses. They can signal through adenylyl cyclase, phospholipase C, phosphodiesterases, and ion channels as effectors (McCudden *et al*., 2005). In turn, they can affect cAMP levels, diacylglycerol levels, and sodium and calcium levels. They can also hydrolase GTP to GTP with their GTPase activity and terminate signaling. Different genes encode these four different family proteins, but they have some conserved regions in the human genome.

Gα11 protein from the Gαq family is expressed in chromosome 19 and has 7 splice variants. The common variant is 359 amino acids long and approximately 42 kDa molecular weight (Silva-Rodríguez *et al*., 2022). Gα12 protein from Gα12/13 family is encoded in chromosome 7 with 8 splice variants. The most abundant one has a length of 381 amino acids, and its molecular weight is approximately 44 kDa (Dhanasekaran & Dermott, 1996). In the same Gα12/13 family, Gα13 protein is expressed in chromosome 17. It has only 2 different splice variants, where the most common one has 377 amino acids and approximately 44 kDa, similar to Gα12 protein in the same family, (Ke *et al*., 2023). Gαi1 is one of the nine proteins in the Gαi family and is coded in chromosome 7 together with 32 splice variants. The most abundant Gαi1 protein is 354 amino acids in length and 41 kDa in weight (Blumer & Tall, 2012). Finally, Gαs protein in the Gαs family is expressed in chromosome 20 with 77 splice variants, and the common one has 394 amino acids and is around 46 kDa molecular mass (Turan & Bastepe, 2013).

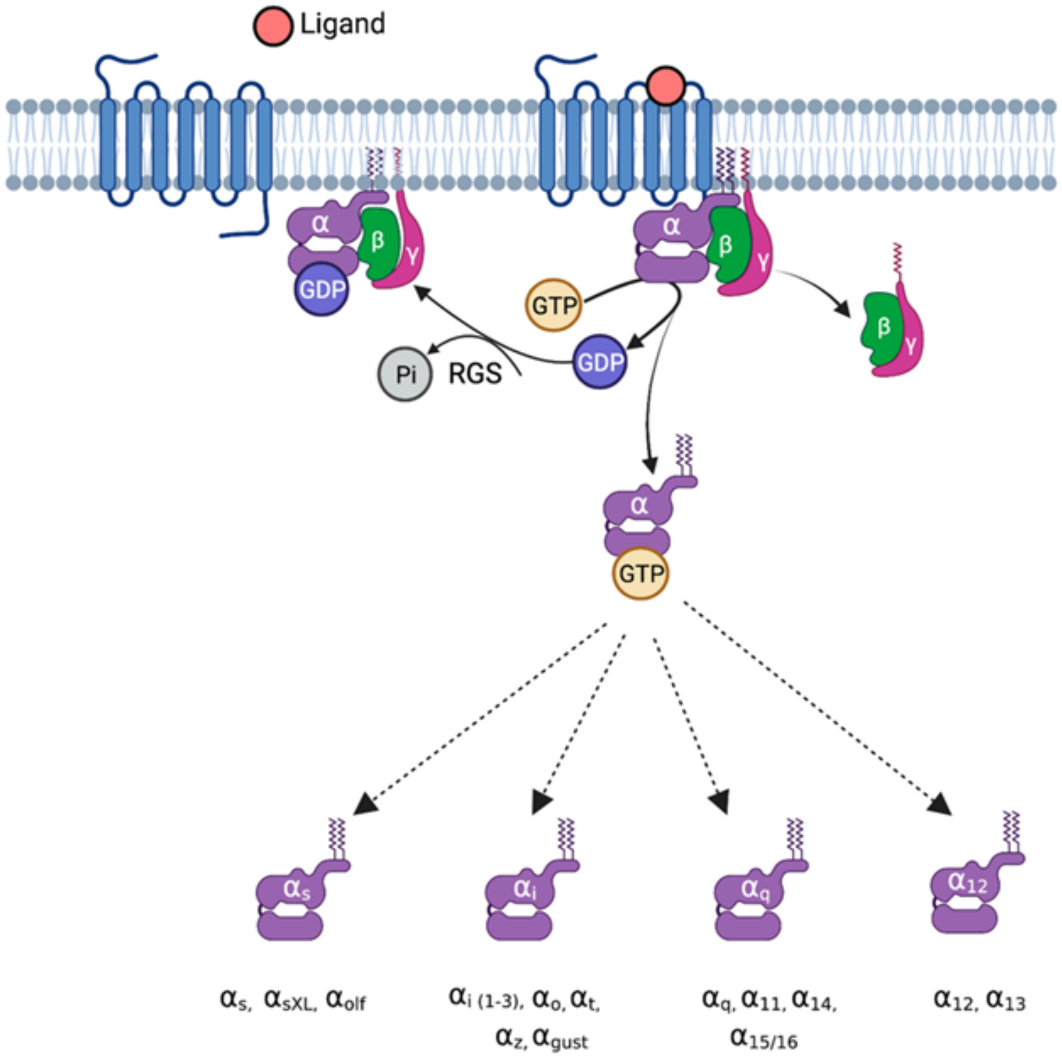

Figure 1.5: Activation of different Gα Protein families. Ligand-bound GPCR activates heterotrimeric G-proteins, and Gα disassociates from the Gβγ subunit. Adapted from Kaur *et al*., 2023.

1.3.1 Structure of Gα Proteins

Similar to Small GTP binding proteins, Gα Proteins have a G-domain that can bind GTP and get activated with conformational changes. Gα Proteins are mostly conserved in structure and have two different domains called helical domain and G-domain (Goricanec *et al*., 2016). G-domain is a site of GTP or GDP binding and performs GTP hydrolysis to GDP during signal transduction. Moreover, it is responsible for binding to GPCRs and effectors. It serves as the binding surface of a dimer of Gβγ subunits of overall heterotrimeric GTP-binding proteins where they can bind various types of GPCRs for relaying signals to their effectors such as adenylyl cyclase, phospholipase C, Rho, and MEKs (Weis & Kobilka, 2018). This GTPase binding domain has 3 loops, called Switch I, Switch II, and Switch III, which are flexible during conformational changes between GDP and GTP binding states and have a P-Loop for phosphate binding (Chung, 2013). On the other hand, the Helical domain has 6 α-helices that serve as a binding pocket for nucleotides and cover them to the core of the protein. It is bound to the GTPase domain with two different linker regions. In addition, the N terminus of the Gα Proteins is subjected to post-translational modifications such as palmitoylation and myristoylated in some Gα Proteins for proper membrane attachment and functioning for all signal transduction events (Oldham & Hamm, 2008). Detailed representation of Gα Protein structures is shown in Figure 1.6.

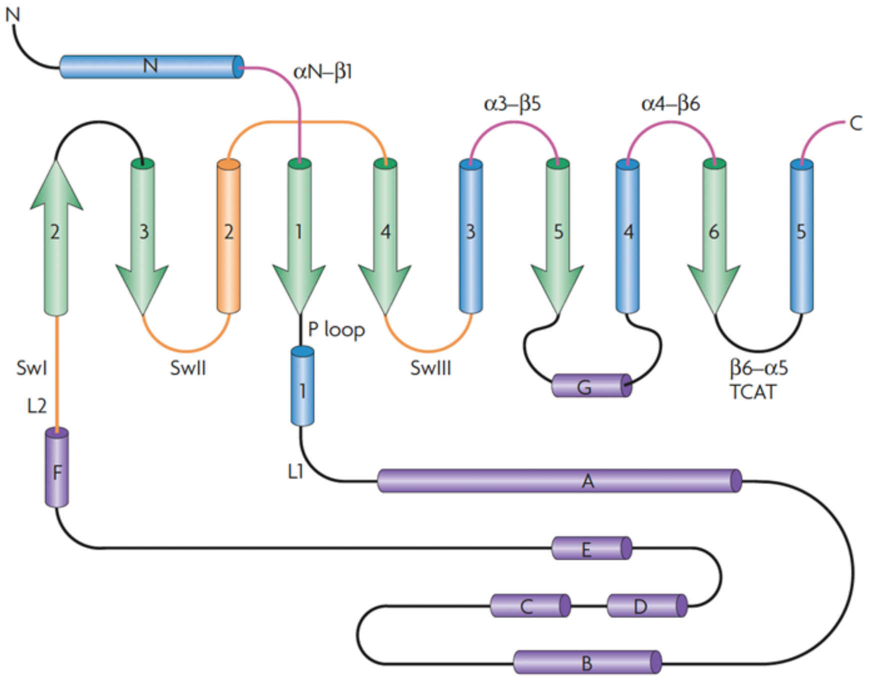

Figure 1.6: Secondary structure of Gα Proteins. Adapted from Oldham & Hamm, 2008.

1.3.2 Localization and Trafficking of Gα Proteins

Gα Proteins have different pathways for correct localization and trafficking in terms of modifications and signals. In common, they require dual signals for modifications and interaction with other subunits of heterotrimeric G proteins that are Gβγ (Marrari *et al*., 2007). Moreover, they are palmitoylated and/or myristoylated covalently, which serves as hydrophobic lipid anchors for membrane localization. Firstly, a type of GEF called Ric-8 protein functions as a chaperon and helps deliver Gα Proteins to ER or Golgi apparatus to be further modified (Wedegaertner, 2012). In these organelles, Gα Proteins are post-transitionally modified with lipid addition. Almost all Gα Proteins are palmitoylated at cysteine amino acid within the first 20 residues in the N terminus of the proteins (Kleuss & Krause, 2003). During palmitoylation, the 16-carbon fatty acid group is attached to the protein reversibly for proper localization to the plasma membrane at the Golgi apparatus where palmitoyl acyltransferases exist (Tsutsumi *et al*., 2008). Moreover, some Gα Proteins, such as Gαi, get myristoylated before palmitoylation during its translation, an irreversible co-translational modification for essential requirements to localization (Galbiati *et al*., 1994). Myristoylation requires the addition of 14-carbon fatty acid myristate via N-myristoyl transferase to the second glycine residue from the N terminus of the protein that is followed by threonine or serine in the position of six (Boutin, 1997). In addition to modifications, Gα Proteins are required to interact with the Gβγ dimer subunit in the ER or Golgi apparatus for correct localization to the plasma membrane, and they are carried to the membrane via Ric-8 chaperon as heterotrimeric formation.

1.3.3 Signaling and Effectors of Gα Proteins

For the overall heterotrimeric G protein signaling, once GPCRs are stimulated with a ligand such as dopamine or epinephrine, its structure conformationally changes and transduces the signal to GDP-bound inactive heterotrimeric G protein. Then, activated GPCRs act as a GEF to induce a conformational change on Gα, triggering binding to GTP. Within this activation, Gα and Gβγ dimer subunits disassociate from each other, and they go different effectors for relaying signals in different pathways (Bondar & Lazar, 2013).

After this initial activation, there are three main pathways for relaying signals. If a GPCR transduces the signal to Gα11 from the Gαq family, it activates Phospholipase C as an effector protein. PL-C can hydrolyze PIP2 into inositol 1,4,5-trisphosphate (IP3) and diacylglycerol (DAG) as secondary messengers (Wu *et al.*, 1992). IP3 is a polar and soluble head group of the phospholipid PIP2, which goes to ER, opens Ca^{+2} ion channels, and causes the release of Ca^{+2} to cytosol (Dickson *et al.*, 2013). On the other hand, DAG is the insoluble part of the tail group of PIP2 that remains on the cell membrane and interacts with effector proteins in there, such as Protein Kinase C, and activates it with the aid of Ca^{+2} that is released via IP3 from ER (Falkenburger *et al.*, 2013). PK-C phosphorylates downstream proteins and causes different gene expressions and responses, such as changing the membrane protein activation and causing different ion conductance or transportation of the cell in and out.

As a second pathway, the Gα12 and Gα13 proteins from the Gα12/13 family stimulate the RhoGEF pathway for signal transduction. Once they are activated by GPCRs, they relay signals to RhoGEF, which is a GEF for the small GTP binding protein Rho (Suzuki *et al.*, 2009). Then, RhoGEF goes and activates Rho-associated kinase (ROCK) which phosphorylates downstream proteins and causes various cell responses.

Finally, the most studied pathway is through Gαs and Gαi1 proteins from Gαs and Gαi families, which affects Adenylyl cyclase (AC) as an effector protein (Ishikawa & Homcy, 1997). The lowercase letters in Gαs and Gαi signify their respective roles, with Gαs acting as stimulatory and Gαi as inhibitory in adenylyl cyclase, resulting in opposite effects. When the ligand binds to GPCR, it relays signal to Gαs, and it goes and stimulates adenylyl cyclase. This enzyme catalyzes ATP to cAMP production as a secondary messenger (Sadana & Dessauer, 2008). Then, cAMP goes and binds to Protein kinase A, which phosphorylates downstream proteins and changes gene expression. On the other hand, Gαi has the opposite effect on adenylyl cyclase compared to Gαs and inhibits adenylyl cyclase and ATP to cAMP production (Taussig *et al*., 1993). Proteins in the Gα Protein family downstream signal transduction are shown in detail in Figure 1.7.

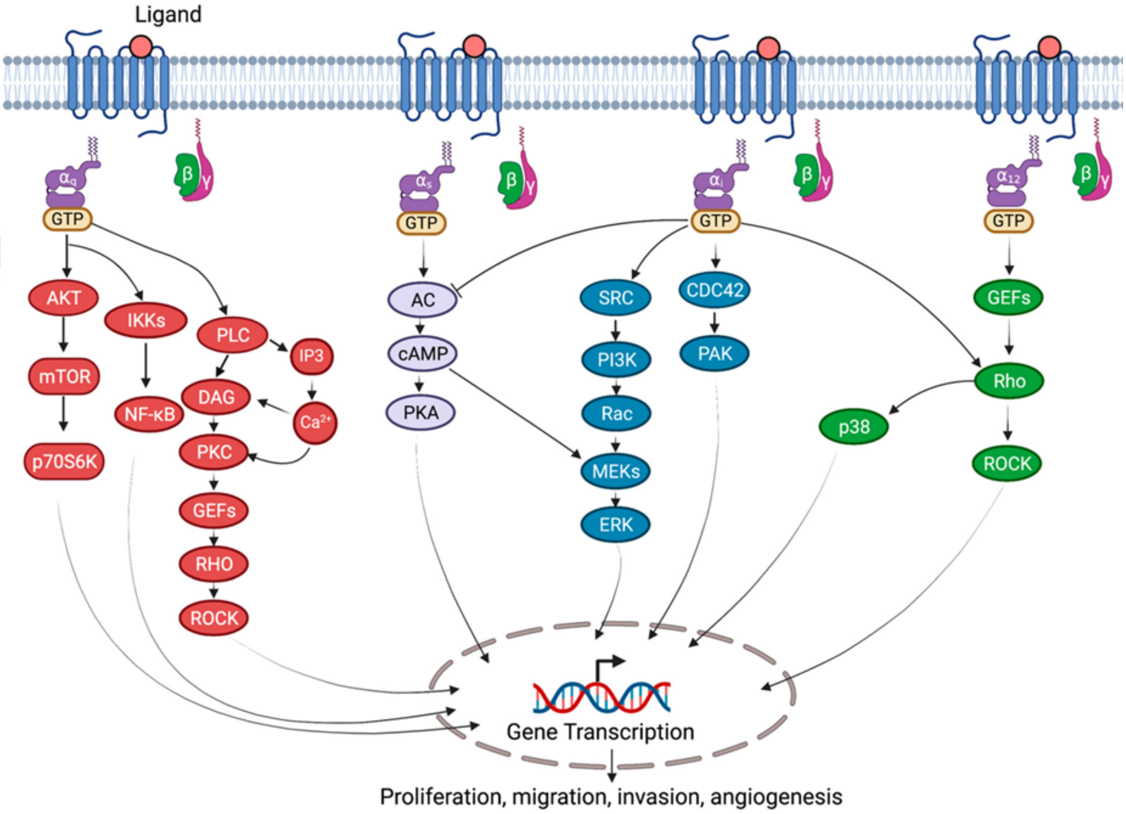

Figure 1.7. Gα Proteins downstream signaling pathways. Gα11 affects the PI3K-AKT pathway, Gαs and Gαi affect the AC-cAMP-PKA pathway, and Gα12 and Gα13 affect the Rho-ROCK pathway. Adapted from Kaur *et al*., 2023.

1.3.4 Gα Proteins in Diseases

Gα Proteins play roles in different signaling pathways and metabolisms; in turn, they can activate a vast number of cellular responses. When any abnormalities occur in Gα Proteins, it causes different dysregulations in these signaling pathways and cellular responses that contribute to many diseases such as cardiovascular diseases, cancer, or endocrine disorders.

Gα Proteins and tumorigenesis have complex relations with each other since Gα Proteins play roles in different signal transduction pathways that affect cell proliferation, migration, and survival. Therefore, the altered function of Gα Proteins stimulates different cancer hallmarks and promotes cancerous cell types and metastasis. Especially the Gα12/13 family is highly associated with tumor progression such as breast, colorectal, and liver, thus known as proto-oncogenes when they are overexpressed and highly activated (Rasheed *et al*., 2021). Moreover, some mutations in Gα13, such as L184R and L197Q, contribute to lymphomas and cause Burkitt Lymphoma with increased activation of the Rho/ROCK pathway (O'Hayre *et al*., 2015). Gα Proteins are also associated with cardiovascular diseases and play roles in regulating heart rate and blood pressure. The increased activation of ROCK protein through Gα12/13 – LPA4 receptor interaction causes hypertension via vasoactive blood-derived lipid lysophosphatidic acid promotion (Yanagida *et al*., 2018). Gα proteins also play a role in regulating immune cells and immune responses. Gα12/13 facilitates B cell maturation and proliferation, and T-cell survival together with differentiation into Th1, Th2, etc. cells, and also, Gα12/13 can interact with chemokines and thrombin receptors, which are crucial for inflammation promotion and recruitment of the immune cells to sites (Yang *et al*., 2020). Therefore, any dysregulation in these Gα proteins can cause malfunctions in immune response, allergy, and autoimmune diseases. Furthermore, Gα protein dysregulations can cause neurodevelopmental disorders where patients have a short life span. Especially when Gαi1 has mutations in its sequence that affect GDP and GTP binding and disrupt proper functioning, patients have intellectual disability, seizures, and developmental delay (Muir *et al*., 2021). Gα proteins are also responsible for maintaining proper endocrine system and metabolic functions. However, some mutations in Gα proteins disrupt all these functions and cause severe disease states. GTP hydrolysis activity is interrupted when Gαs is mutated on Arginine 201 or Glutamine 227 residues. It causes McCune-Albright syndrome, which is described as fibrous dysplasia, irregular skin pigmentation, and precocious puberty, where estrogen or testosterone starts functioning earlier than normal stage (Levine, 1999). In addition, these mutations on the pituitary, thyroid, or adrenal glands may cause acromegaly, Cushing syndrome, and hyperthyroidism (Albani *et al*., 2018). Gα proteins play a role in hepatic metabolism regarding glucose and lipid metabolism. Once Gα12 is defective in these cells, it causes obesity and hepatic steatosis via disturbed mitochondrial respiration and dynamics (Kim *et al*., 2018).

1.4 Protein-Protein Interactions

The proper functioning of the cells requires many different interactions between organic and inorganic molecules. Protein-Protein interactions (PPi) are one of the most important interactions in the cell. PPi occurs when two or more proteins come together in close physical proximity and function further (Sharma *et al*., 2021). These interactions are crucial for the regulation of cell activation and metabolism. There are different types of PPi, such as structural, enzymatic, signaling, and transporting. In structural PPi, one protein gets into a stable complex with other proteins or proteins physically through different forces such as electrostatic, hydrogen bonding, and van der Waals. For enzymatic PPi, proteins come together for catalyzing reactions in the cell where one protein, in this case, enzyme, facilitates another proteins' or substrates' chemical transformation. PPi is also a part of signaling pathways. Proteins are usually members of a signaling pathway where signals relay the cell membrane to the cell nucleus and vice versa. During these transductions, many different proteins interact with each other and cause various cell responses. Lastly, PPi happens during transportation in the cell, which enables different molecules to ship to other organelles or compartments of the cells, such as ion channels and transporters where different proteins work together.

1.4.1 Protein-Protein Interaction Detection Techniques

In order to understand the importance and mechanism of PPi, many different techniques are developed at the cellular or tissue level under *in vitro* conditions. These techniques enable developing and understanding new drug targets, disease mechanisms, or functional insights into the cells. There are two-hybrid systems, such as Yeast Two-Hybrid or Bacterial Two-Hybrid systems, where one target protein and potential interacting partner proteins are expressed in cells. In the case of interaction, reporter gene activation occurs (Mehla *et al*., 2017). Affinity approaches are another technique for detecting PPi. In the case of a pull-down assay, a matrix is designed to bind the target protein, and potentially interacting proteins bind this matrix to be pulled together with the target protein (Louche *et al*., 2017). Co-immunoprecipitation assay in affinity approaches relies on antibody and target protein interaction and pulling down from the solution with its potential interacting proteins (Nam *et al*., 2023). Moreover, mass spectrometry is one of the widely used techniques for PPi detection, with its quantitative and high-throughput information via a combination of various methods (Richards *et al*., 2021). Finally, Fluorescence tagging methods are widely used techniques for PPi. Förster Resonance Energy transfer is used for tracking PPi during the energy transfer between two different fluorophores (Lin *et al*., 2018).

1.4.1.1 Confocal Fluorescence Microscopy

The confocal microscope is one of the advanced fluorescence microscope types that can provide better contrast and resolution of imaging fluorescence samples with the help of its improved properties compared to other commonly used microscopes such as having high axial resolution and optical sectioning to obtain 3D images (Peterson, 2010). In a confocal microscope, light sources (such as lasers), pinholes, excitation and emission filters, collimating lens, dichromatic mirror, objective, and photomultiplier tube are in its components. A laser is used as a light source, which is monochromatic, to excite the desired wavelength at a single point. Exciting specific points instead of exciting everything all at once can help to increase contrast and resolution on the lateral plane. To obtain better imaging of the samples in the axial direction, pinholes are used (Wilson, 1995). There is usually one pinhole after the laser, and the other pinhole is before the photomultiplier tube. A laser pinhole can help the desired excitation wavelength pass through the excitation filter better and prevent interference signals from the surroundings. On the other hand, the pinhole of the photomultiplier tube allows emitted light to come from the focal point by eliminating the out-of-focus light, which helps optical sectioning obtain 3D images. It simply blocks the light coming from below or above the desired focal plane, and also, the light hits the near sites of the pinhole and only allows emitted light to come from the desired focal point. Therefore, it improves axial resolution in addition to increased contrast and lateral resolution. Excitation and emission filters help only desired excitation and emission wavelengths pass through the system. With the aid of a collimating lens, light can be collected and linearized to excite the sample after the beam splitter, which increases the signal. Also, with the objectives, lights can be gathered to illuminate the sample. The dichromatic mirror reflects the excitation light to the sample and transfers the emitted light from the sample. Also, there are bandpass filters in dichromatic mirrors, which work as excitation light reaches the mirror; it reflects the light below the pass point to the sample and allows the pass of emitted light from the sample above the pass point to the emission filter. A photomultiplier tube can be used as a detector. It collects the photons that pass from the pinhole and senses charges due to its photosensitivity property, counts the photons, and converts photon energy to electrical energy. A confocal microscope is also connected to a computer system with proper software to visualize and arrange the setups.

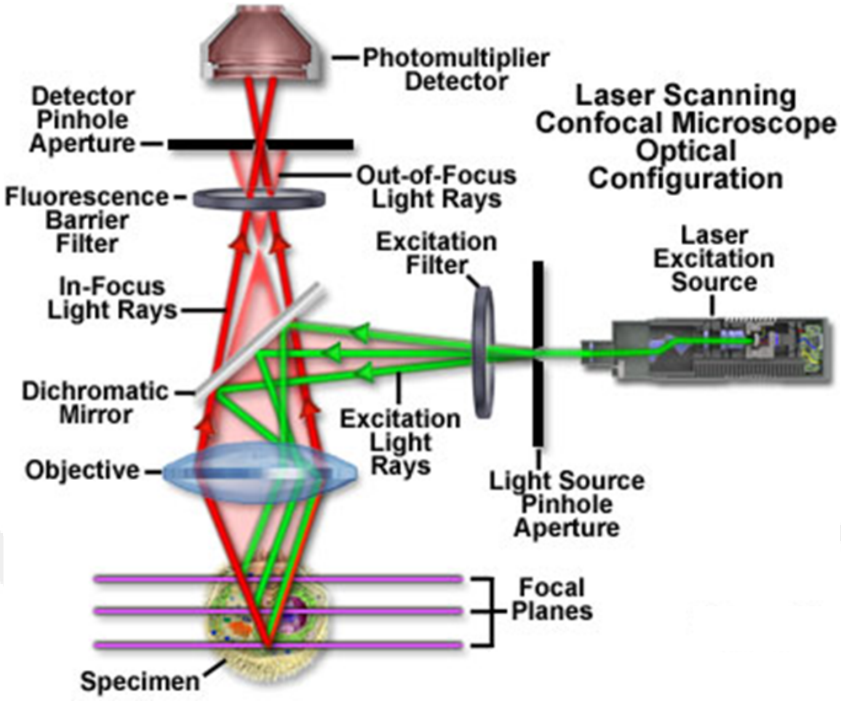

Figure 1.8: Representation of imaging components of confocal microscopy. Adapted from EVIDENT, 2024.

1.4.1.2 Förster Resonance Energy Transfer (FRET)

Förster Resonance Energy Transfer (FRET) is a technique that enables the examination of protein-protein or molecular interactions, the location of the proteins, and the distance of the proteins in live cell imaging, which was developed by Theodore Förster in the twentieth century (Kramer & Fischer, 2011). FRET relies on the resonance energy transfer between molecules with a long-range dipole-dipole interaction up to 10 nm within the Förster distance; that is, energy transference is in 50% efficiency (Sekar & Periasamy, 2003). FRET can be measured using different techniques such as donor or acceptor photobleaching, spectral imaging, and the 3cube method (Rebenku *et al.*, 2023).

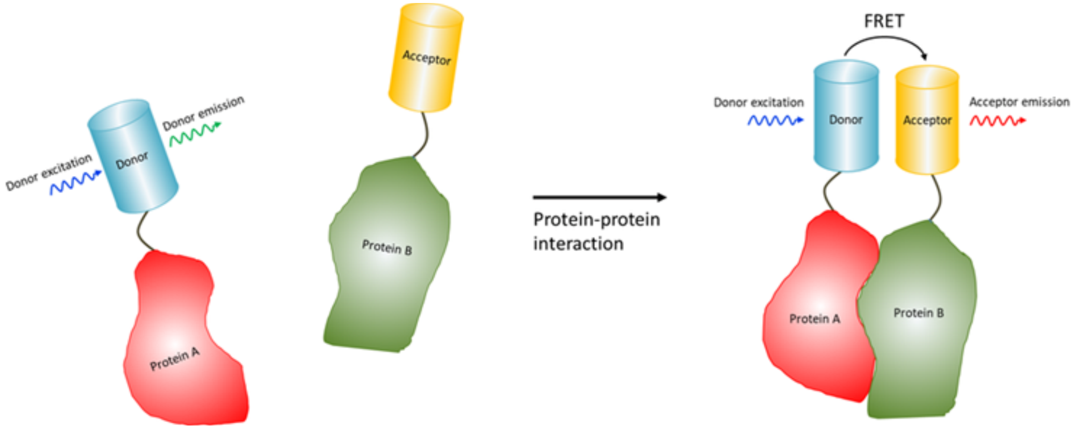

Figure 1.9: FRET technique in protein-protein interactions. When two fluorophore-tagged proteins come in close proximity, non-radiative energy transfer enables the study of this interaction dynamics. Adapted from the University of Gothenburg, 2024.

Energy transfer in FRET can be calculated using a formula given below in Formula 1.1 (Berney & Danuser, 2003). $k_T(r)$ stands for the energy rate that is transferred from donor to acceptor, τ_D stands for donor's decay time, R_0 stands for Förster distance, and r is the distance between donor and acceptor.

$$k_T(r) = \frac{1}{\tau_D}\left(\frac{R_0}{r}\right)^6 \tag{1.1}$$

In FRET, fluorophores can be used to measure this energy transfer, and these fluorophores should meet some criteria to understand the dynamics of interactions. Firstly, the excitation and emission spectrum of the two candidate fluorophores should be well known. Since in FRET, the donor's excitation energy is transferred to the acceptor ground state energy in long-range dipole-dipole interaction, the donor's emission spectrum and the acceptor's excitation spectrum should overlap as much as possible. However, the emission spectrum and excitation spectrum of the donor and acceptor should not overlap since this could cause bleedthrough, which will be interpreted as a false positive or false negative signal. Also, the quantum yield of the donor fluorophore should be high. Thus, its emitted number of photons should be as high as the absorbed number of photons with low non-radiative decay. Thus, the donor can transfer its excited energy to the acceptor in the most efficient way (Bajar *et al*., 2016). Also, the extinction coefficient of the acceptor, which is the best absorption for a given wavelength, should be high. Moreover, fluorophores should be at Förster Distance, which is the range of 20 A° to 90 A° to transfer the energy efficiently with a proper orientation of the fluorophores that is important for energy transfer to provide better resonance energy transfers between pairs in appropriate dipole moments.

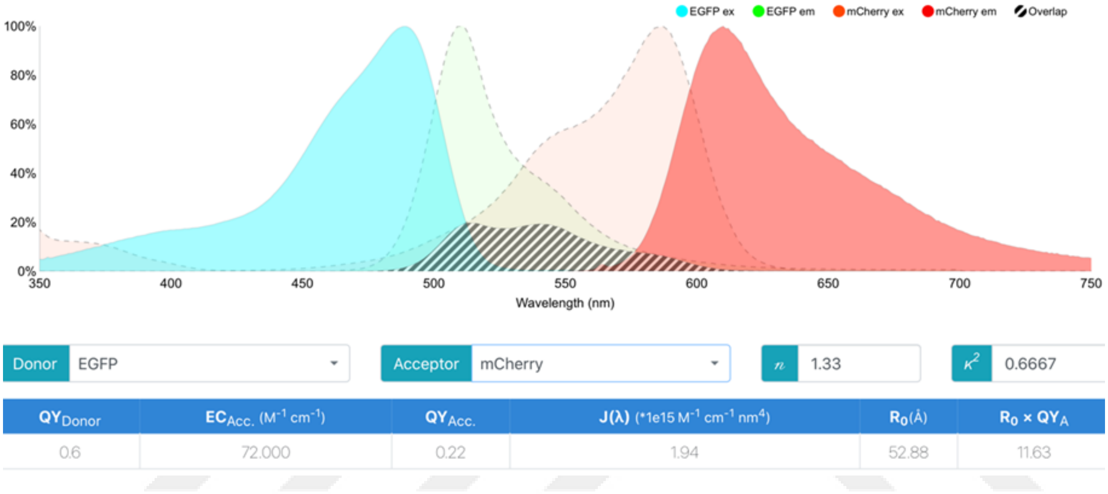

Donor: EGFP

Acceptor: mCherry

n: 1.33

κ^2: 0.6667

QY_{Donor}	$EC_{Acc.}$ (M^{-1} cm^{-1})	$QY_{Acc.}$	J(λ) (*1e15 M^{-1} cm^{-1} nm^4)	R_0(Å)	$R_0 \times QY_A$
0.6	72,000	0.22	1.94	52.88	11.63

Figure 1.10: Wavelength spectrum of EGFP and mCherry fluorophores and their spectral overlaps. Förster distance between donor EGFP and acceptor mCherry is 52.88 20 A°. Adapted from Wu & Brand, 1994.

When the distance between the donor and the acceptor is equal to the Förster distance, the decay rate of the donor becomes equal to the energy transfer rate; then, energy transfer occurs at 50% efficiency. With this information, energy transfer efficiency can be calculated below in Figure 1.11 with proper rearrangements in the values. E stands for efficiency of energy transfer, R_0 is Förster distance, and r is the distance between donor and acceptor.

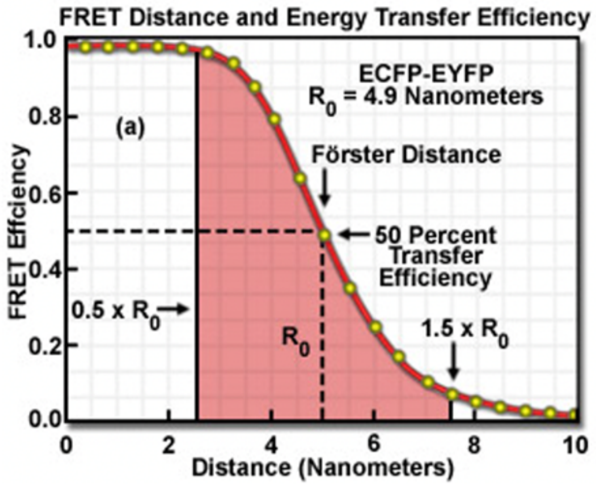

$$E = \frac{R_0^6}{R_0^6 + r^6}$$

Figure 1.11: Relation between FRET efficiency-distance of fluorophores and adjusted. FRET Efficiency formula regarding distances. Adapted from EVIDENT, 2024.

However, FRET has some problems due to the nature of fluorophores, such as bleed-through. When the emission spectrum of multiple fluorophores overlaps, it is possible to get crosstalk or bleed-through from one signal to another signal (Chen *et al.*, 2007). Due to the broad emission spectrum and the spilling of one wavelength to other wavelengths in the filter system, it is hard to get exact measurements when multiple fluorophores exist. It can be prevented by selecting fluorophores carefully, such as they can be at different ends of the spectrum, and specific filters can be used.

1.5 Aim of the Thesis

K-Ras is a peripheral plasma membrane protein belonging to the small G-protein Ras family. It plays vital roles in signal transduction, cell proliferation, survival, and differentiation with its GDP/GTP transition. Therefore, K-Ras dysfunctions are associated with tumorigenesis. Similarly, Gα proteins are peripheral membrane proteins belonging to the Heterotrimeric G-protein family. These proteins are generally activated with G protein-coupled receptors, which act as Guanine exchange factor (GEF) switching GDP/GTP activating Gα proteins. Like K-Ras, Gα proteins are also associated with many disease states. In recent years, studies have shown that K-Ras forms dimers through the G-domain, which plays a vital role in GTPase activity (Muratcioglu *et al.*, 2020). In addition to current research on K-Ras dimerization, studies in our laboratory showed that Gα proteins (specifically Gαi1-Gαi1) can also dimerize in live cells. These findings unveiled new possibilities that G-proteins can function and activate alternative signaling pathways through homo- and/or hetero-dimerization. Thus, this study aims to investigate the role and importance of G-Domain on K-Ras and Gα protein dimerization in live cells.

CHAPTER 2

MATERIALS AND METHODS

2.1 Protein Modelling and Structure Prediction

Protein modeling studies were carried out using Chimera software version 1.16.0 (University of California, USA). For studying protein models, the Research Collaboratory for Structural Bioinformatics Protein Data Bank, RCSB PDB, was used. From this experimentally determined protein structure data bank, for K-Ras PDB ID: 3GFT, Gα11 PDB ID:6OIJ, Gα12 PDB ID:1ZCA, Gα13 PDB ID:3AB3, Gαi1 PDB ID:1KJY and Gαs PDB ID:6AUG were picked and modeled under Chimera MatchMaker tool for dimerization interface studies and amino acid simulations. Also, for the K-Ras – K-Ras dimerization model, the study that was published by Muratcioglu was used as a reference.

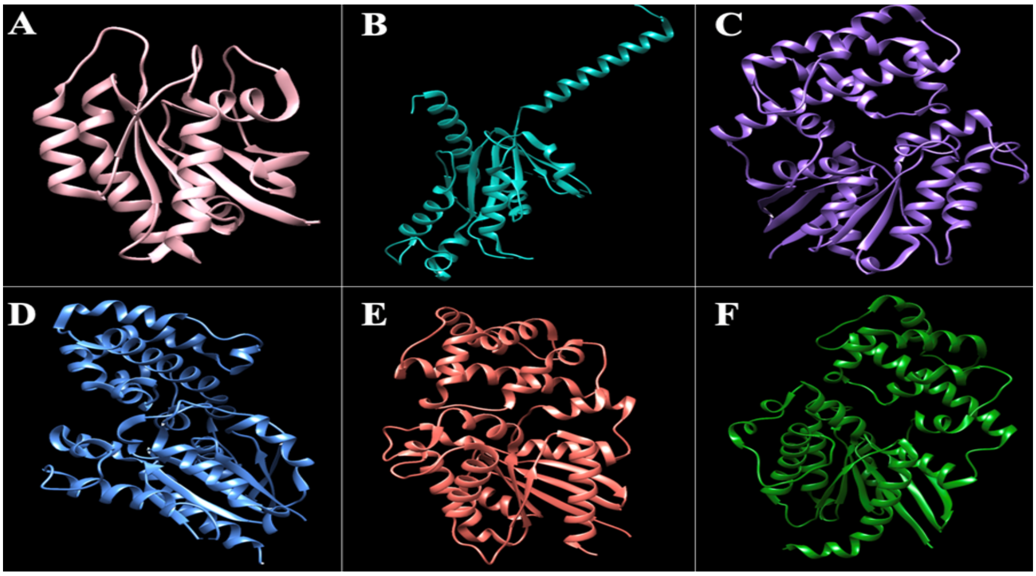

Figure 2.1: 3D protein structures taken from Protein Data Bank. (A) K-Ras PDB ID: 3GFT. (B) Gα11 PDB ID:6OIJ (C) Gα12 PDB ID:1ZCA. (D) Gα13 PDB ID:3AB3. (E) Gαi1 PDB ID:1KJY. (F) Gαs PDB ID:6AUG.

2.2 Bacterial Cell Culture

2.2.1 Bacterial Strain & Growth Media & Maintenance

In this study, as a bacterial strain *Escherichia coli* XL-1 Blue strain was used for plasmid transformation. Lysogeny Broth, LB, medium was used for *E. coli* growth after performing autoclave sterilization for 20 minutes at 121°C in an autoclave machine. For the selection marker of *E. coli*, antibiotic ampicillin in 100 µg/ml concentration was used in LB medium. Transformed *E. coli* cells were grown in LB agar medium with ampicillin for 16 hours at 37°C in the incubator. Transformed single colonies were selected and inoculated to liquid LB medium for plasmid isolation and allowed to grow for 16 hours at 37°C in a rotary shaker at 200 rpm.

2.3 Molecular Cloning

2.3.1 Preparation of E. coli Competent Cells via RbCl2 Method

A single colony from E. coli XL-1 Blue strain plate was inoculated to a blood tube with 4 mL liquid LB medium without any selection marker and left to grow at 37°C for 16 hours in a rotary shaker. 1 mL of an overnight grown culture was inoculated to a fresh 100 mL liquid LB medium containing 20 mM $MgSO_4$ and continued growing till OD_{600} reached 0.4-0.6. Once confluency reached the desired level, 100 mL subculture was centrifuged at 2700 rpm for 7 minutes at 4°C. Then, the supernatant was discarded, and the pellet was resuspended in 40% volume of the initial subculture of ice-cold TFBI and incubated on ice for 5 minutes. Another round of centrifugation was applied at 2700 rpm for 7 minutes at 4°C, and the pellet was resuspended with TBFII, which was 4% volume of the initial subculture, and left for incubation on ice for 45 minutes. End of the incubation, cells were aliquoted to Eppendorf tubes in 50 µL volume, quick-freezed in liquid nitrogen, and stored at -80°C.

2.3.2 Construction of Coding Sequences in Mammalian Expression Vector pcDNA 3.1(-)

GNA11, GNA12 and GNA13 tagged with EGFP in pcDNA3.1 (-) vectors were obtained from 113Z639 numbered TÜBİTAK Project “Adenozin 2a ve Dopamin 2 Reseptörlerinin Homo ve/veya Heteromerlerinin G Proteinleri İle Etkileşiminin Canlı Nöron Hücrelerinde Analizi ve Bu Etkileşimlerin Sinyal Yolakları Üzerindeki Etkileri ” with GNA11 Gene ID:2767, GNA12 Gene ID:2768 and GNA13 Gene ID:10672; GNAI1 and GNAS tagged with EGFP in pcDNA 3.1 (-) vectors were obtained from 117Z868 numbered TÜBİTAK project “Investigation of Gα protein dimerization mechanisms in live cells” with GNAI1 GeneID:2770 and GNAS Gene ID:2778. EGFP and mCherry vectors were gifted by Prof. Dr. Henry Lester, California Institute of Technology, USA. pcDNA3.1(-) was gifted by Prof. Dr. Ayşe Elif Erson Bensan, Middle East Technical University, Turkiye. K-Ras G12D oncogenic form, Gene ID: 3854, coding vector was gifted by Assoc. Prof. Dr. Kwang-Jin Cho, Wright State University, USA. Positive and negative FRET control groups were prepared by a former Master's student, Hüseyin Evci, Middle East Technical University, Turkiye.

In this project, Firstly, the K-Ras G12D oncogenic form of the K-Ras gene named “K-Ras *onc*” was mutated to the K-Ras wild type form named “K-Ras *wt*” detailed below (2.3.4. Site-Directed Mutagenesis). Then, K-Ras *wt* and K-Ras *onc* coding sequences were constructed in a mammalian expression vector pcDNA 3.1(-).

2.3.2.1 Primer Design

In order to amplify the K-Ras gene, NheI (GCTAGC) and BamHI (GGATCC) restriction sites were added to primers for cloning genes with proper restriction sites into pcDNA 3.1(-). Moreover, in order to increase the binding efficiency of primers GTTGTTGTT sequences were added beginning of the primer. Designed primers were shown below in Table 2.1 in a 5’ to 3’ DNA replication direction.

Table 2.1 : Designed primers used for K-Ras *wt* and K-Ras *onc* genes, bold characters indicate restriction sites.

Primer Name	**Sequences**
K-Ras NheI Forward	GTTGTTGTT**GCTAGC**ATGACTGAATATAAACTTGTGGTAGTTGGA
K-Ras BamHI Reverse	GTTGTTGTT**GGATCC**TTACATAATTACACACTTTGTCTTTGA

2.3.2.2 Polymerase Chain Reaction (PCR)

For cloning coding sequences to pcDNA 3.1 (-), firstly, the amplification of K-Ras *wt* and K-Ras *onc* coding sequences was performed, PCR was run with proper primers, and new restriction sites were introduced at the beginning and end of the genes. End of the reaction, blunt end coding sequences were obtained. As a polymerase, Phire Hot Start II Green Master Mix (Thermo Fisher Scientific, CAT#F126L) which has optimized reaction buffers, nucleotides, and $MgCl_2$ was used. Below, optimized PCR reaction ingredients and PCR conditions are shown.

Table 2.2 : Optimized PCR conditions and ingredients for amplifying K-Ras *wt* and K-Ras *onc*.

Reagent	**Amount**				
DNA Template	300 ng	Initial Denaturation	98°C	30sec	
Forward Primer (0.5 µM)	1.25 µL from 20 mM stock	Denaturation	98°C	5sec	
Reverse Primer (0.5 µM)	1.25 µL from 20 mM stock	Annealing	68°C	5sec	33X
Phire Hot Start II Green Master Mix	25 µL	Extension	72°C	45sec	
Nuclease Free Water	Completed to 50 µL	Final Extension	72°C	1min	
TOTAL	50 µL				

2.3.2.3 PCR Purification

At the end of the PCR reaction, in addition to amplified PCR products, buffers, enzymes, and MgCl2 also stay in the reaction, which is unwanted for further cloning steps. In order to get rid of these undesired products, a PCR purification technique is applied. GeneJET PCR Purification Kit (Thermo Fisher Scientific, CAT#K0702) was used as the manufacturer's instruction to purify the PCR products. In addition, instead of elution buffer, pre-heated nuclease-free water was used in 30 µL instead of 50 µL to obtain a higher concentration.

2.3.2.4 Agarose Gel Electrophoresis

To visualize and validate the existence of amplified products in the expected size, products were loaded in agarose gel, run under an electric field, and imaged under

UV light. To visualize amplified constructs, 0.8% (w/v) agarose gel in 1X TAE and 0.5 µg/mL Ethidium Bromide, which intercalates itself into DNA and emits light under UV excitation, was prepared (Sigmon & Larcom, 1996). For the preparation of the gel, 0.48 g agarose was weighed and added into 60 mL 1X TAE, which was diluted with dH_2O from 50X TAE stock solution. Till agarose melted in TAE completely, the mixture was heated in a microwave and cooled under tap water for 30 seconds. Then, 25 µL EtBr was added, and the mixture was poured into a gel tray with a proper comb. Once the gel polymerized, samples were mixed with loading dye to track migration and sinkage of the samples to wells using Purple Gel loading dye (NEB, CAT# B7024S). Moreover, as a reference for size determination of samples, GeneRuler DNA Ladder Mix (Thermo Fisher Scientific, CAT#SM0331) or GeneRuler 1 kb DNA Ladder (Thermo Fisher Scientific, CAT#SM0313) were used. Then, the gel was run under 100V in 1X TAE buffer for 35-45 minutes and visualized under UV.

2.3.2.5 Restriction Enzyme Digestion

After confirmation of desired products in expected size in agarose gel electrophoresis, PCR products, blunt end K-Ras *wt,* and K-Ras *onc* genes were cut with introduced restriction sites in PCR, which are NheI (NEB, CAT#R3131M) and BamHI (NEB, CAT#R0136M) at 37°C for 3 hours. In addition to cutting genes, pcDNA 3.1(-) was also cut with the same enzymes under the same conditions. According to the manufacturer's instruction, 1 µL enzyme is supposed to be used for cutting 1000 ng DNA with the proper concentration of CutSmart buffer (NEB, CAT#B6004). At the end of the restriction digestion, both genes and the vector get sticky ends, which enables gene insertion into the vector after ligation. However, at the end of the reaction, the mixture has a buffer and restriction enzyme that can interfere with the proper ligation reaction. To prevent that, the end products of reactions were subjected to PCR purification, which purifies DNA as mentioned above in the “2.3.2.3. PCR Purification” section. Below, ingredients and their optimized amount for double restriction digestion are shown.

Table 2.3 : Optimized double restriction digestion reagents and amounts.

Reagents	**Amount**
Target DNA	33 µL
Restriction Enzyme I	1.5 µL
Restriction Enzyme II	1.5 µL
CutSmart Buffer (10X)	4 µL
TOTAL	40 µL

2.3.2.6 Ligation

After digested products were purified, their concentrations and purity were quantified using Nanodrop. To clone inserts in this case K-Ras *wt* and K-Ras *onc* genes to vector pcDNA 3.1 (-), T4 ligase (Thermo Fisher Scientific, CAT# EL0011) was used provided by manufacturer’s T4 Ligase Buffer (Thermo Fisher Scientific, CAT#B69). For the reaction, considering the mass and sizes of inserts and vector, 1:5 or 1:10 insert: vector molar ratios were calculated, and at least 200 ng vector was used. Then, the mixture was incubated for 3 hours at room temperature. Below, reagents and amounts are shown.

Table 2.4 : Optimized ligation reagents and amounts.

Reagents	**Amount**
Vector	200 ng
Insert	Ratio depended
T4 Ligase	1 μL
T4 Ligase Buffer (10X)	2 μL
Nuclease Free Water	Completed to 20 μL
TOTAL	20 μL

2.3.2.7 Transformation

In order to obtain ligated plasmids, ligation reactions were transformed into competent cells. As a competent cells, *E. coli* XL-1 Blue strain was used. For long-term storage, competent cells were kept at -80°C, and at the beginning of the procedure, they were thawed on ice for 15 minutes. Then, 3 μL from the ligation reaction mixture was added in sterile conditions and incubated on ice for 30 minutes. After incubation, competent cells were subjected to heat shock at 42°C for 45 seconds and put back to ice incubation for 5 minutes. Later, 950 μL LB was added to cells and incubated in a rotary shaker at 180 rpm at 37°C for 1 hour. End of the incubation, competent cells were centrifuged at 4000 rpm for 4 minutes, 700 μL supernatant was discarded, and the remaining cells were resuspended in the supernatant and then plated on selective media, that is Ampicillin agar plates, and incubated at 37°C for 16 hours to pick single bacterial colonies.

2.3.2.8 Plasmid Isolation

Transformed plasmids were able to amplify in competent cells, and lysing single colonies enabled the obtaining of desired plasmids. After transformation, a single colony from agar plates was inoculated to 4 mL liquid LB medium containing ampicillin in sterile conditions and incubated in a rotary shaker at 180 rpm at 37°C for 16 hours. After this incubation, grown cells were collected to isolate their desired plasmid. For plasmid isolation, the GeneJET Plasmid Miniprep Kit (Thermo Fisher Scientific, CAT#K0503) was performed according to the manufacturer's instructions. In a similar manner to PCR purification, instead of elution buffer, 90 µL pre-heated NFW was used to increase the yield, and plasmid concentrations were measured using Nanodrop.

2.3.2.9 Control Restriction Enzyme Digestion

During the transformation, competent cells can uptake self-ligated vector from ligation reaction and may give false positive results by forming single colonies on agar plates. Control restriction enzyme digestion was performed to test whether the desired isolated plasmids were the desired. In the same manner as Restriction Enzyme Digestion, reaction amounts were decreased to small volumes to see if insertion exists in determined vector sites, and the reaction was incubated at 37°C for 2 hours. Below, optimized control restriction enzyme digestion ingredients and their amounts are shown.

Table 2.5 : Optimized double restriction digestion reagents and amounts.

Reagents	**Amount**
Target DNA	300 ng
Restriction Enzyme I	0.25 µL
Restriction Enzyme II	0.25 µL
CutSmart Buffer (10X)	1.5 µL
Nuclease Free Water	Completed to 15 µL
TOTAL	15 µL

2.3.3 PCR Integration Method

In this study, K-Ras *wt* and K-Ras *onc* proteins were internally tagged with mCherry and EGFP at the 62nd amino acid position in the structure. This 62nd position on K-Ras proteins was chosen according to EGFP tagged Gα Proteins to efficient energy transfer in FRET studies, considering Förster distance between EGFP and mCherry at their positions. For the position tagging, the PCR Integration method was used. This method required two PCR reactions back-to-back in different PCR conditions (Geiser *et al*., 2001). The first primer was designed to target the amplification of EGFP or mCherry together with approximately 30 bp overhang sequences belonging to protein to be tagged. The final product end of the first PCR reaction was used as a primer in the second PCR reaction, and the protein was tagged during this amplification with fluorophores.

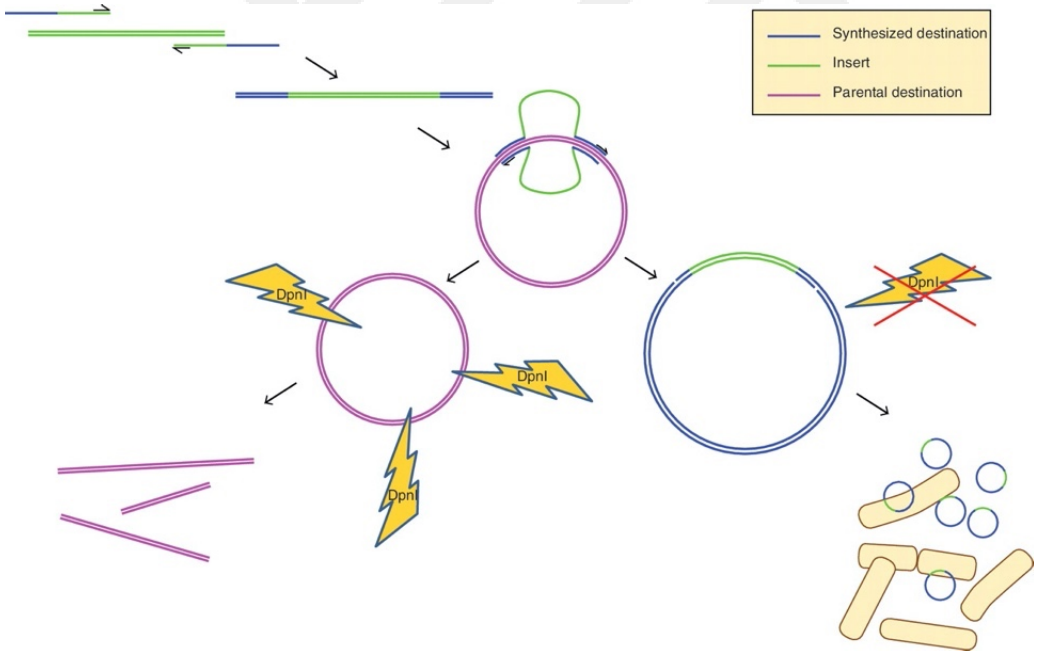

Figure 2.2: A schematic representation of PCR integration method. Adapted from Geiser *et al*., 2001

2.3.3.1 Primer Design

To tag K-Ras *wt* and K-Ras *onc* proteins with EGFP and mCherry at the 62nd amino acid position, the first primer pairs were designed to anneal EGFP and mCherry, and the beginning and end of the primers have approximately 30 bp sequences from before and after K-Ras 62nd amino acid as overhangs. In the second PCR, no primers were used since the first PCR reaction product, which anneals the K-Ras coding gene with its 30 bp overhangs, was used as a primer. In addition, since mCherry and EGFP have identical sequences at the beginning and end of their sequences for 21 bp length, the same primers were used to amplify both of them.

Table 2.6 : Designed primers for tagging K-Ras *wt* and K-Ras *onc* proteins at 62nd position with EGFP and mCherry in 5’ to 3’ direction. Underlined sequences anneal to EGFP or mCherry, overhangs anneal to K-Ras.

Primer Name	**Sequences**
K-Ras-62 EGFP/mCherry Forward	CTCTTGGATATTCTCGACACAGCAGGTCAAGAGATGGTGAGCAAGGGCGAGGAG
K-Ras-62 EGFP/mCherry Reverse	CCTCATGTACTGGTCCCTCATTGCACTGTACTCCTTGTACAGCTCGTCCATGCCG

2.3.3.2 Integration Polymerase Chain Reaction (PCR)

2.3.3.2.1 First PCR

First PCR reaction was performed in a similar manner amplifying any gene explained above in the section “2.3.2.2. Polymerase Chain Reaction (PCR)” with using the same conditions and ingredients. For EGFP amplification, EGFP in pcDNA 3.1 (-) and for mCherry amplification mCherry in pcDNA 3.1 (-) were used as DNA templates.

2.3.3.2.2 Second PCR

The second PCR reaction was performed using the first PCR products as primers, which are called Mega Primers, and proper high-fidelity PCR conditions. In the reaction, high-fidelity Phusion HS II DNA Polymerase (Thermo Fisher Scientific, CAT#F549S), which has 52 times more fidelity compared to Taq polymerase, was used. In this step, K-Ras *wt* and K-Ras *onc* were used as a template to tag with EGFP and mCherry in desired positions. Here below, the second PCR reagents and their high-fidelity conditions are shown.

Table 2.7 : Optimized second PCR conditions and ingredients for tagging K-Ras *wt* and K-Ras *onc* with EGFP and mCherry fluorophores.

Reagent	**Amount**				
DNA Template	25 ng	Initial Denaturation	98°C	3 min	
Mega Primer	125 ng	Denaturation	98°C	30 sec	
dNTP mix (10mM)	0.4 µL	Annealing	57°C	45 sec	18X
Phusion HS II DNA Polymerase	0.3 µL	Extension	69°C	10 min	
5X Phusion HF Buffer	4 µL	Final Extension	69°C	12 min	
Nuclease Free Water	Completed to 20 µL				
TOTAL	20 µL				

2.3.3.3 DNA Extraction from Agarose Gel

When the First PCR was performed, whole products were loaded into agarose gel, and electrophoresis was applied. Then, the gel was visualized under UV light, and sizes were confirmed according to the DNA ladder. Later, related DNA fragments were cut with a scalpel and put in separate Eppendorf tubes to be weighed. DNA fragments inside the gel were purified according to the manufacturer's instructions using the GeneJET Gel Extraction Kit (Thermo Fisher Scientific, CAT#K0692). The elution step was done similarly to other DNA purification kits. After the purification, products were used as a primer in the second PCR step.

2.3.3.4 DpnI Enzyme Digestion

The end products of the second PCR also contain an untagged template. In order to remove the template plasmid from the reaction mixture, DpnI (NEB, CAT# R0176S) restriction enzyme digestion was applied (incubated at 37°C for 3 hours). DpnI enzyme recognizes its recognition site only when the site is methylated; therefore, parental plasmids can be cleaved in the reaction (Weiner et al., 1994). Then, the products were transformed into bacterial cells; the plasmid was isolated using a plasmid isolation kit, and control restriction digestion was applied.

2.3.4 Site-Directed Mutagenesis

In this study, the K-Ras *onc* construct was mutated to its *wild-type* form, K-Ras *wt*, via site-directed mutagenesis (SDM). Moreover, K-Ras and Gα proteins were mutated at the dimerization interface. Following protein sequence alignment, amino acids of Gα proteins aligned with the two crucial K-Ras amino acids at the dimerization interface were mutated to mimic K-Ras residues. Also, charge reversal mutations on K-Ras residues were carried out in order to disrupt the dimerization. For SDM, proper primers with desired mutations were designed, and high-fidelity PCR was performed. Then, similar to the "2.3.3.4. DpnI Enzyme Digestion" part, DpnI enzyme digestion was applied, and the reaction mixture was transformed into *E. coli* competent cells, plasmids were purified. Table 2.8 below shows the desired mutations after performing Site-directed mutagenesis.

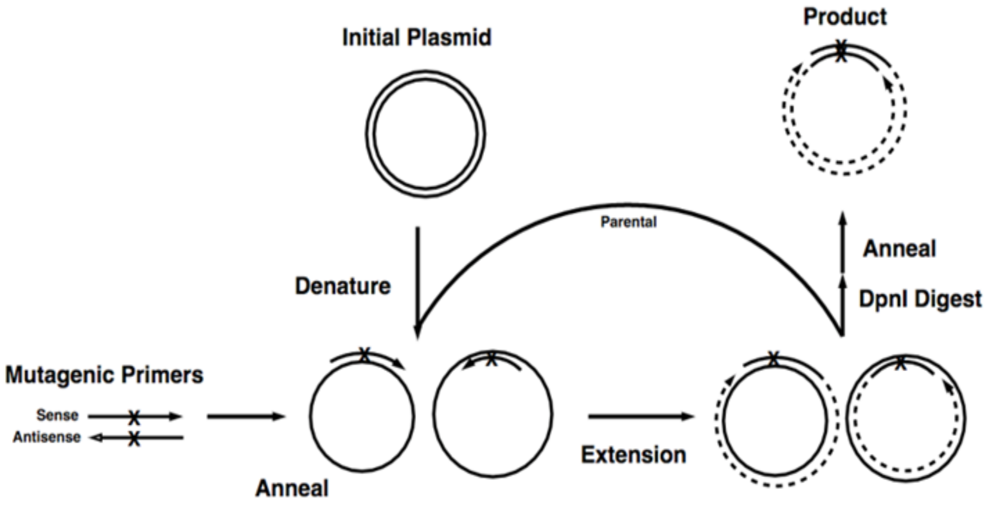

Figure 2.3: A schematic representation of Site-Directed Mutagenesis. Adapted from Laible & Boonrod, 2009.

Table 2.8 : Desired mutation on K-Ras and Gα proteins after site-directed mutagenesis to interfere with dimerization interfaces.

Constructs	**Sites before mutation**	**Desired mutation on site after SDM**
K-Ras *onc*	D12	D12G
K-Ras *wt*	K101 & R102	K101D&R102E
K-Ras *onc*	K101 & R102	K101D&R102E
GNAI1	N256 & K257	N256K & K257R
GNA11	Y261 & P262	Y261K&P262R
GNA13	N278	N278K

2.3.4.1 Primer Design

For site-directed mutagenesis reactions, desired mutations were put in the middle of the sequence with at least 9 bp flanking nucleotides, and more extended complementary sequences were added on both primers for proper annealing. Below, designed primer sequences are shown.

Table 2.9 : Designed primers that were used for mutating K-Ras *onc* form to its wild-type form and EGFP/mCherry tagged K-Ras *wt*, K-Ras *onc* and Gα proteins. Underlined sequences show mutated regions.

Primer name	**Sequence**
K-Ras D12G Forward	GTTGGAGCTGGTGGCGTAGGCAAGAGTGCC
K-Ras D12G Reverse	GCCTACGCCACCAGCTCCAACTACCACAAG
K-Ras SDM K101D&R102E Forward	GAACAAATTGACGAAGTTAAGGACTCTGAAGATG
K-Ras SDM K101D&R102E Reverse	GTCCTTAACTTCGTCAATTTGTTCTCTATAATGG
GNAI1 N256K & K257R Forward	GCATATGTAACAAAAGGTGGTTTACAGATACATCC
GNAI1 N256K & K257R Reverse	CTGTAAACCACCTTTTGTTACATATGCTGTCAAAC
GNA11 Y261K&P262R Forward	CCGGACCATCATCACCAAGCGCTGGTTCCAGAACTCCTCCG
GNA11 Y261K&P262R Reverse	CTGGAACCAGCGCTTGGTGATGATGGTCCGGAACAGGGC
GNA13 N278K Forward	CAATCGTCAATAAACGGGTTTTCAGCAATGTCTCC
GNA13 N278K Reverse	GCTGAAAACCCGTTTATTGACGATTGTTTCAAAATG

2.3.4.2 SDM Polymerase Chain Reaction (PCR)

SDM PCR reaction required high-fidelity PCR conditions for proper primer annealing to plasmids to perform its substitutions in the sequences. Therefore, similar to the “2.3.2.2.1. Second PCR” section, the same polymerase was used.

Table 2.10 : Optimized SDM PCR conditions and ingredients for mutating K-Ras *onc* to K-Ras *wt* and tagged K-Ras *wt*, K-Ras *onc* and Gα proteins.

Reagent	**Amount**				
DNA Template	25 ng	Initial Denaturation	98°C	3 min	
Forward Primer (0.5 µM)	0.5 µL from 20 mM stock	Denaturation	98°C	30 sec	22X
Reverse Primer (0.5 µM)	0.5 µL from 20 mM stock	Annealing	58°C	45 sec	
dNTP mix (10mM)	0.4 µL	Extension	70°C	10 min	
Phusion HS II DNA Polymerase	0.3 µL	Final Extension	70°C	12 min	
5X Phusion HF Buffer	4 µL				
Nuclease Free Water	Completed to 20 µL				
TOTAL	20 µL				

2.4 DNA Sequencing

After constructing the desired plasmids, their sequence confirmation was done by Sanger sequencing. Sequencing primers were chosen from upstream and downstream regions from multiple cloning sites sequences of pcDNA 3.1 (-) and designed accordingly. Once sequences were confirmed, all constructs were cut from the plasmid from PCR and ligated to a new empty pcDNA 3.1 (-) vector to eliminate any possible mutations generated by HF polymerase that could interfere with gene expression. Table 2.11 shows pcDNA 3.1(-) sequencing primers.

Table 2.11 : Designed primers for sequencing of constructs.

Primer Name	**Sequences**
pcDNA 3.1(-) Forward	GTGTACGGTGGGAGGTCTAT
pcDNA 3.1(-) Reverse	GCCTTCCTTGACCCTGGAA

2.5 Mammalian Cell Culture

2.5.1 *Mus musculus* Neuro-2a (N2-a) Cell Line

The N2-a cell line is obtained from neuroblasts of the mouse (*Mus musculus*) brain tissue, and as the name indicates, it is a tumor cell line. Since the N2-a cell is a good candidate for understanding the dynamics of GTP binding proteins, this cell line was used for imaging and investigating the interaction between K-Ras and Gα proteins in this study. N2-a cells are adherent cells, and their doubling time is approximately 24 hours to 36 hours. The N2-a cell line was purchased from ŞAP Enstitüsü, Turkiye.

2.5.1.1 Maintenance of N2-a Cell Line

N2-a cell subculturing and cultivation were done using T-25 flasks (Greiner, CAT#690175) in a sterile laminar flow hood. The growth media contained 89% Dulbecco's Modified Eagle Medium, DMEM (Gibco, CAT#41966029) supplemented with high glucose and pyruvate. In addition to DMEM, media contained 10% Fetal Bovine Serum, FBS (Gibco, CAT#10500064), and 1% antibiotic Penicillin/Streptomycin (Gibco, CAT#15140122) in Penicillin 100 IU/mL and Streptomycin 100 µg/mL concentrations. A complete medium was prepared accordingly, and the filter was sterilized with a 0.22 µm pore size vacuum filtration apparatus (Nest, CAT#34300). The N2-a cell line requires passage twice per week once it reaches approximately 80% confluency. The cell medium was first discarded during the passage, and cells were washed with 3 mL 1X phosphate-buffered saline (PBS). Since they were adherent cells, 0.5 mL TrypLE (Gibco, CAT#12605028) was used for disassociation of cells from the surface of the flask and incubated for 5 minutes at 37°C under 5% CO_2. Then, 8 mL fresh media was added to detached cells and collected into a falcon tube for centrifuging at 900 rpm for 5 minutes to eliminate TrypLE. After centrifugation, the supernatant was discarded, and 5 mL of fresh media was added to resuspend the cell pellet. Then, 10 µL resuspended cells were counted using a Neubauer Hemocytometer (Marienfeld, #CAT0640010). Then, viable cells were counted, and an approximate cell number in 1 mL cell was found. Then, the desired number of cells were seeded in a new T-25 flask with fresh 8 mL medium and incubated till later passaging at 37°C under 5% CO_2.

Figure 2.4: A schematic representation of cell counting on a Neubauer Hemocytometer.

2.5.2 Transfection

Transient transfection was applied to introduce desired expression vectors to mammalian N2-a cells using Lipofectamine LTX (Invitrogen, CAT# 15338100). Before transfection day, 180.000 cells were seeded on a 35 mm glass bottom dish (Cellvis, CAT#D35-20-1.5-N). For transfection, 400-600 ng from each plasmid and 3 µL Lipofectamine Plus Reagent were mixed in 100 µL Opti-MEM (Gibco, CAT#31985070) and incubated at room temperature for 15 minutes. During this incubation, in another tube, 3 µL Lipofectamine LTX reagent was diluted in 100 µL Opti-MEM. After incubation, plasmid tubes and Lipofectamine LTX reagent tubes were mixed and incubated for an additional 15 minutes at room temperature. At the end of the incubation, the medium of cells in dishes was discarded, and the cells were washed with 1 mL PBS. Then, the transfection mixture and 1 mL Opti-MEM were added to the cells gently and incubated for 3 hours at 37°C under 5% CO_2. After 3 hours, fresh cell medium was added to the cells, and incubation continued for 48 hours prior to imaging.

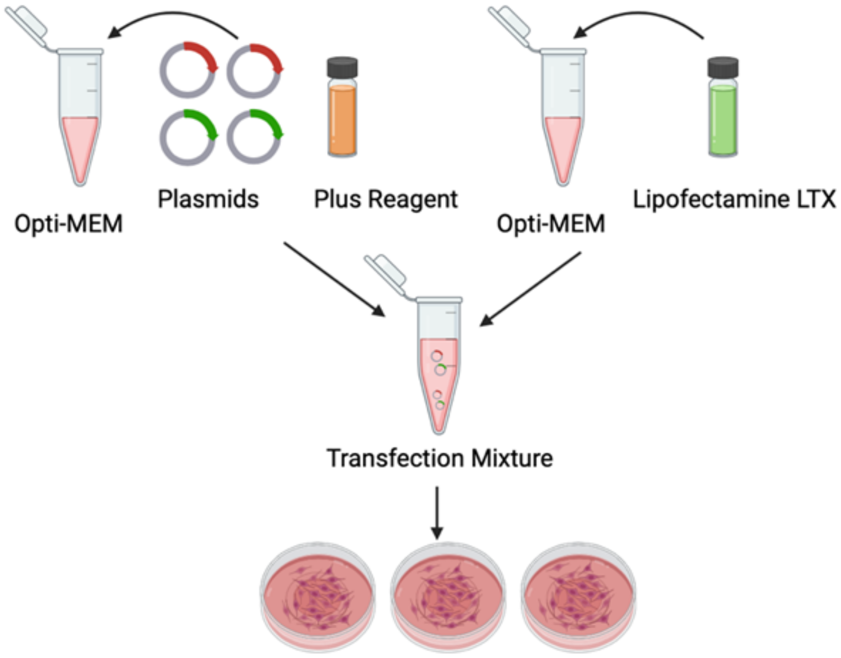

Figure 2.5: A schematic representation of the transfection protocol.

2.6 Protein Isolation

In this study, transfected cell total proteins were isolated for further studies. 500.000 cells were seeded for transfection, and the transfection protocol was applied as described in section "2.5.2. Transfection". 48 hours after transfection, the cell medium was discarded in laminar hood flow, and 200 µL Radioimmunoprecipitation assay buffer (RIPA) (Serva, CAT# 39244.01) that contained protease inhibitor PMSF (Serva, CAT# 32395.02) in 1 mM concentration was added on cells and incubated on ice for 5 minutes. Then, cells were detached from the surface of the dishes using a scraper, transferred to Eppendorf tubes, and centrifuged at 14.000xg for 15 minutes. After centrifugation, the supernatant containing isolated proteins was collected and transferred to another Eppendorf tube.

2.6.1 Quantification of Protein Concentrations

Protein concentrations were determined by Bradford Assay. The Bradford Protein Assay Kit (Thermo Fisher Scientific, CAT#23200) based on Coomassie-dye was used to conduct the assay. 5 µL isolated proteins were loaded on a clear 96 well plate (Sarstedt, CAT# 83.3924), and then 250 µL from the kit's Coomassie reagent was added and incubated at room temperature for 10 minutes. After incubation, using the Multiskan-GO microplate reader (Thermo Fisher Scientific, CAT# N10588), protein concentration was measured at OD_{595}. Before measuring protein concentration, a protein standard curve was generated using Bovine Serum Albumin between 0-2000 µg range, and concentration calculations were done according to the standard curve.

2.7 Western Blot

Firstly, protein samples were prepared in dilution and loading buffer and denatured at 98ºC for 5 minutes in a heat block. Proteins were separated according to their sizes with polyacrylamide-based gel using the SDS-PAGE technique. For this separation, a discontinuous gel system was prepared with 10% separating gel at the bottom and 4% stacking gel at the top between glass cassettes. Electrophoresis was done at 80V for 1.5 hours at room temperature with loading reference protein sizes to determine corresponding size prestained protein ladder (Thermo Fisher Scientific, CAT#26616) was used in 10 kDa to 180 kDa protein size ranges. Once separation was done, proteins in the gel were transferred to Polyvinylidene Fluoride, PVDF, membrane (Biorad, CAT#162-0177) at constant voltage (25V) for 20 minutes at room temperature using a semi-dry transfer method. Then, proteins on the membrane were blocked with 5% skim milk in TBS-T solution for 1 hour at room temperature to prevent nonspecific antibody binding. Later, the primary antibody diluted in blocking solution, incubation was done at room temperature for 1.5 hours using anti-K-Ras antibody (Santa Cruz Biotechnology, CAT#sc-30) and anti-GAPDH (Santa Cruz Biotechnology, CAT#sc-25778) as loading control. Then, excess antibodies were removed from the membrane via washing with TBS-T buffer three times for 10 minutes. Then, a secondary antibody with Horse Radish Peroxidase (HRP) was used for 1-hour. The membrane was washed with TBS-T buffer three times for 10 minutes following the removal of secondary antibodies. To detect the protein of interest, the chemiluminescence technique was conducted based on enzyme-substrate interaction using HRP substrate (Biorad, CAT# 1705060) and sensing byproduct of the reaction, which emitted light. The HRP Substrate reagent was used according to the manufacturer's instructions, and the membrane was visualized by a Bio-Rad ChemiDoc imaging device.

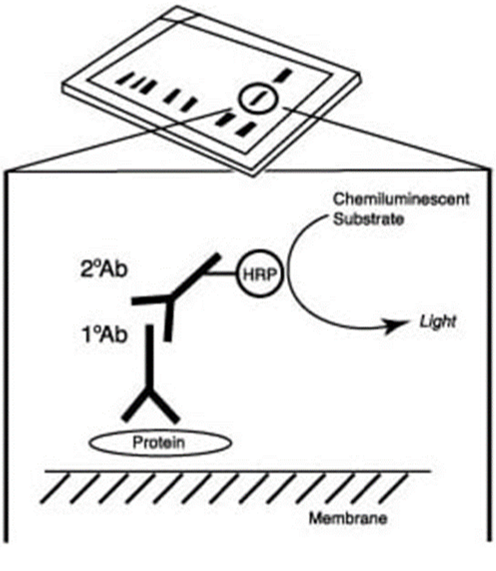

Figure 2.6: A schematic representation of Antibody detection in Western Blot.

2.8 Imaging

Imaging of the transfected cells was conducted using a Leica DMI4000 B automated inverted microscope equipped with Andor Metal Halide Light Source, DSD2 spinning disc, and Zyla 5.5 sCMOS camera with 63X magnification and 1.4 numerical aperture oil objective.

Imaging of tagged proteins was done by specific excitation and emission filters according to tags. Protein-protein interaction studies were done by separating proteins into specific groups to perform FRET analysis. Table 2.12 shows protein groups transfected to cells on glass bottom dishes. For positive FRET control, GAP43-mCherry-RGSLVPR-EGFP construct, and for negative FRET control, GAP43-EGFP and GAP43-mCherry constructs were used. For proper FRET calculations, pcDNA 3.1(-) was transfected with donor or acceptor plasmids for imaging under the same plasmid load during transfection.

Table 2.12 : Dish numbers and constructs during imaging order. “X” after Gα stands for specified Gα protein in the context of Gα11, Gα12, Gα13, Gαi1, Gαs. SDM stands for specific mutations in proteins mentioned in the “2.3.4. Site-Directed Mutagenesis” section.

Dish number	Transfected Constructs
1.	Donor (EGFP tagged construct) + pcDNA 3.1(-)
2.	Acceptor (mCherry tagged construct) + pcDNA 3.1 (-)
3.	Positive FRET control
4.	Negative FRET control
5.	K-Ras *wt* mCherry + GαX EGFP
6.	K-Ras *wt* mCherry + GαX SDM EGFP
7.	K-Ras *wt* SDM mCherry + GαX SDM EGFP
8.	K-Ras *onc* mCherry + GαX EGFP
9.	K-Ras *onc* mCherry + GαX SDM EGFP
10.	K-Ras *onc* SDM mCherry + GαX SDM EGFP

2.8.1 Imaging with Spinning Disc and FRET Technique Settings in Confocal Microscope

For the FRET technique, the 3-Cube method was performed. In the 3-Cube method, as the name indicates, three different filter cubes were used for proper FRET analysis and bleed-through subtraction. The first filter was arranged for EGFP excitation and emission called ***EGFP channel***, and the second filter was arranged for mCherry excitation and emission called ***mCherry channel***. The final filter cube was arranged for EGFP excitation and mCherry emission called ***FRET channel***. For donor bleed-through calculation, ***FRET and EGFP channels*** were used, and for acceptor bleed-through calculation, ***FRET and mCherry channels*** were used during imaging. All channels (FRET, EGFP, and mCherry) were used to obtain Net FRET images.

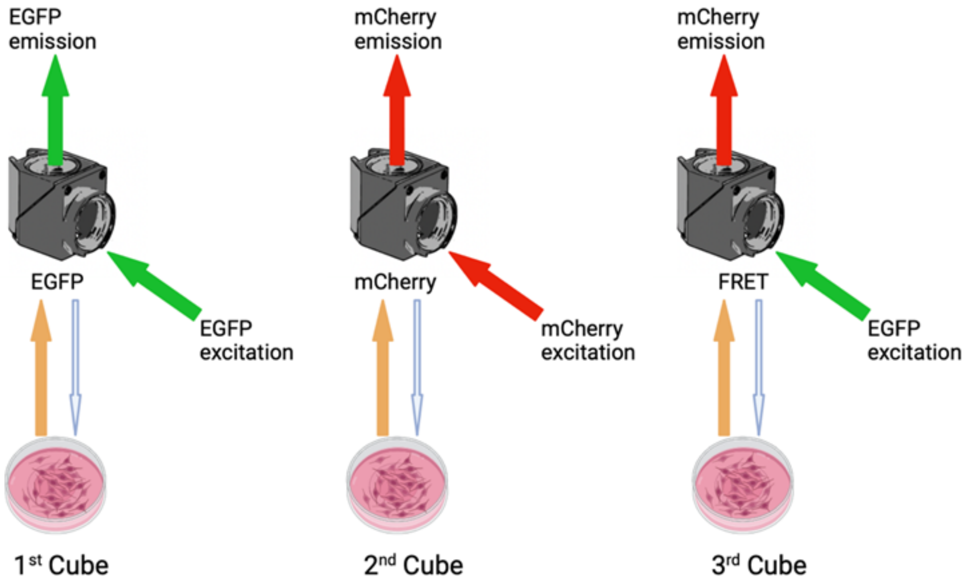

Figure 2.7: A schematic representation of the 3-Cube method.

2.9 Image Analysis

After FRET studies in the confocal microscope, images were analyzed using ImageJ version 1.53 software with PixFRET plug-in (Feige et al., 2005). With the aid of the PixFRET plug-in, bleed-through signals were eliminated. As mentioned before, during energy transfer in FRET, the fluorophore spectrum overlaps cause crosstalk between signals, eventually leading to misinterpretation of FRET results. The PixFRET plug-in eliminates donor and acceptor spectral bleed-through from images, preventing misinterpretation. Firstly, to eliminate donor spectral bleed-through, two image stacks that include both FRET and EGFP channels were analyzed in the algorithm; similarly, two image stacks that have FRET and mCherry channels were analyzed in the algorithm of plug-in to eliminate acceptor spectral bleed-through. After these two analyses, the algorithm calculated different equations according to pixel intensity values in the images, and the fittest equation was picked to further FRET analysis, which included three image stacks from FRET, EGFP, and mCherry channels and values were normalized for calculating Net FRET efficiencies. For each condition, approximately 40 images and 100 cells with detectable net FRET signals were analyzed for FRET efficiency calculations.

2.10 Statistical Analysis

In this study, independently replicated experiments' statistical analysis and their graphical representative figures were conducted in GraphPad Prism 9.5.0 version. A T-test was performed to compare mean differences between two groups in one condition. One-way ANOVA was used to analyze mean differences between more than two groups in one condition. Mean ± standard error of the mean (SEM) was used to represent statistical results, and p values less than 0.05, $p<0.05$, were considered statistically significantly different. In statistically significant results, "*" was denoted for $p<0.05$, "**" was denoted for $p<0.01$, "***" was denoted for $p<0.001$, and "****" was denoted for $p<0.0001$.

CHAPTER 3

RESULTS

3.1 Dimerization Interface Simulations

According to the literature, K-Ras dimerization occurs on either α or β interfaces. For α interface dimerization, K-Ras dimerizes through α3 and α4 helical interfaces, and there are hot spot amino acids identified as directly playing a role in this dimerization through hydrogen bonding and salt bridges such as amino acid Glu98 interacts with Arg97 and Lys101 while Arg102 interacts with Asp105 and Glu107 (Muratcioglu et al., 2020). Figure 3.1 shows the α-helical dimerization interface, and in this study, residues corresponding to this dimerization interface are investigated to test possible interactions between K-Ras and Gα proteins.

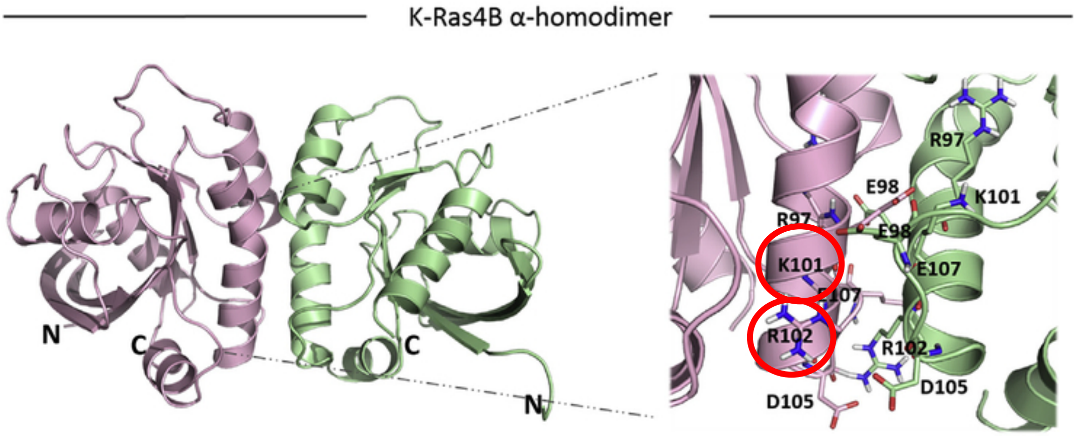

Figure 3.1: K-Ras4B α-homodimer and hot spot residues. Adapted from Muratcioglu, 2020.

All Gα proteins used in this study were aligned to K-Ras protein according to 3D structures via Chimera MatchMaker plug-in. These structural alignments were further used to understand the possible interaction interface between them. Figure

3.2 shows Gα11, Gα12, Gα13, Gαi1, and Gαs proteins structural alignments with K-Ras protein. The 3D structures were experimentally determined and submitted to the Protein Data Bank (PDB). All these structures were resolved either by X-Ray Diffraction or Electron Microscopy method. Except for Gα12, all other proteins are originated from *Homo sapiens*. Gα12 is *Mus musculus* origin in its only resolved structure.

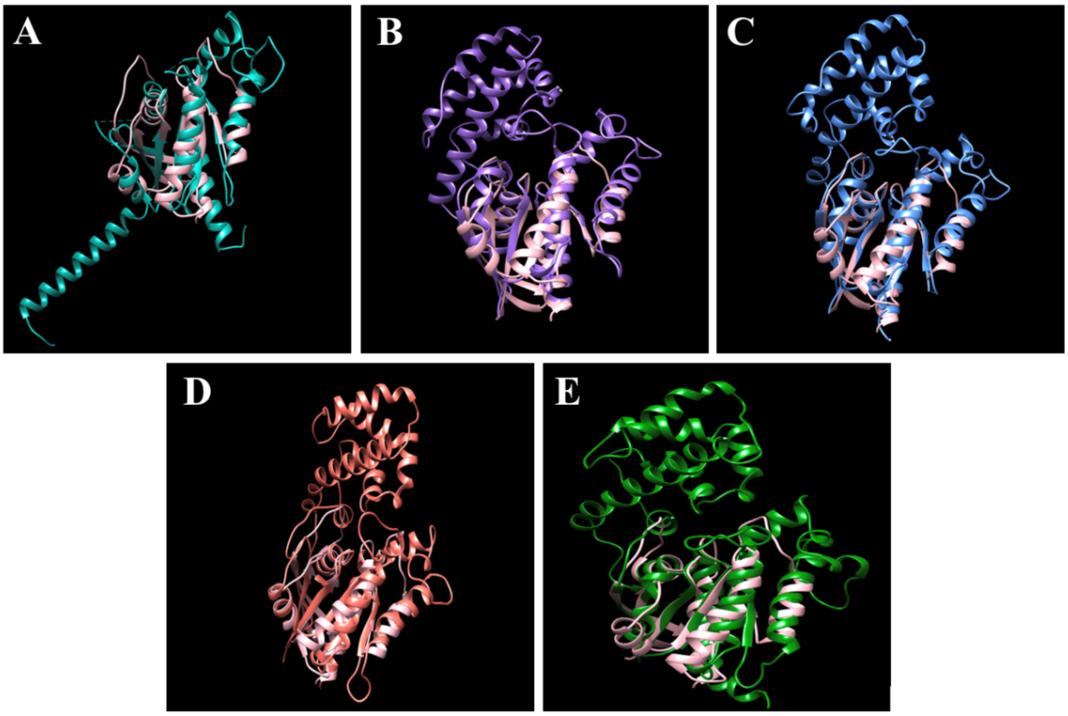

Figure 3.2: K-Ras and Gα proteins 3D protein structural alignments on Chimera. (A) K-Ras - Gα11 alignment. (B) K-Ras - Gα12 alignment. (C) K-Ras - Gα13 alignment. (D) K-Ras - Gαi1 alignment. (E) K-Ras - Gαs alignment.

K-Ras structure and Gα proteins were aligned at their G-domains since this region is functionally homologous (hydrolyze GTP to GDP). K-Ras α-homodimer interface corresponding amino acids on Gα proteins were identified after the structural alignment. While some Gα proteins share similar amino acids with K-Ras, others showed variations in this region. Comparison of hetero dimerization of Gα proteins and K-Ras proteins was analyzed considering these similarities. Mainly for the Gα proteins that showed significant variability in this region, SDM studies were carried out to mimic K-Ras dimerization interface residues in order to check if these residues would be enough to increase dimerization.

3.2 Construction of K-Ras *wt*/K-Ras *onc* coding sequences in pcDNA3.1(-)

The coding sequence of K-Ras *onc* was gifted by Assoc. Prof. Dr. Kwang-Jin Cho, Wright State University, USA. Firstly, the K-Ras *onc* coding sequence was amplified with NheI and BamHI restriction sequence containing primers to insert into pcDNA 3.1 (-). Figure 3.3 and Figure 3.4 below show the K-Ras coding sequence and its desired ligation region flanked by selected restriction digestion sites in the pcDNA 3.1(-) vector.

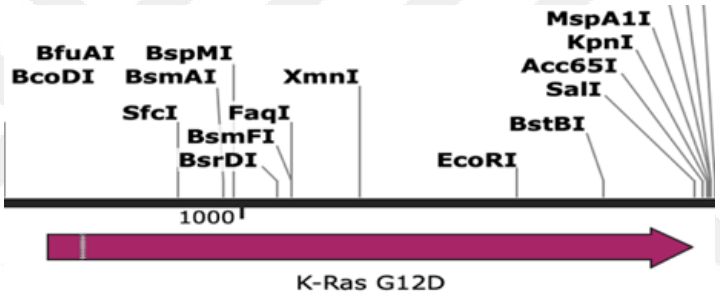

Figure 3.3: Coding sequence of K-Ras G12D gifted from Assoc. Prof. Dr. Kwang-Jin Cho.

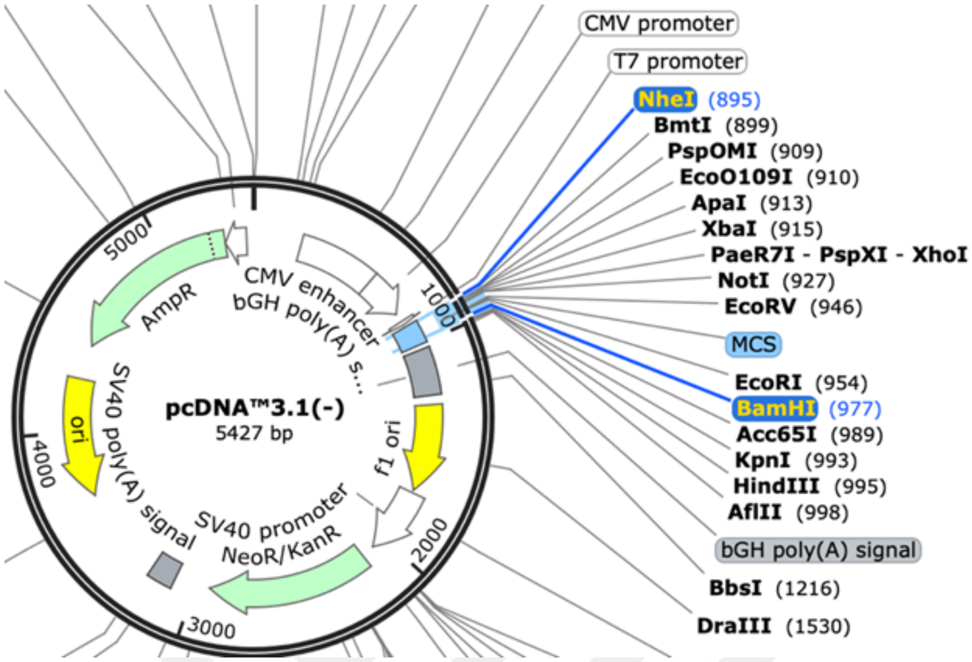

Figure 3.4: Insertion sites of K-Ras *onc* to pcDNA 3.1(-), NheI and BamHI.

PCR for amplification of coding sequence K-Ras *onc* was performed, and PCR products were purified using a kit to get rid of contaminants from the reaction. Then, 2 µL PCR product was loaded on 0.8% Agarose gel to confirm the amplification at the desired size, which is 567 bp length. Figure 3.5 shows amplified PCR products of K-Ras *onc* with determined restriction digestion sites.

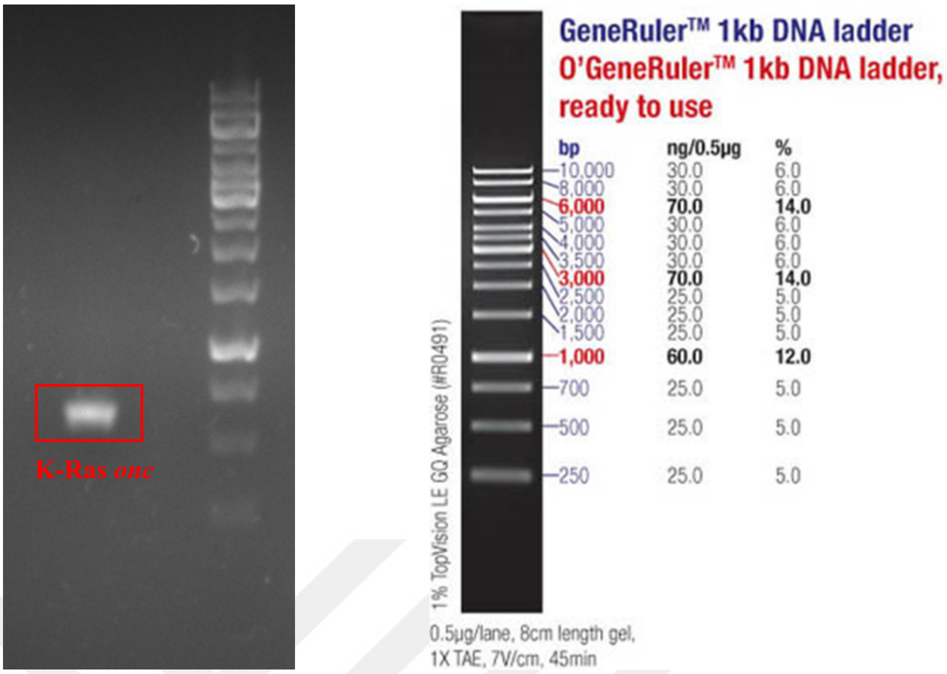

(A) **(B)**

Figure 3.5: PCR product of K-Ras *onc* on agarose gel. (A) Amplified K-Ras *onc* 567 bp. (B) GeneRuler 1kb DNA ladder.

After this confirmation, PCR product K-Ras *onc* and pcDNA 3.1(-) vector were cut with NheI and BamHI. Then, PCR purification was applied to eliminate the restriction digestion enzymes before ligation. Then, K-Ras *onc* was ligated to pcDNA 3.1(-) mammalian expression vector. Control restriction digestion was performed with these two restriction enzymes to confirm if ligation was successful, and the reaction was loaded on 0.8% agarose gel for size confirmation. The expected K-Ras *onc* sequence size was 567 bp, and the pcDNA 3.1(-) vector was 5427 bp. Figure 3.6 shows digested vector pcDNA 3.1(-) that drops its K-RAS *onc* gene at the size between 500-700 bp, and according to the DNA ladder, digestion control suggests the success of ligation.

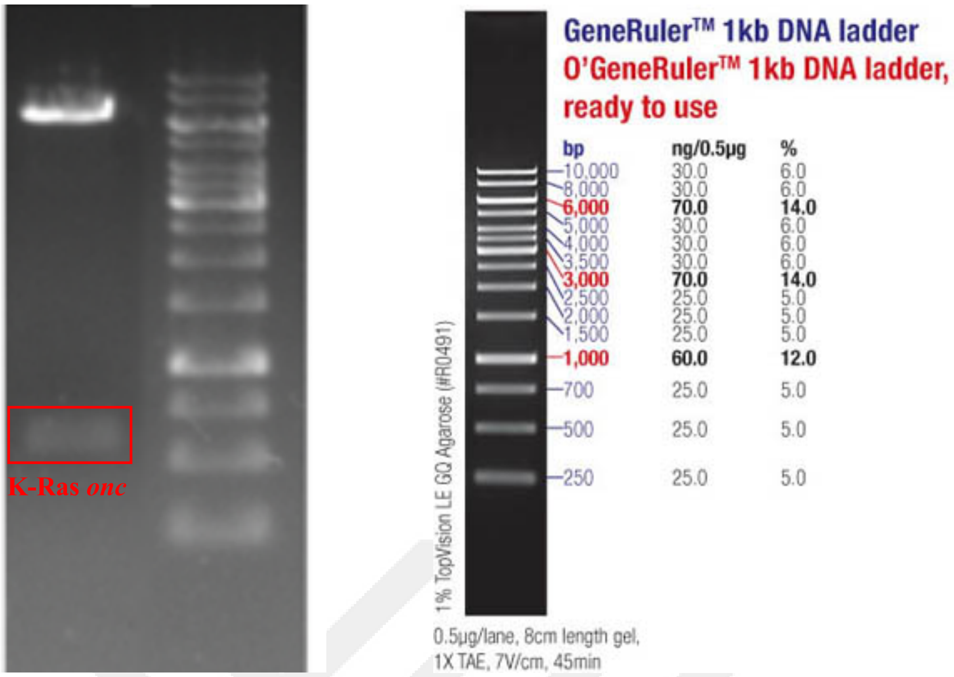

(A) **(B)**

Figure 3.6: Control restriction with NheI and BamHI of K-Ras *onc* in pcDNA 3.1(-) on agarose gel. (A) Digested K-Ras *onc* 567 bp. (B) GeneRuler 1kb DNA ladder.

Once K-Ras *onc* in pcDNA 3.1(-) construct was obtained, it was mutated to K-Ras *wt* form via site-directed mutagenesis method. Using designed primers, PCR reaction, and subsequent experiments were carried out and sent to sequencing to confirm the mutation. K-Ras *onc* form has aspartic acid (D) with GAT codon at the 12th position instead of glycine (G). After mutagenesis, this amino acid is converted to glycine using the GGT codon, generating the K-Ras *wt* form. Figure 3.7 shows both forms of the K-Ras sequences, and the mutation of D(GAT) to G(GGT) was confirmed after sequencing. Thus, K-Ras *wt* in pcDNA 3.1(-) was obtained.

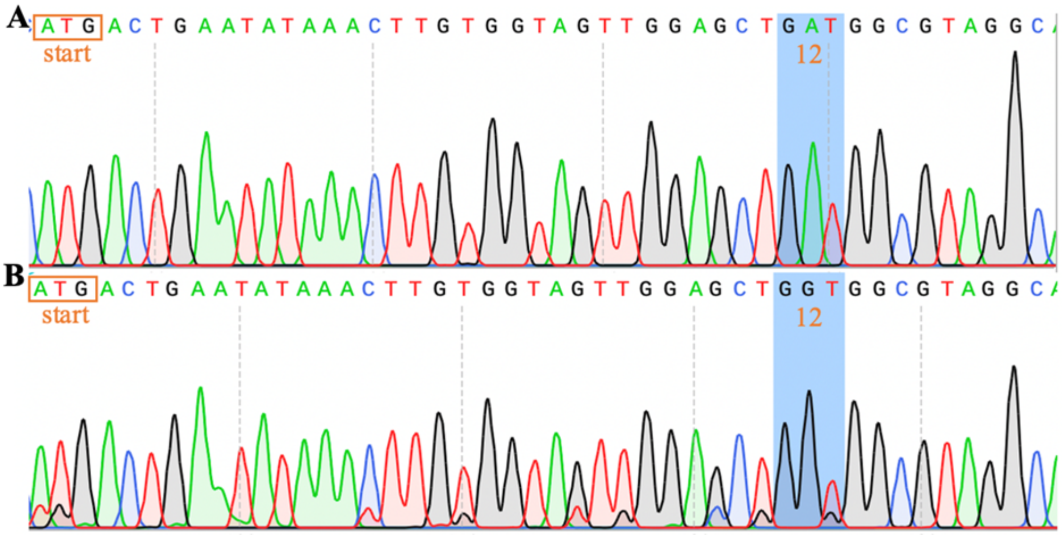

Figure 3.7: Sanger sequencing results of K-Ras *wt* and K-Ras *onc*. (A) K-Ras *onc* D12 sequence. (B) K-Ras *wt* G12 sequence.

3.3 Labeling Proteins with EGFP/mCherry via PCR Integration Method

K-Ras *wt* and K-Ras *onc* proteins were labeled with fluorophores EGFP and mCherry in the Switch II loop at 62nd and 63rd amino acids. For this integration, the first PCR was performed to amplify fluorophores with flanking regions at the end of genes, which were complementary to K-Ras before and after the 62nd amino acid, and fluorophores stop codons were deleted. These PCR products, called Mega primers, were loaded on 0.8% agarose gel and isolated from it. Figure 3.8 shows PCR products of EGFP, 717 bp, mCherry, 708 bp, and additional flanking regions in expected size according to DNA Marker.

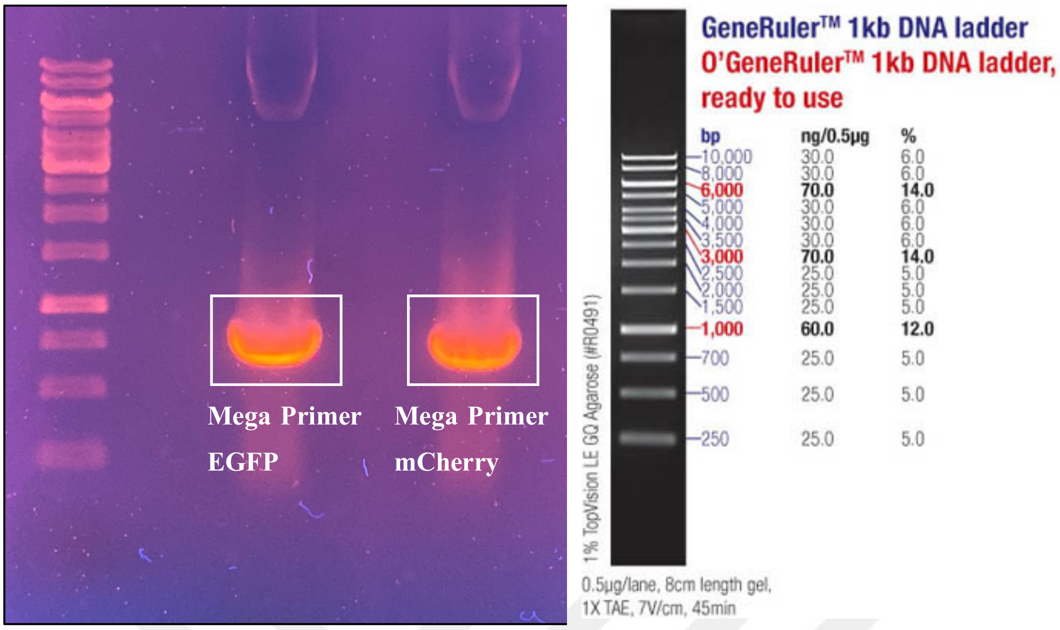

(A) **(B)**

Figure 3.8: The first PCR products on agarose gel from PCR integration method to tag K-Ras on 62nd position. (A) Amplified first PCR products, EGFP and mCherry. (B) GeneRuler 1kb DNA ladder.

Extracted PCR products were used as mega primers for tagging K-Ras *wt* and K-Ras *onc*. After the second PCR, products were transformed into bacterial cells, and plasmids were isolated. Insertion of fluorescence tags was verified with control restriction digestion enzymes NheI and BamHI, where K-Ras *wt* and K-Ras *onc* genes reside. Expected sizes of tagged K-Ras genes are 567 bp and additional EGFP or mCherry lengths, which are 1285 bp and 1275 bp, respectively. Figures 3.9 and Figure 3.10 show that cut plasmid sizes are between 1000 bp and 1500 bp in the DNA marker, which suggests that the insertion of EGFP and mCherry fluorophores is successful.

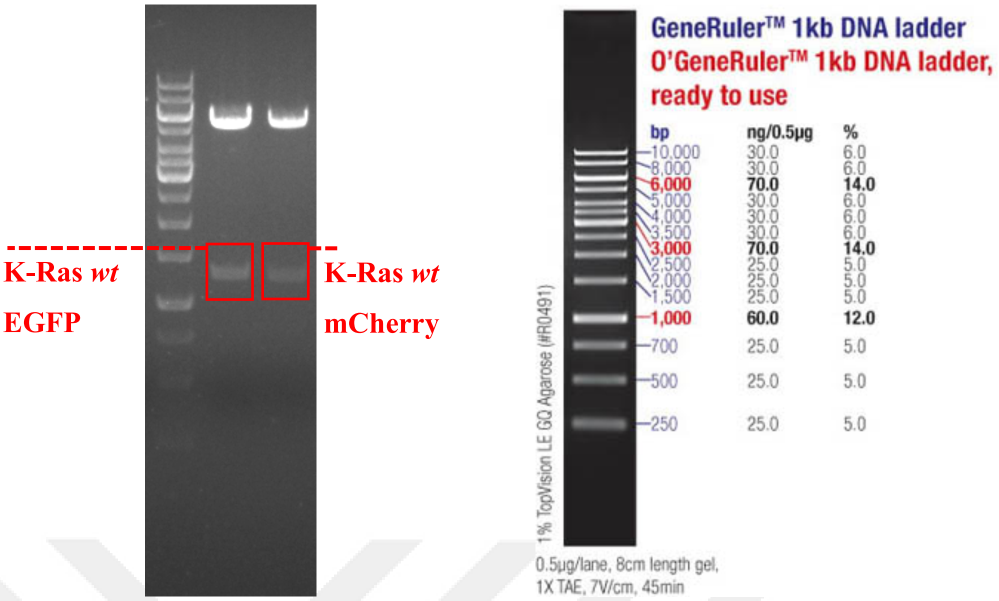

(A) **(B)**

Figure 3.9: Control restriction with NheI and BamHI, K-Ras *wt* tagged with EGFP and mCherry in pcDNA 3.1(-) on agarose gel. (A) Digested K-Ras *wt EGFP* 1285 bp, digested K-Ras *wt mCherry* 1275 bp. (B) GeneRuler 1kb DNA ladder.

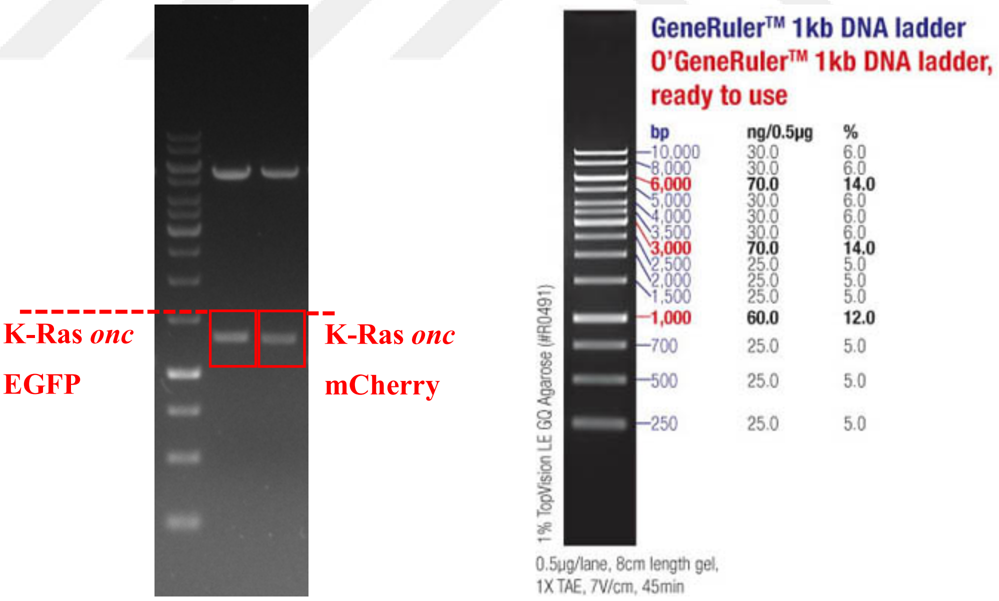

(A) **(B)**

Figure 3.10: Control restriction with NheI and BamHI, K-Ras *onc* tagged with EGFP and mCherry in pcDNA 3.1(-) on agarose gel. (A) Digested K-Ras *onc EGFP* 1285 bp, digested K-Ras *onc mCherry* 1275 bp. (B) GeneRuler 1kb DNA ladder.

3.4 Positive and Negative FRET Controls

For positive FRET control, the GAP43-mCherry-RGSLVPR-EGFP construct was used as a reference. GAP43 is a membrane protein, and it is linked to the EGFP and mCherry fluorophore with a seven amino acid linker, which are in close proximity 1-10 nm in length. Therefore, resonance energy transfer is expected between these fluorophores to calculate FRET efficiency further. On the other hand, for negative FRET control, GAP43-EGFP and GAP43-mCherry constructs were used to show when there is no interaction between proteins. GAP43 proteins do not interact on the plasma membrane; therefore, they were tagged separately with EGFP and mCherry, knowing insufficient resonance energy transfer between them. Figure 3.11 shows a schematic representation of positive and negative FRET control behavior on the plasma membrane.

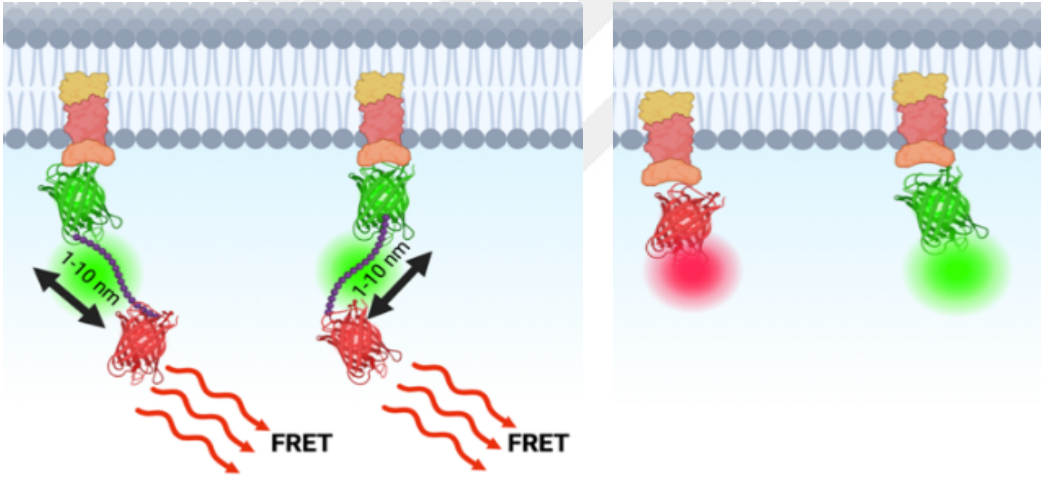

(A) **(B)**

Figure 3.11: A schematic representation of Positive and Negative FRET controls on the cell membrane. (A) Positive FRET control, GAP43-mCherry-RGSLVPR-EGFP. (B) Negative FRET control, GAP43-mCherry + GAP43-EGFP.

The PixFRET plug-in in the ImageJ program was used for efficiency analysis in the FRET technique to detect interactions between desired proteins. FRET images were analyzed in three different channels (donor only, acceptor only, and FRET) to determine the net FRET value and calculate the bleedthrough signal. FRET efficiency analysis was conducted by examining approximately 100 different cells. Regions of interest (ROI) were drawn over the plasma membrane where the signal was expected to be present, and histograms providing the pixel counts in these ROI areas were obtained. Subsequently, pixel counts in % FRET efficiency intervals and total FRET pixel counts were determined using these histograms.

The FRET images were color-coded based on pixel intensity color channels called 5 Ramps to distinguish differences between pixel intensities on FRET regions. These FRET efficiencies range from 0.1-10% are represented in blue, 10-20% in green, 20-30% in yellow, 30-40% in red, and 40-50% in white color, as shown in Figure 3.12. The % FRET Efficiency images are illustrated in Figure 3.12 with their respective efficiencies.

Figure 3.12: 5 Ramps color scale on ImageJ. FRET efficiencies are represented accordingly, 0-10% blue, 10-20% green, 20-30% yellow, 30-40% red, and 40-50% white.

Figure 3.13 shows the Positive FRET control's confocal microscopy images in donor, acceptor, and FRET channels and its calculated FRET efficiency frame under a 10 µm scale bar. As expected, the same cells gave both EGFP and mCherry signals in the respective channels since these two fluorophores were linked and translated simultaneously. In the FRET channel, a signal indicates the interaction between two fluorophores to calculate FRET efficiency. According to the FRET efficiency frame, signal colors range from blue to green, indicating that FRET efficiency is around 10-15% visually.

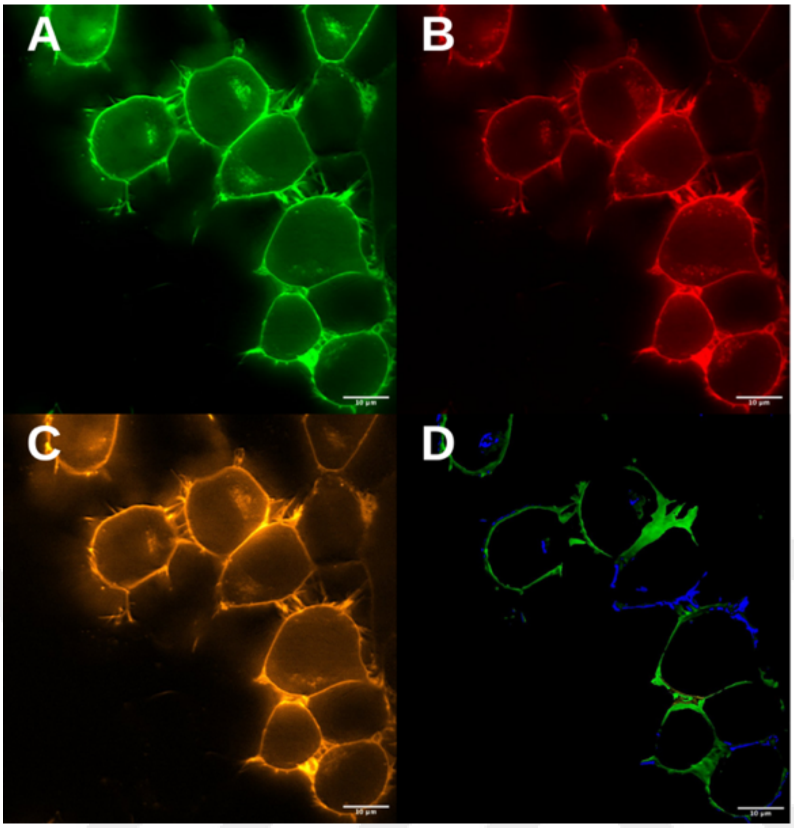

Figure 3.13: Confocal FRET images of Positive FRET control GAP43-mCherry-Linker-EGFP in live N2-a cells, 63X magnification, 10 µm scale line. (A) Image of the EGFP channel. (B) Image of the mCherry channel. (C) Image of the FRET channel. (D) Image of the FRET efficiency in color scale.

On the other hand, figure 3.14 shows Negative FRET control where fluorophores do not interact and give no signal in the FRET channel, though they give signals in both EGFP and mCherry channels. Therefore, the calculatable FRET efficiency was low and used as a non-interaction indicator.

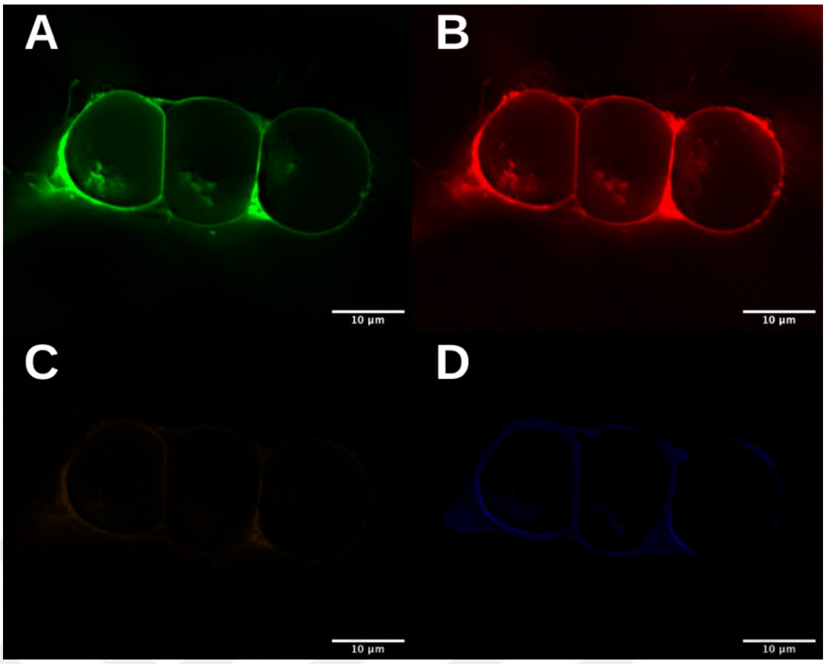

Figure 3.14: Confocal FRET images of Negative FRET control GAP43-mCherry and Gap43-EGFP in live N2-a cells, 63X magnification, 10 µm scale line. (A) Image of the EGFP channel. (B) Image of the mCherry channel. (C) Image of the FRET channel. (D) Image of the FRET efficiency in color scale.

Figure 3.15 shows the graph of calculated FRET efficiencies of positive and negative FRET controls according to their pixel intensities on the cell membrane. Positive control has 10-15% FRET efficiency on the cell membrane, while negative control has lower than 5% FRET efficiency. Calculated FRET efficiency graphs are also displayed in box plots to show cells' %FRET Efficiency means with SEM values and their statistical analysis. The positive control %FRET efficiency mean is 12.58 ±0.39,and the negative control %FRET efficiency mean is3.16±0.39.. According to T-test statistical analysis, there is a significant difference between these two FRET controls.

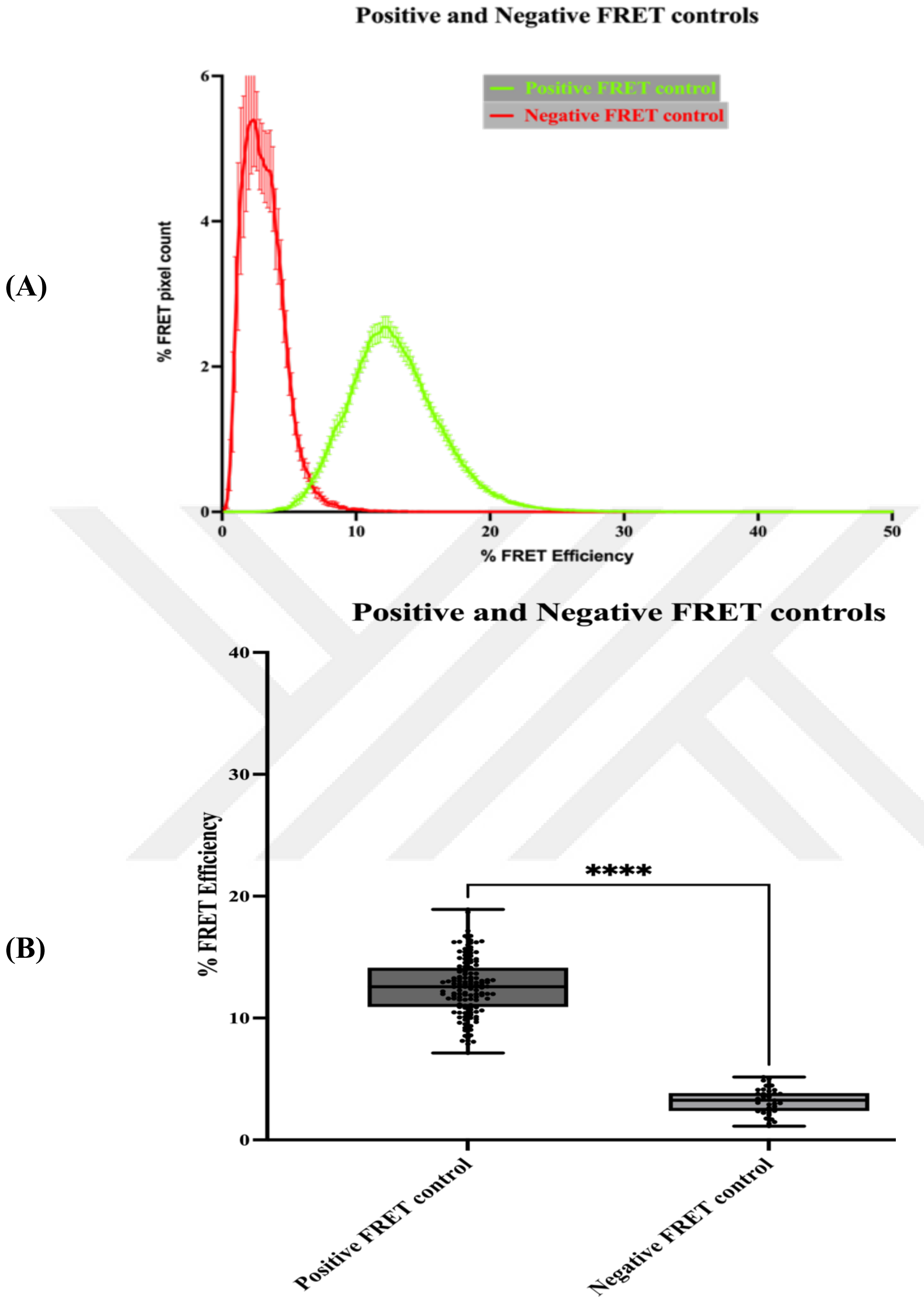

Figure 3.15: Positive and Negative FRET controls FRET efficiency in line graph and box plot. (A) FRET efficiency in line graph, FRET efficiency mean±SEM values distribution in the range. (B) FRET efficiency in box plot, all cells mean FRET Efficiency. T-test statistical analysis was performed, significance level $p<0.05$.

3.5 Localization Detection of EGFP/mCherry labeled proteins in live cells using a confocal microscope

3.5.1 Visualization of EGFP/mCherry labeled K-Ras *wt* & K-Ras *onc* proteins in Neuro2-a cells

To see the localization of EGFP and mCherry tagged K-Ras *wt* & K-Ras *onc*, constructs were transiently transfected to N2-a cells and visualized live under the confocal microscope. Figure 3.16 shows that most proteins are on the plasma membrane where K-Ras reside naturally to function.

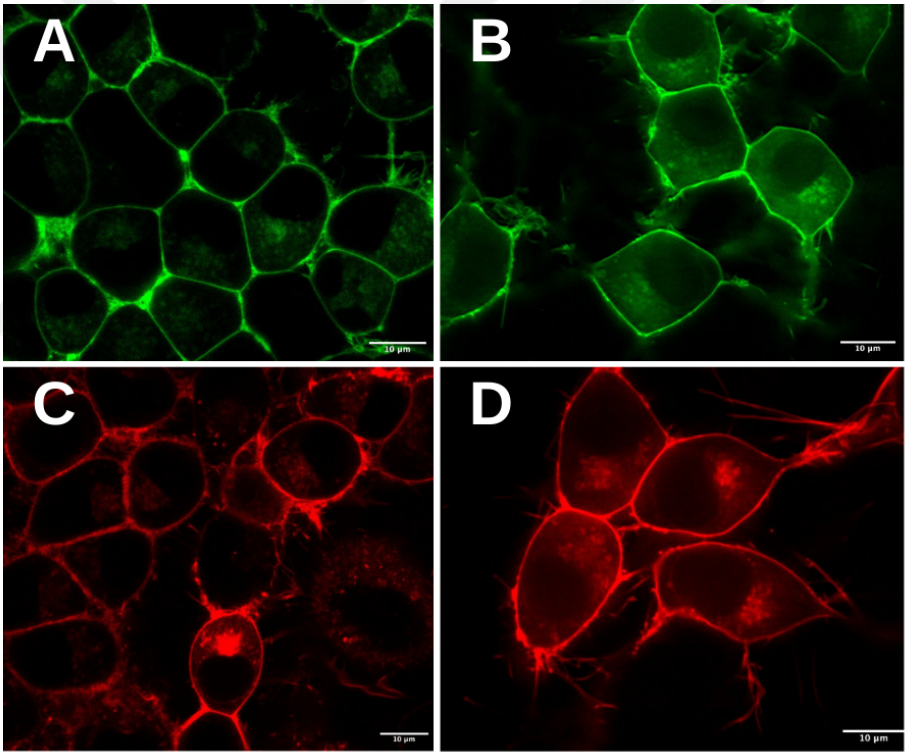

Figure 3.16: Confocal images of K-Ras *wt* & K-Ras *onc* 62nd position labeling with EGFP and mCherry in live N2-a cells, 63X magnification, 10 µm scale line. (A) Image of the of K-Ras *wt* 62nd EGFP in EGFP channel. (B) Image of the of K-Ras *onc* 62nd EGFP in EGFP channel. (C) Image of the of K-Ras *wt* 62nd mCherry in mCherry channel. (D) Image of the of K-Ras *onc* 62nd mCherry in mCherry channel.

3.5.2 Visualization of EGFP labeled Gα Proteins in Neuro2-a cells

In this study, EGFP tagged Gα Proteins were used as a donor protein in FRET technique to examine K-Ras - Gα Proteins interactions. Therefore, to check their proper functioning site on the cell, that is, on the plasma membrane, Gα11, Gα12, Gα13, Gαi, and Gαs proteins were visualized live under the confocal microscope. Representative images are shown in Figure 3.17 and used later for FRET studies.

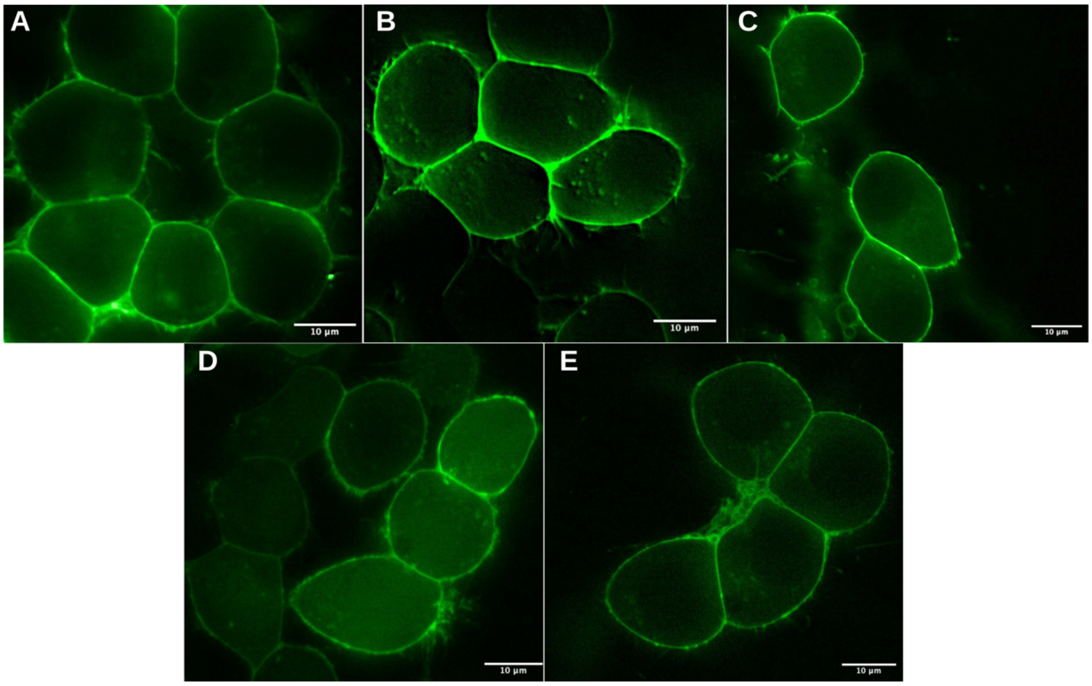

Figure 3.17: Confocal images of mutated Gαs, Gαi, Gα11, Gα12, and Gα13 in live N2-a cells, 63X magnification, 10 µm scale line. (A) Image of the of Gαs 73-85th EGFP in EGFP channel. (B) Image of the Gαi 121st EGFP in EGFP channel. (C) Image of the Gα11 246th EGFP in EGFP channel. (D) Image of the Gα12 265th EGFP in EGFP channel. (E) Image of the Gα13 215th EGFP in EGFP channel.

3.6 Interaction of K-Ras *wt*/K-Ras *onc* in terms of homodimerization detection with FRET technique & analysis

In recent years, studies have shown that K-Ras dimerizes or oligomerizes, on the cell membrane and continues signal transduction, using different techniques (Güldenhaupt *et al.*, 2012; Nan *et al.*, 2015). In this study, the FRET technique was used to show the interaction under different experimental setups, such as labeling proteins with different fluorophores. Figure 3.18 shows the interaction between K-Ras *wt* - K-Ras *wt* in terms of their homodimerization. K-Ras constructs tagged on their 62nd position with EGFP or mCherry were used together in the double transient transfection to N2-a cells, and signals were collected for FRET imaging. In accordance with the literature, a significant signal was obtained in the FRET channel, indicating the homodimerization and FRET efficiency was calculated.

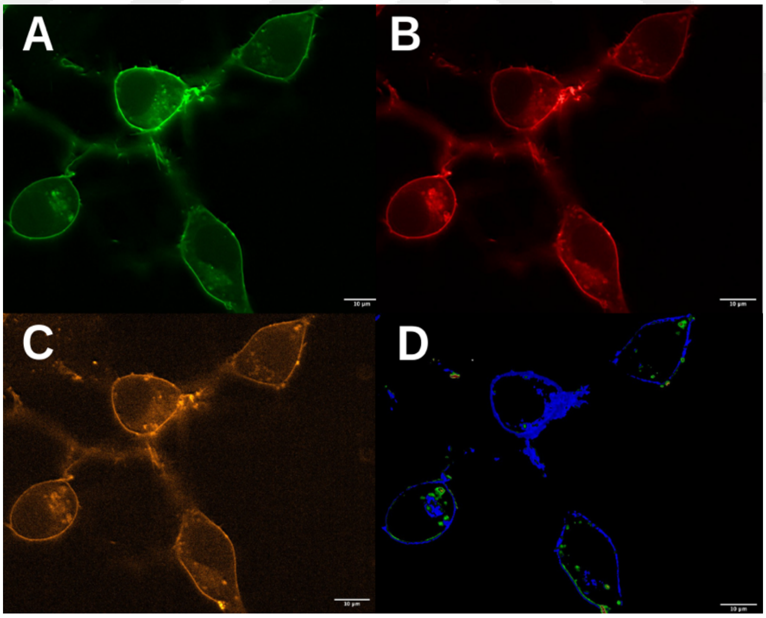

Figure 3.18: Confocal FRET images of K-Ras *wt* mCherry - K-Ras *wt* EGFP in live N2-a cells, 63X magnification, 10 µm scale line. (A) Image of the EGFP channel. (B) Image of the mCherry channel. (C) Image of the FRET channel. (D) Image of the FRET efficiency in color scale.

The distribution of calculated FRET efficiencies from the cells is shown in the line graph below Figure 3.19A. The pink line belongs to the %FRET efficiency of K-Ras *wt* - K-Ras *wt* homodimerization in addition to positive and negative FRET controls. Even though K-Ras *wt* homodimerization and positive control's peak points are similar, K-Ras *wt* homodimerization shows a broader distribution in the FRET efficiencies compared to positive control due to the dynamic interaction of the constructs on the plasma membrane. In contrast, positive FRET control might correspond to more restricted dynamics due to the linker between fluorophores. The means of the %FRET efficiencies are shown in the box plots below Figure 3.19 B. As can be seen the K-Ras *wt* - K-Ras *wt* interaction is significantly different from the negative control, and there is no significant difference between K-Ras *wt* - K-Ras *wt* interaction and the positive FRET construct according to One Way ANOVA statistical analysis, and this indicates homodimerization of K-Ras.

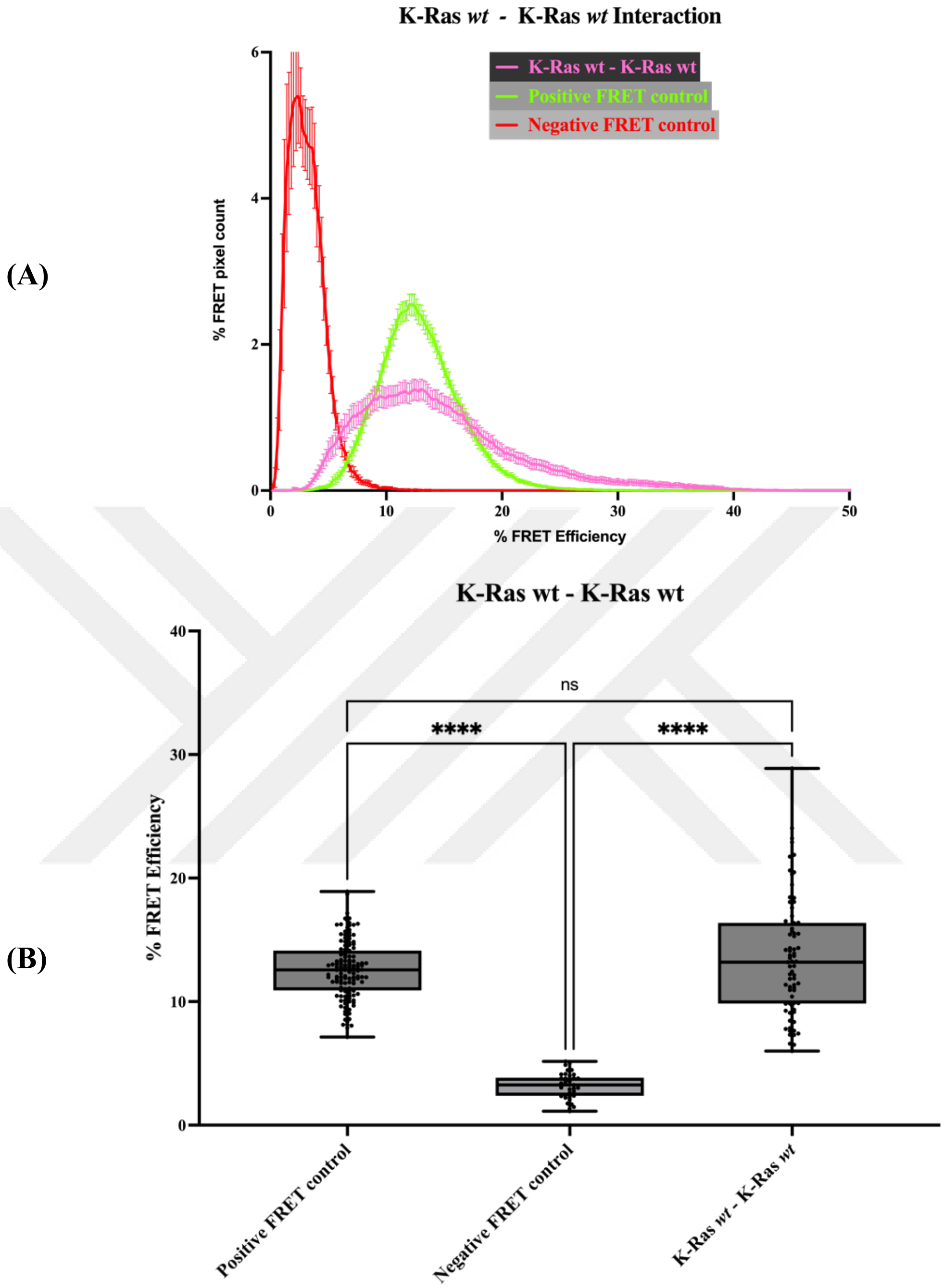

Figure 3.19: K-Ras *wt* - K-Ras *wt* interaction FRET efficiency in line graph and box plot. (A) FRET efficiency in the line graph, FRET efficiency mean±SEM values distribution in the range. (B) FRET efficiency in the box plot, all cells mean FRET Efficiency. T-test statistical analysis was performed, significance level $p<0.05$.

Similarly, with K-Ras *wt* - K-Ras *wt* interaction, K-Ras *onc* - K-Ras *onc* interaction was examined with FRET technique. Therefore, the interaction of the oncogenic form of K-Ras protein on K-Ras - K-Ras was tested. Figure 3.20 shows the interaction study of K-Ras *onc* - K-Ras *onc* proteins tagged at 62nd position with EGFP or mCherry. FRET signal was obtained in the FRET channel, and %FRET efficiency was calculated.

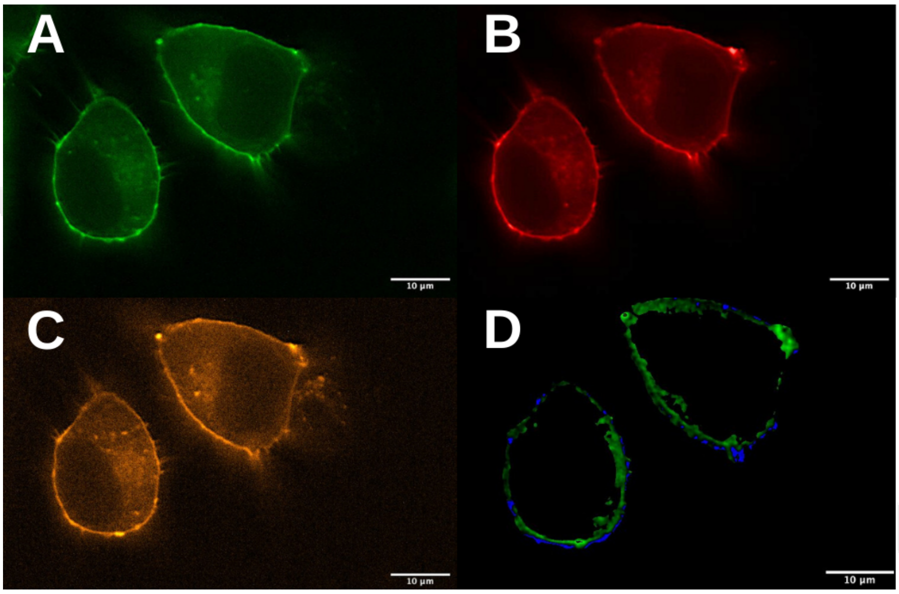

Figure 3.20: Confocal FRET images of K-Ras *onc* mCherry - K-Ras *onc* EGFP in live N2-a cells, 63X magnification, 10 µm scale line. (A) Image of the EGFP channel. (B) Image of the mCherry channel. (C) Image of the FRET channel. (D) Image of the FRET efficiency in color scale.

Compared to the positive control in Figure 3.21A, K-Ras *onc* - K-Ras *onc* shows a similar trend in its distribution to K-Ras *wt* - K-Ras *wt* efficiency distribution in protein interaction dynamics. Their average %FRET efficiencies were represented with the box plot, and there is no significant difference between K-Ras *onc* - K-Ras *onc* and positive control. However, it is highly significant compared to negative control under the One-Way ANOVA test. Therefore, results suggest K-Ras *onc* - K-Ras *onc* proteins homodimerize under these conditions.

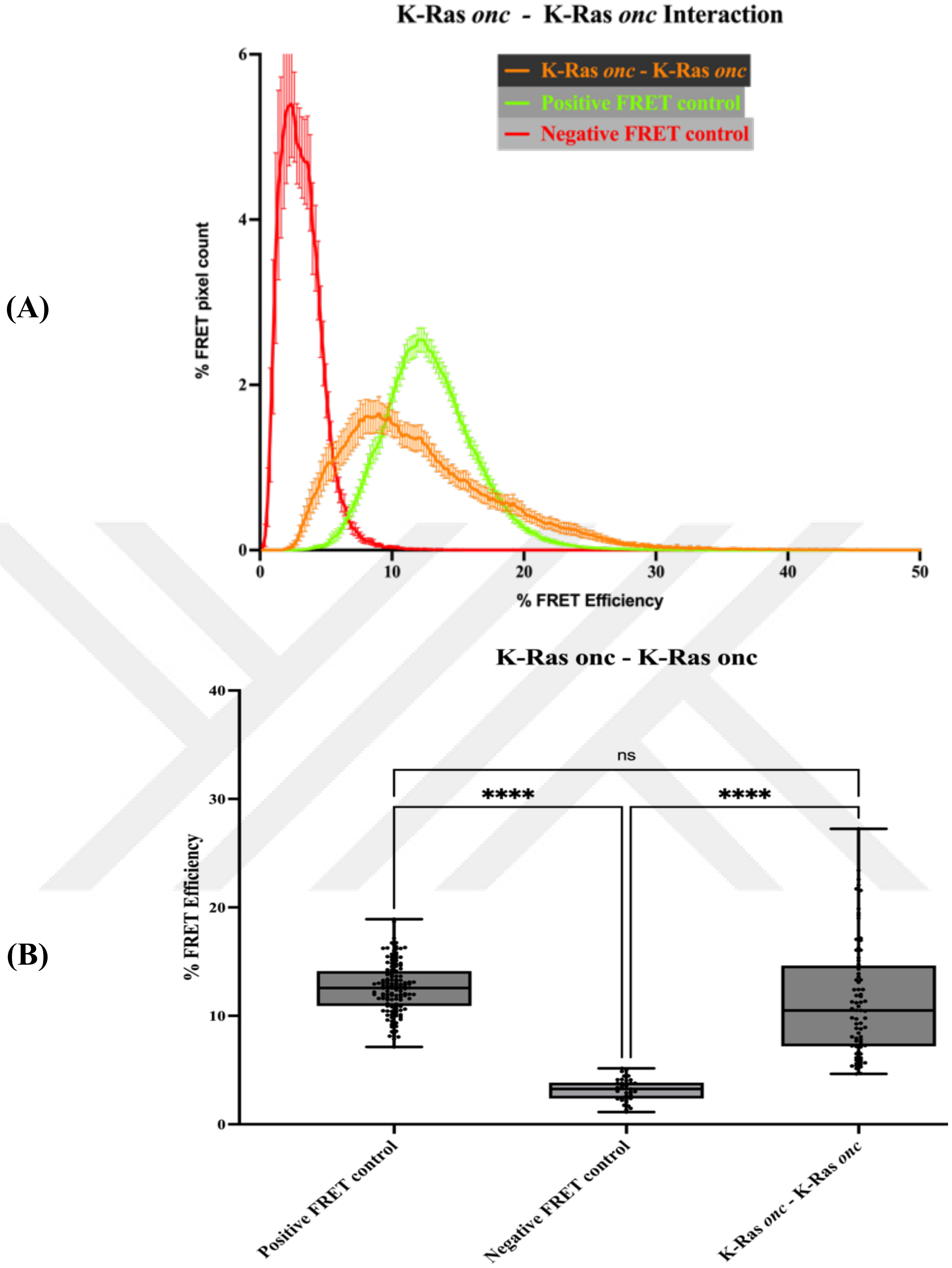

Figure 3.21: K-Ras *onc* - K-Ras *onc* interaction FRET efficiency in line graph and box plot. (A) FRET efficiency in the line graph, FRET efficiency mean±SEM values distribution in the range. (B) FRET efficiency in the box plot, all cells mean FRET Efficiency. T-test statistical analysis was performed, significance level $p<0.05$.

In addition to individual visualization and analysis, K-Ras *wt* - K-Ras *wt* and K-Ras *onc* - K-Ras *onc* interactions, were tested to see whether there are any differences in these interactions. Figure 3.22A shows their complete distribution in FRET efficiencies. As it is seen, the %FRET efficiency showed a similar, broad distribution. Besides, their distribution means were shown in a box plot, and according to T-test analysis, there is no significant difference between the interaction of K-Ras *wt* - K-Ras *wt* and K-Ras *onc* - K-Ras *onc* in Figure 3.22B.

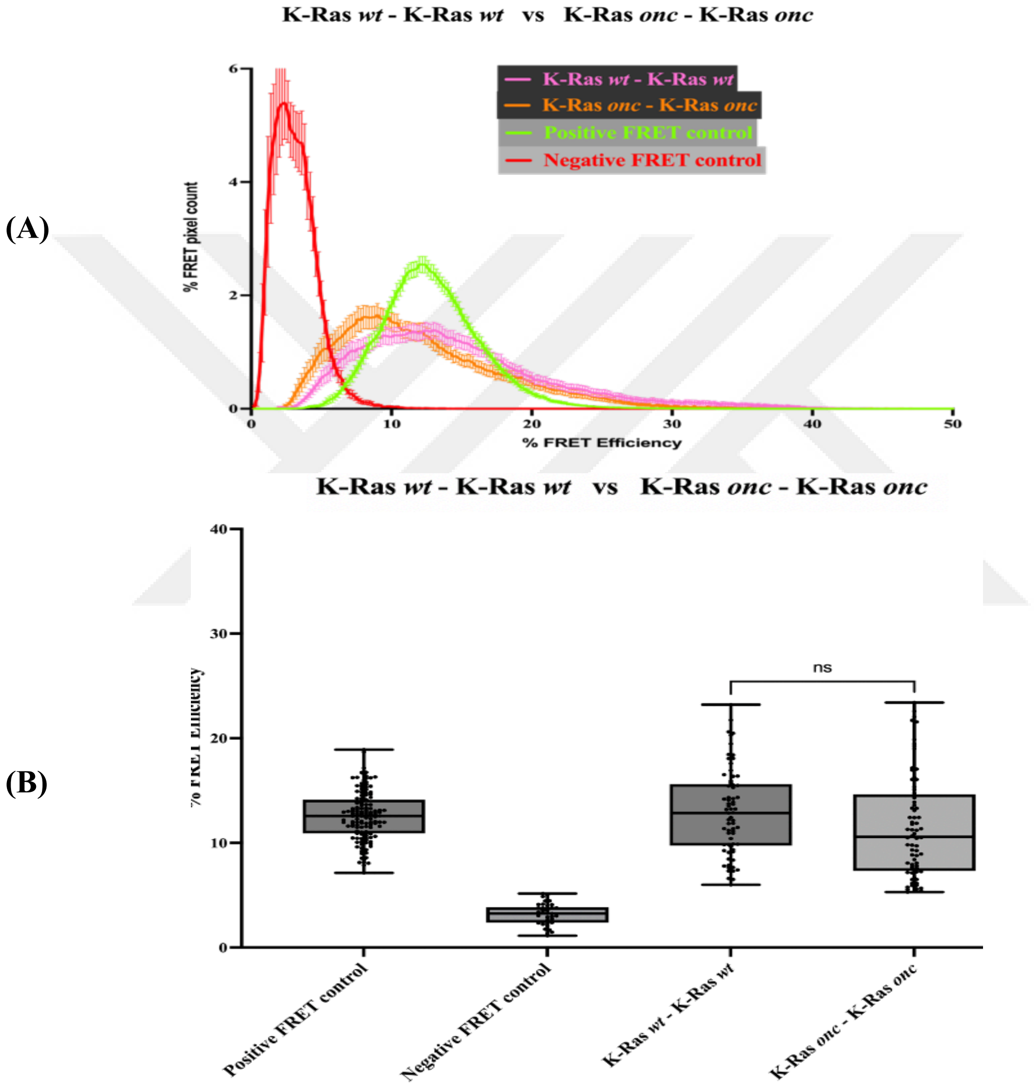

Figure 3.22: K-Ras *wt* - K-Ras *wt* interaction vs K-Ras *onc* - K-Ras *onc* interaction FRET efficiency in line graph and box plot. (A) FRET efficiency in the line graph, FRET efficiency mean±SEM values distribution in the range. (B) FRET efficiency in the box plot, all cells mean FRET Efficiency. T-test statistical analysis was performed, significance level $p<0.05$.

3.7 Interaction of K-Ras *wt*/K-Ras *onc* – Gαs Proteins heterodimerization detection with FRET technique & analysis

After homodimerization studies of K-Ras proteins, heterodimerization of K-Ras with its structural homologs was tested, and K-Ras *wt* – Gαs possible interaction was examined with the FRET technique. 62nd position mCherry tagged K-Ras *wt* was used as an acceptor and 73-85th position EGFP tagged Gαs was used as a donor. As seen in the donor and acceptor channels, K-Ras and Gαs proteins were expressed in N2-a cells. Detectable signal on the FRET channel suggests a possible interaction between K-Ras *wt* – Gαs in Figure 3.23.

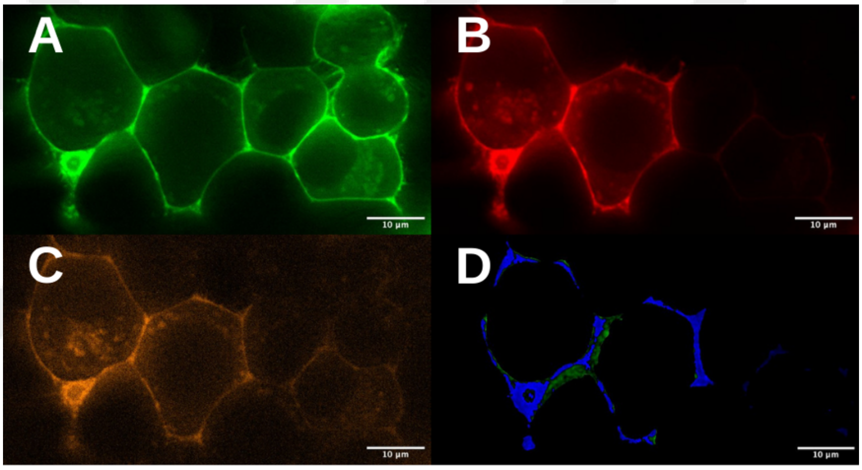

Figure 3.23: Confocal FRET images of K-Ras *wt* mCherry - Gαs EGFP in live N2-a cells, 63X magnification, 10 µm scale line. (A) Image of the EGFP channel. (B) Image of the mCherry channel. (C) Image of the FRET channel. (D) Image of the FRET efficiency in color scale.

After calculating K-Ras *wt* – Gαs FRET efficiencies, data was compared with K-Ras *wt* – K-Ras *wt* interaction studies. According to the line graph in Figure 3.24A, the K-Ras *wt* – Gαs interaction shows less dynamic nature than the K-Ras *wt* – K-Ras *wt* interaction, indicated by the narrow distribution of the K-Ras *wt* – Gαs interaction graph. When their mean FRET efficiencies values are calculated, it is seen in Figure 3.24B that K-Ras *wt* – Gαs interaction is significantly different from negative FRET control, which implies the interaction between them. However, this interaction mean is lower than the K-Ras *wt* – K-Ras *wt* interaction mean.

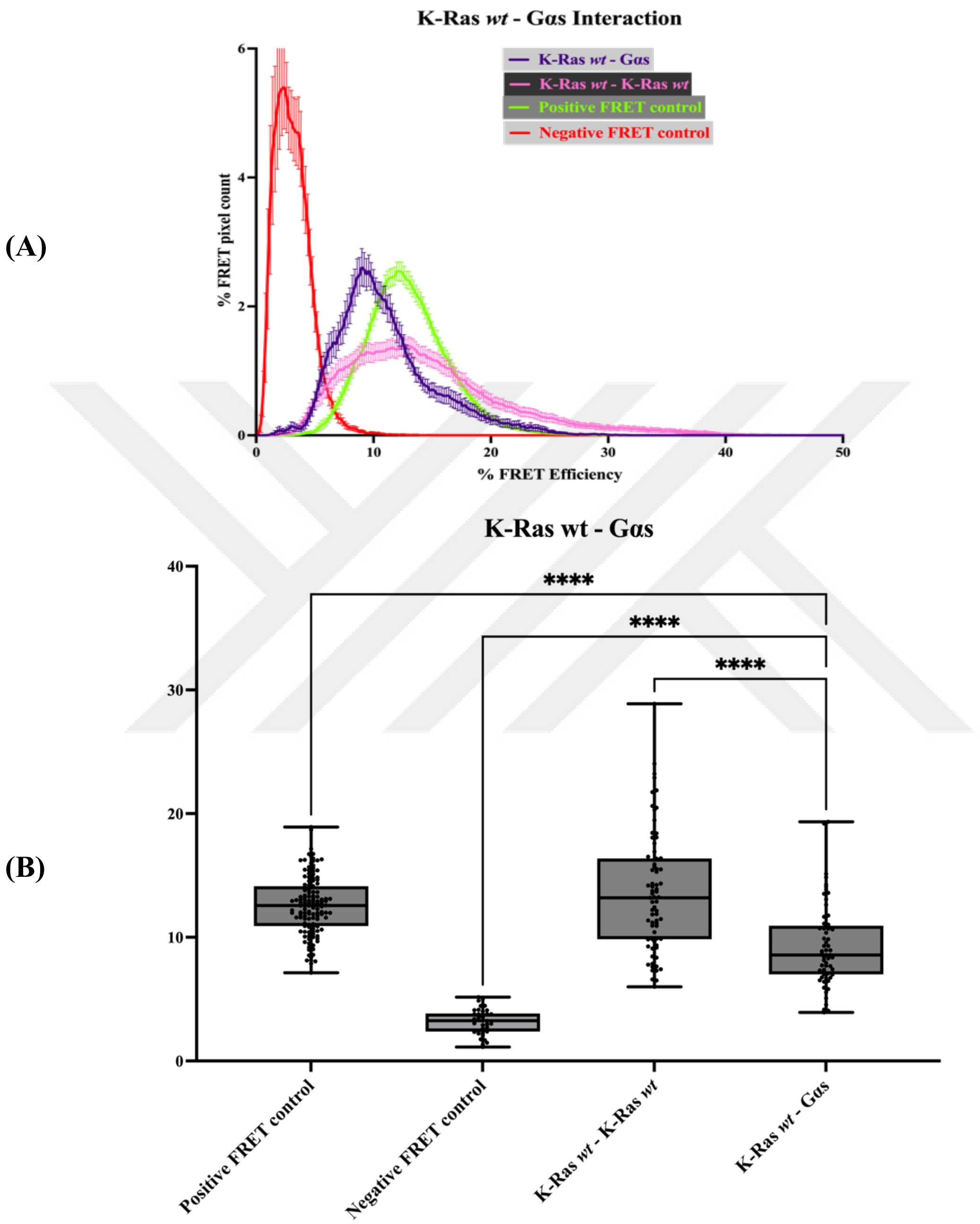

Figure 3.24: K-Ras *wt* – Gαs interaction FRET efficiency in line graph and box plot. (A) FRET efficiency in line graph, FRET efficiency mean±SEM values distribution in the range. (B) FRET efficiency in box plot, all cells mean FRET Efficiency. T-test statistical analysis was performed, significance level $p<0.05$.

In addition to K-Ras *wt* – Gαs interaction, K-Ras *onc* – Gαs interaction was studied to test if there is any interaction with the oncogenic form of K-Ras. Again, K-Ras was used as an acceptor pair while Gαs was the donor. FRET signal was obtained in the FRET channel of Figure 3.25 after transfection of both constructs, and FRET efficiency was calculated.

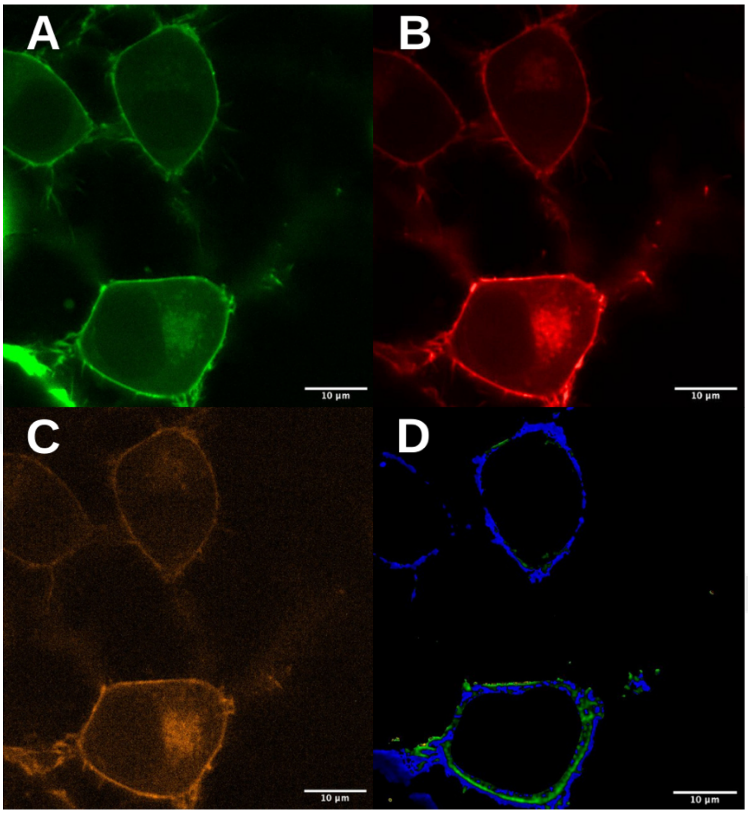

Figure 3.25: Confocal FRET images of K-Ras *onc* mCherry - Gαs EGFP in live N2-a cells, 63X magnification, 10 µm scale line. (A) Image of the EGFP channel. (B) Image of the mCherry channel. (C) Image of the FRET channel. (D) Image of the FRET efficiency in color scale.

The calculated FRET efficiency of K-Ras *onc* – Gαs was compared with K-Ras *onc* – K-Ras *onc* interaction efficiencies. As a result, similar to K-Ras *wt* – Gαs heterodimerization, it shows a narrow distribution in pixel intensities of cells compared to K-Ras homodimerization, shown in Figure 3.26A. Compared to the negative control, K-Ras *onc* – Gαs interaction is significantly higher in their mean results in Figure 3.26B. However, K-Ras *onc* – Gαs interaction FRET efficiency is lower than K-Ras homodimerization.

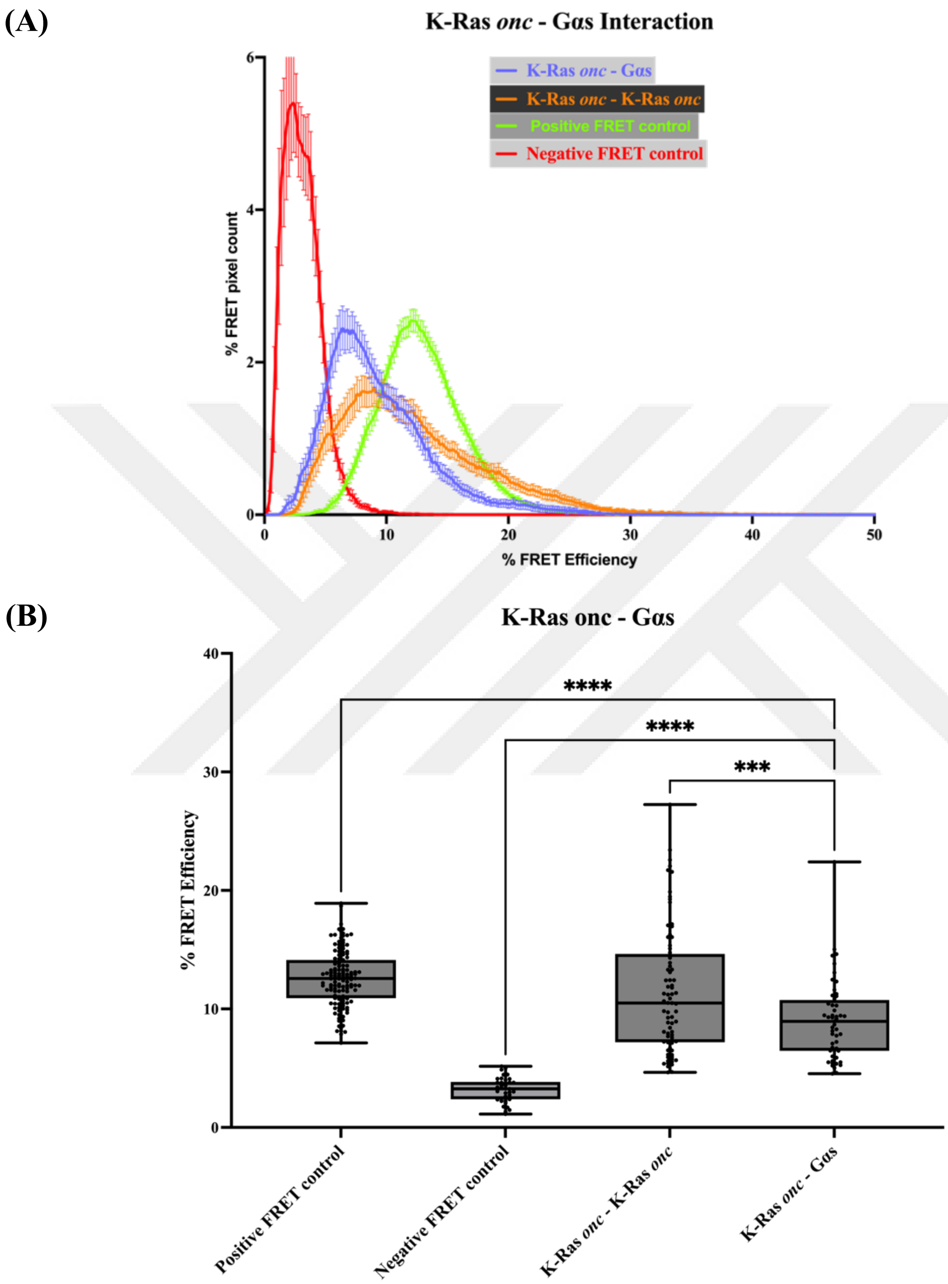

Figure 3.26: K-Ras *onc* – Gαs interaction FRET efficiency in line graph and box plot. (A) FRET efficiency in line graph, FRET efficiency mean±SEM values distribution in the range. (B) FRET efficiency in box plot, all cells mean FRET Efficiency. T-test statistical analysis was performed, significance level $p<0.05$.

3.8 Interaction of K-Ras *wt*/K-Ras *onc* – Gαi1 Proteins heterodimerization detection with FRET technique & analysis

Another Gα protein, Gαi1, was tested for K-Ras *wt* interaction. 62nd mCherry tagged K-Ras *wt* was used as an acceptor in FRET pairs, while 121st EGFP tagged Gαi1 was a donor for the technique. The interaction was observed on the FRET channel in Figure 3.27, and the efficiency of this interaction was calculated.

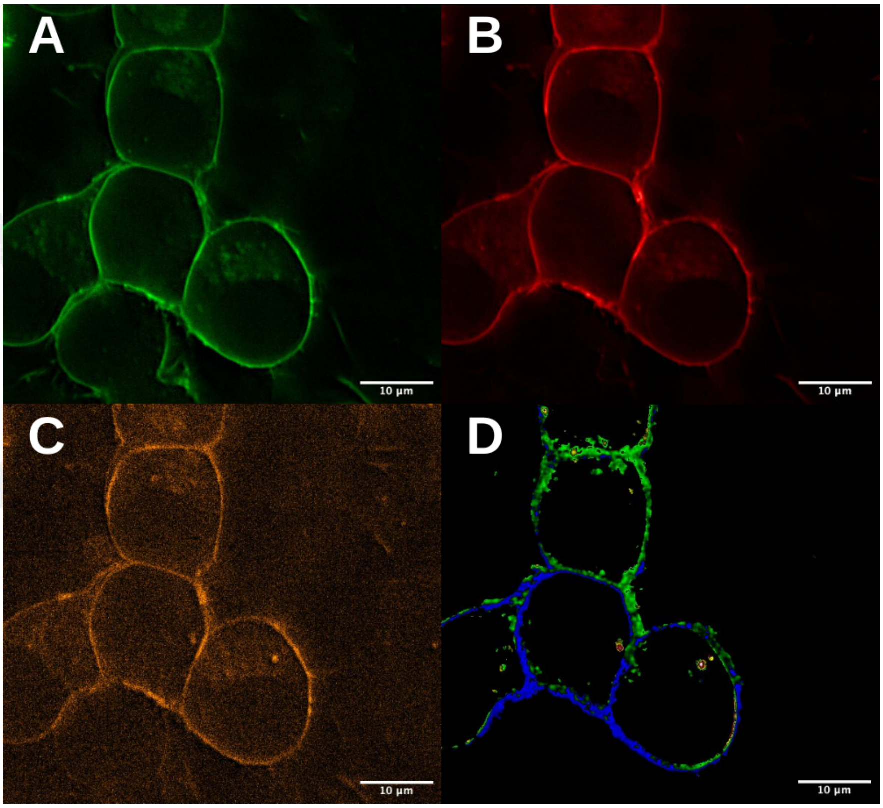

Figure 3.27: Confocal FRET images of K-Ras *wt* mCherry - Gαi EGFP in live N2-a cells, 63X magnification, 10 µm scale line. (A) Image of the EGFP channel. (B) Image of the mCherry channel. (C) Image of the FRET channel. (D) Image of the FRET efficiency in color scale.

In K-Ras *wt* – Gαi1 FRET efficiency distribution, when compared with K-Ras *wt* – K-Ras *wt*, it is observable that their line graphs overlap and show similar trends in interaction ranges in Figure 3.28A. According to Figure 3.28B, K-Ras *wt* – Gαi1 interaction is significantly higher than negative FRET control, and no significant changes with positive FRET control suggest the interaction. Also, net FRET values are slightly lower than the K-Ras *wt* – K-Ras *wt* interaction.

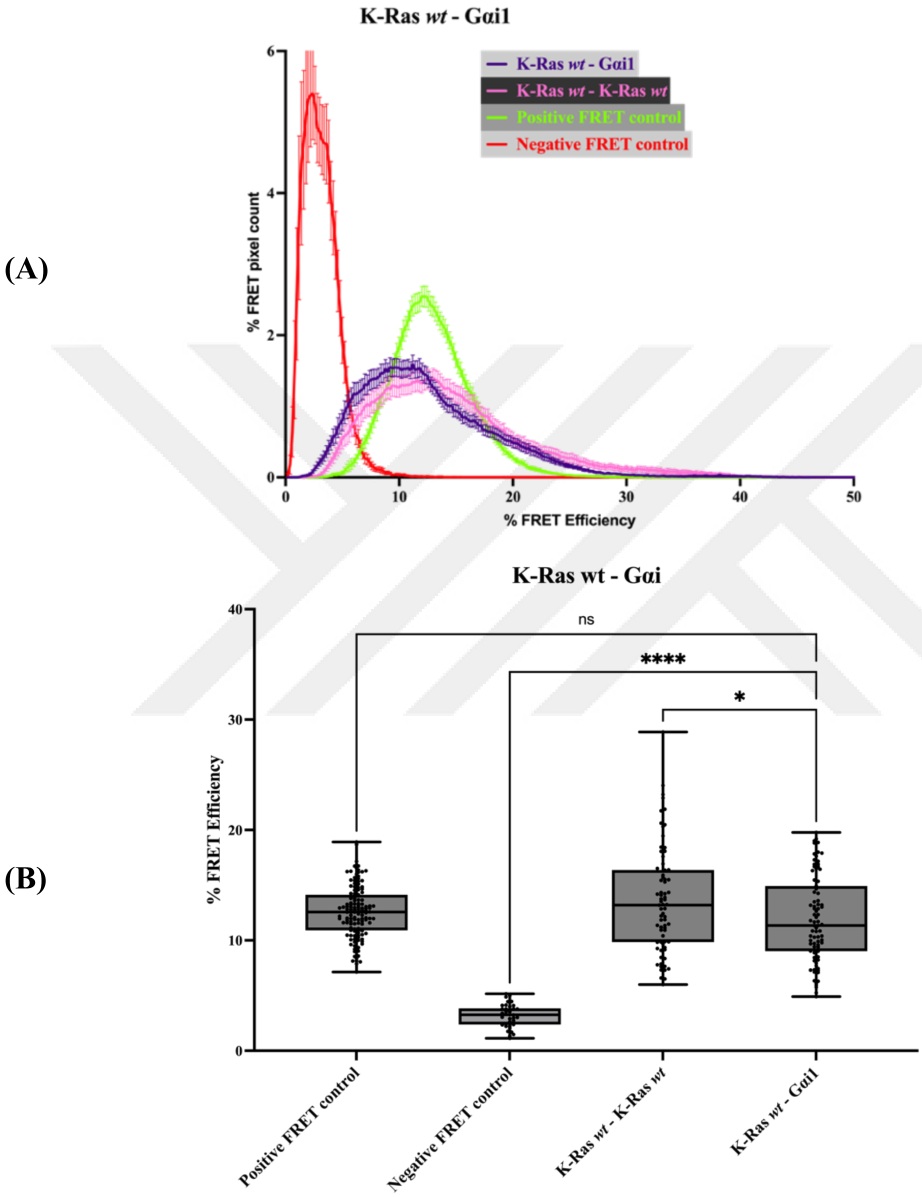

Figure 3.28: K-Ras *wt* – Gαi interaction FRET efficiency in line graph and box plot. (A) FRET efficiency in the line graph, FRET efficiency mean±SEM values distribution in the range. (B) FRET efficiency in the box plot, all cells mean FRET Efficiency. T-test statistical analysis was performed, significance level p<0.05.

In addition to K-Ras *wt* – Gαi1 interaction, K-Ras *onc* interaction with Gαi1 was also tested. Similarly, an indication of interaction was observed in the FRET channel in Figure 3.29, and the FRET efficiency was calculated accordingly.

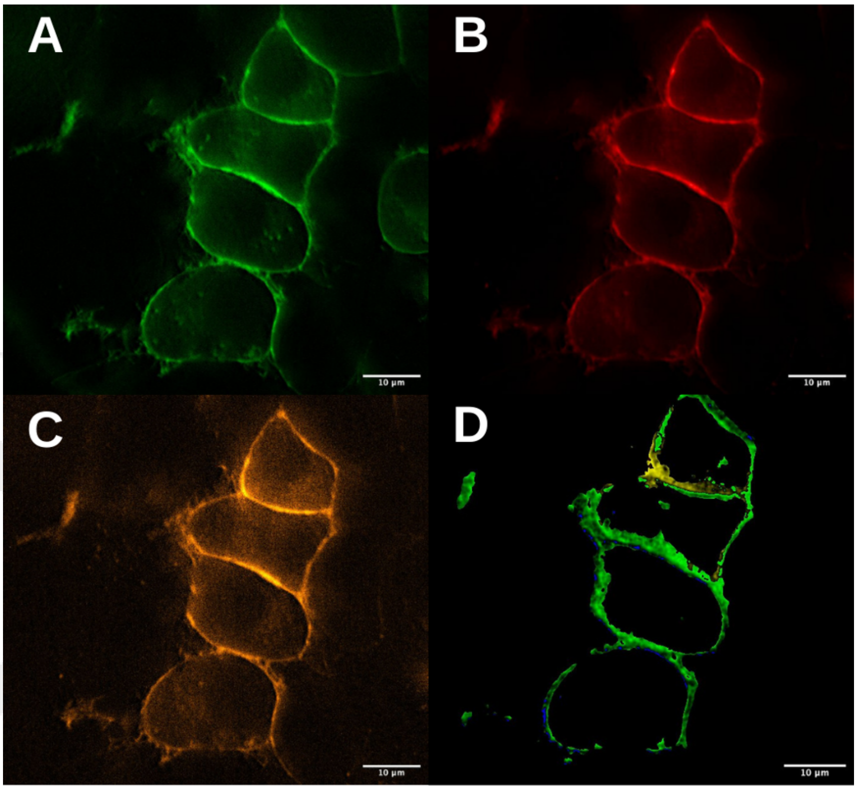

Figure 3.29: Confocal FRET images of K-Ras *onc* mCherry - Gαi EGFP in live N2-a cells, 63X magnification, 10 μm scale line. (A) Image of the EGFP channel. (B) Image of the mCherry channel. (C) Image of the FRET channel. (D) Image of the FRET efficiency in color scale.

The K-Ras *onc* – Gαi1 interaction efficiency graph in Figure 3.30A shows a similar wide distribution with K-Ras *onc* – K-Ras *onc* interaction. The mean efficiency values in K-Ras *onc* – interaction are shown in Figure 3.30B. According to the One-Way ANOVA statistical test, it is significantly higher than K-Ras *onc* homodimerization and slightly higher than positive FRET control.

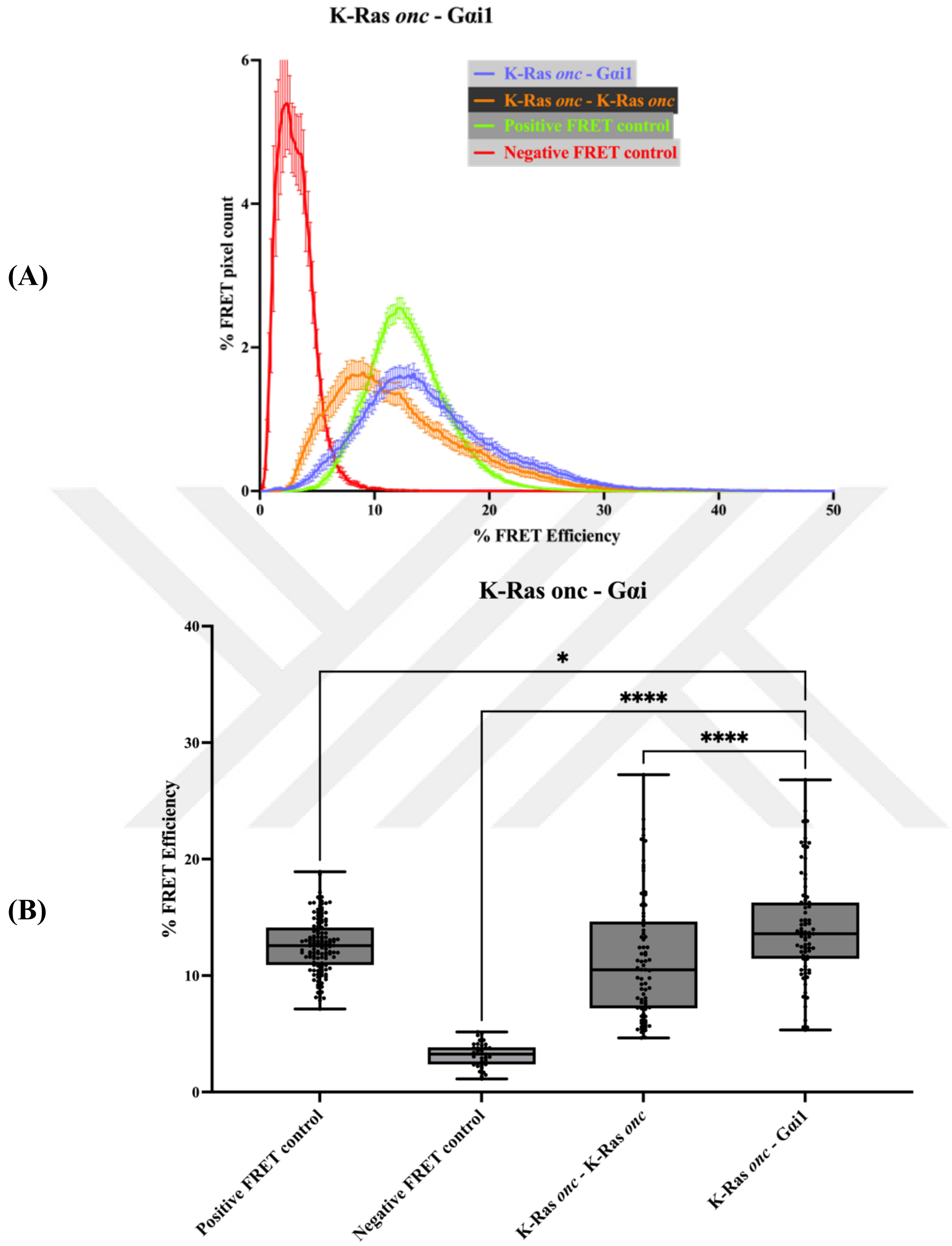

Figure 3.30: K-Ras *onc* – Gαi interaction FRET efficiency in line graph and box plot. (A) FRET efficiency in the line graph, FRET efficiency mean±SEM values distribution in the range. (B) FRET efficiency in the box plot, all cells mean FRET Efficiency. T-test statistical analysis was performed, significance level $p<0.05$.

3.9 Interaction of K-Ras *wt*/K-Ras *onc* – Gα11 Proteins heterodimerization detection with FRET technique & analysis

Gα11 protein's possible interaction with K-Ras *wt* was examined with the FRET technique. K-Ras *wt* was used as an acceptor in its 62nd position labeled with mCherry, while Gα11 was a donor tagged with EGFP in the 246th amino acid position. Compared to other Gα proteins, Gα11 does not interact with K-Ras *wt* protein in these conditions. According to Figure 3.31, even though both proteins were expressed simultaneously in the same cells, no FRET signal was observed in the FRET channel, and pixel intensity was so low and was not appropriately visualized.

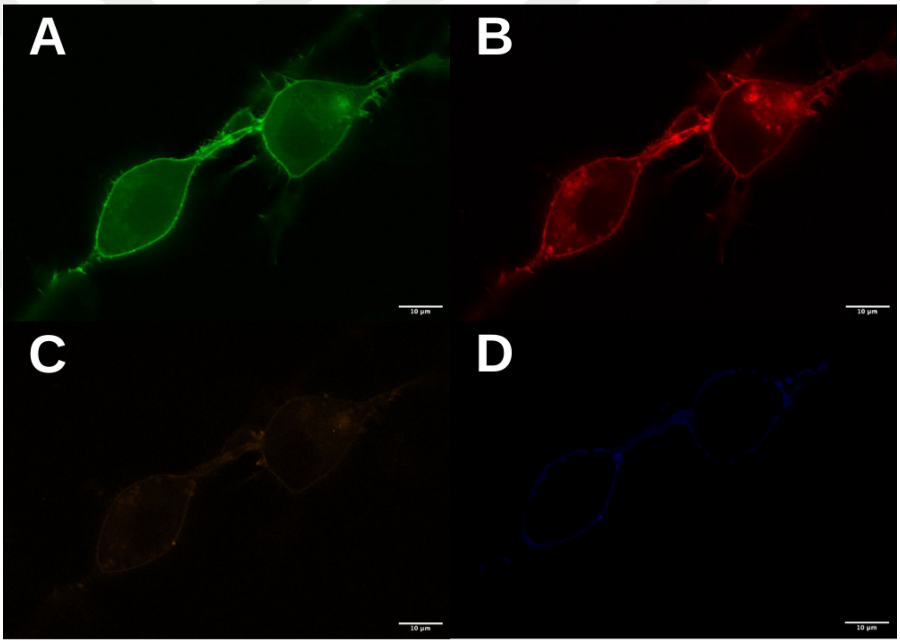

Figure 3.31: Confocal FRET images of K-Ras *wt* mCherry – Gα11 EGFP in live N2-a cells, 63X magnification, 10 µm scale line. (A) Image of the EGFP channel. (B) Image of the mCherry channel. (C) Image of the FRET channel. (D) Image of the FRET efficiency in color scale.

The FRET efficiency graph of K-Ras *wt* - Gα11 interaction shows the overlap in the lines with negative FRET control in Figure 3.32A. When means of FRET efficiency in the cells were calculated in this interaction, it is seen that there is no significant difference between K-Ras *wt* - Gα11 interaction and negative control below in Figure 3.32B.

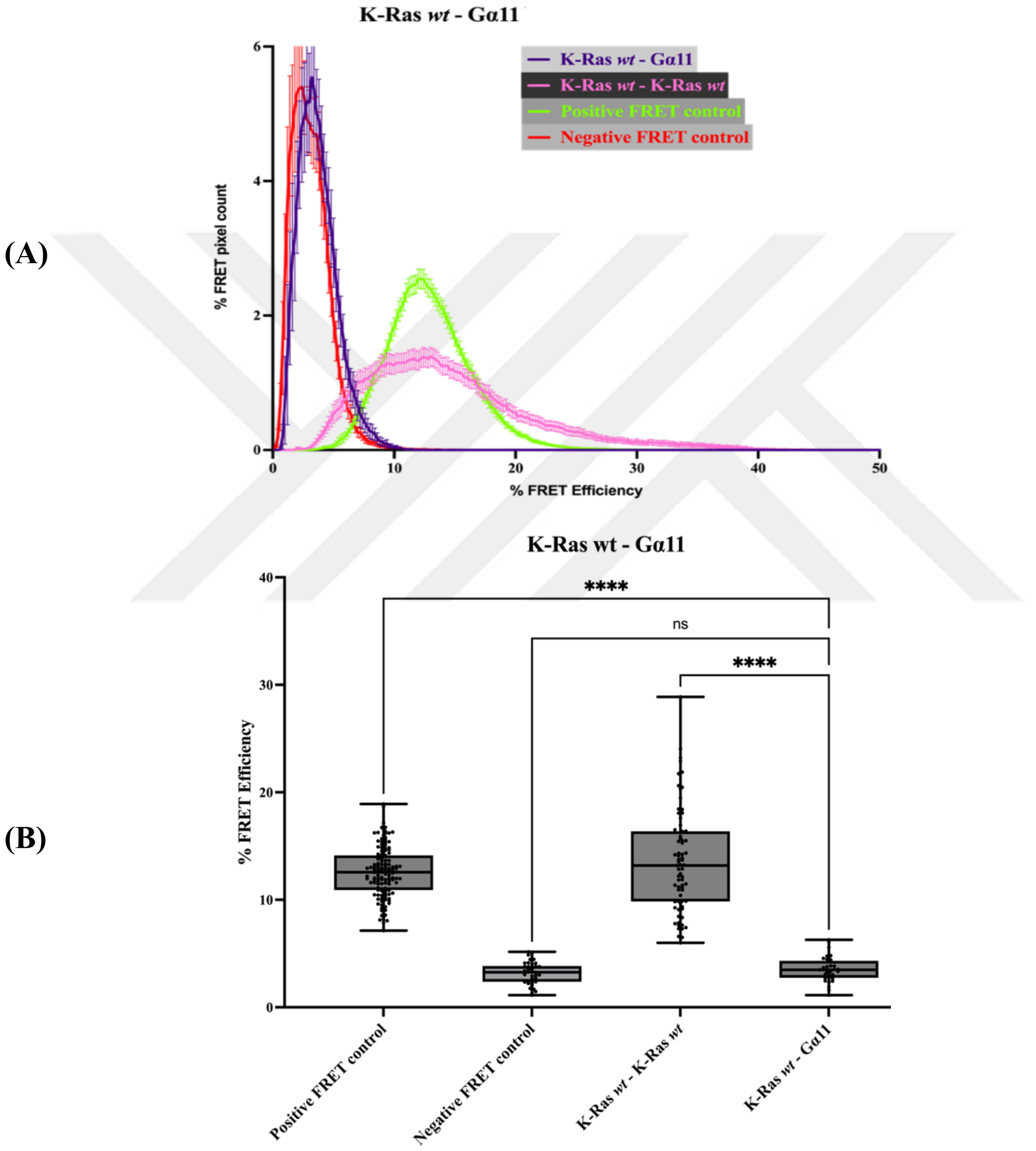

Figure 3.32: K-Ras *wt* – Gα11 interaction FRET efficiency in line graph and box plot. (A) FRET efficiency in the line graph, FRET efficiency mean±SEM values distribution in the range. (B) FRET efficiency in the box plot, all cells mean FRET Efficiency. T-test statistical analysis was performed, significance level $p<0.05$.

Like the K-Ras *wt* - Gα11, the K-Ras *onc* - Gα11 expressing cells were examined to see if there is an interaction between these proteins, a representative result was shown in Figure 3.33. However, similar to K-Ras *wt* interaction, no FRET signal in the FRET channel indicates no interaction between these proteins under these conditions.

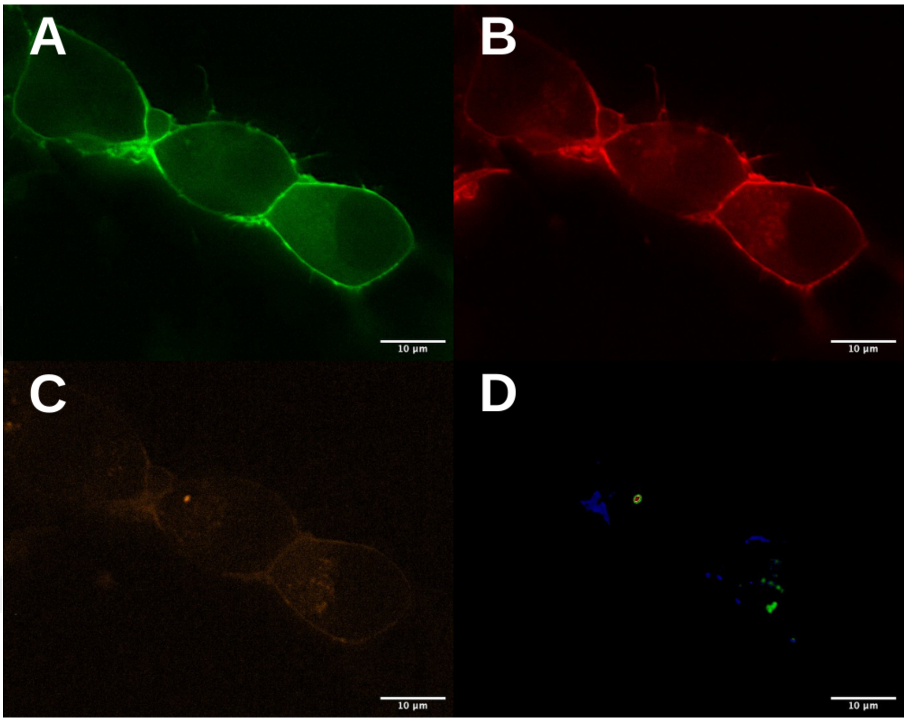

Figure 3.33: Confocal FRET images of K-Ras *onc* mCherry – Gα11 EGFP in live N2-a cells, 63X magnification, 10 μm scale line. (A) Image of the EGFP channel. (B) Image of the mCherry channel. (C) Image of the FRET channel. (D) Image of the FRET efficiency in color scale.

K-Ras *onc* - Gα11 FRET efficiency distribution line graph overlaps with negative control in Figure 3.34A with lower than 5% FRET efficiency. When K-Ras *onc* - Gα11 FRET efficiencies of cells were calculated, it is seen in Figure 3.34B that there is no significant difference between this interaction and the negative control's mean according to One Way ANOVA statistics.

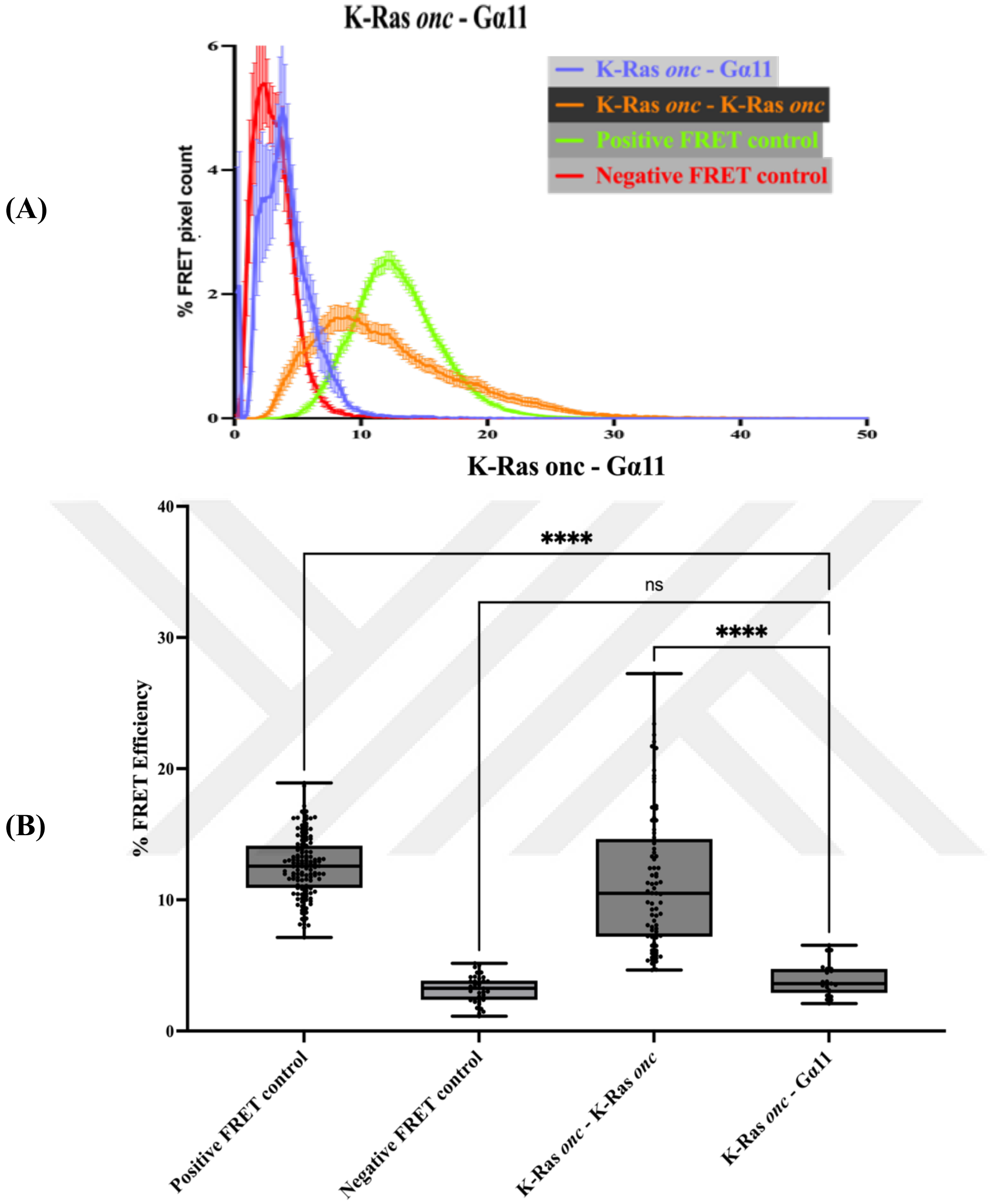

Figure 3.34: K-Ras *onc* – Gα11 interaction FRET efficiency in line graph and box plot. (A) FRET efficiency in the line graph, FRET efficiency mean±SEM values distribution in the range. (B) FRET efficiency in the box plot, all cells mean FRET Efficiency. T-test statistical analysis was performed, significance level p<0.05.

3.10 Interaction of K-Ras *wt*/K-Ras *onc* – Gα12 Proteins heterodimerization detection with FRET technique & analysis

K-Ras *wt* – Gα12 interaction was also tested with the FRET technique under the confocal microscope in live cells. Gα12 tagged with EGFP at 265th amino acid position as a donor and transfected to N2-a cells with K-Ras *wt* tagged with mCherry in 62nd position as an acceptor. According to microscope images in Figure 3.35, proteins were expressed at the same time, and the FRET signal was detected in the FRET channel.

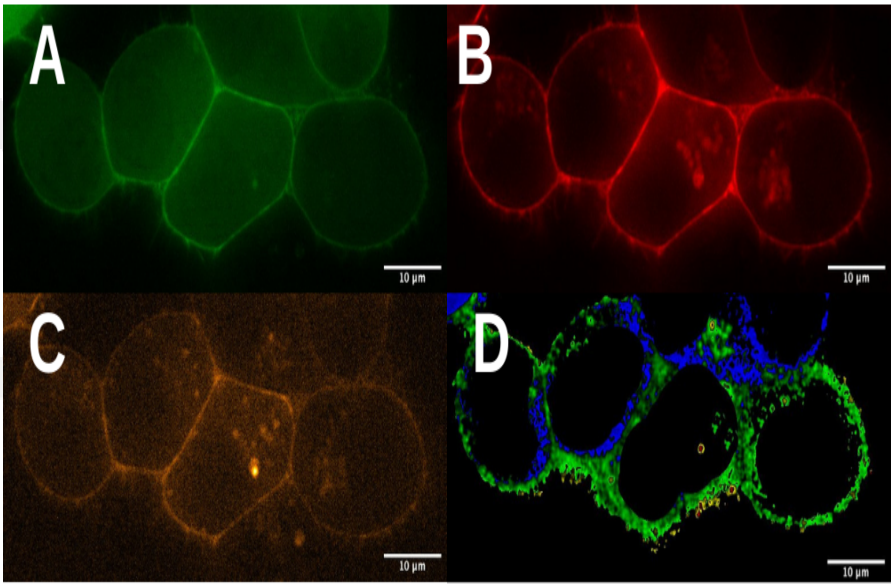

Figure 3.35: Confocal FRET images of K-Ras *wt* mCherry – Gα12 EGFP in live N2-a cells, 63X magnification, 10 µm scale line. (A) Image of the EGFP channel. (B) Image of the mCherry channel. (C) Image of the FRET channel. (D) Image of the FRET efficiency in color scale.

Once this interaction's efficiency for FRET was calculated, it is seen that interaction shows almost the same trend as positive FRET control in both distribution and percentage in Figure 3.36A. Moreover, it is less dynamic than the K-Ras *wt* - K-Ras *wt* interaction. The calculated mean of FRET efficiencies shows no significant difference between K-Ras *wt* - Gα12 interaction and K-Ras *wt* - K-Ras *wt* interaction or positive FRET control in Figure 3.36B.

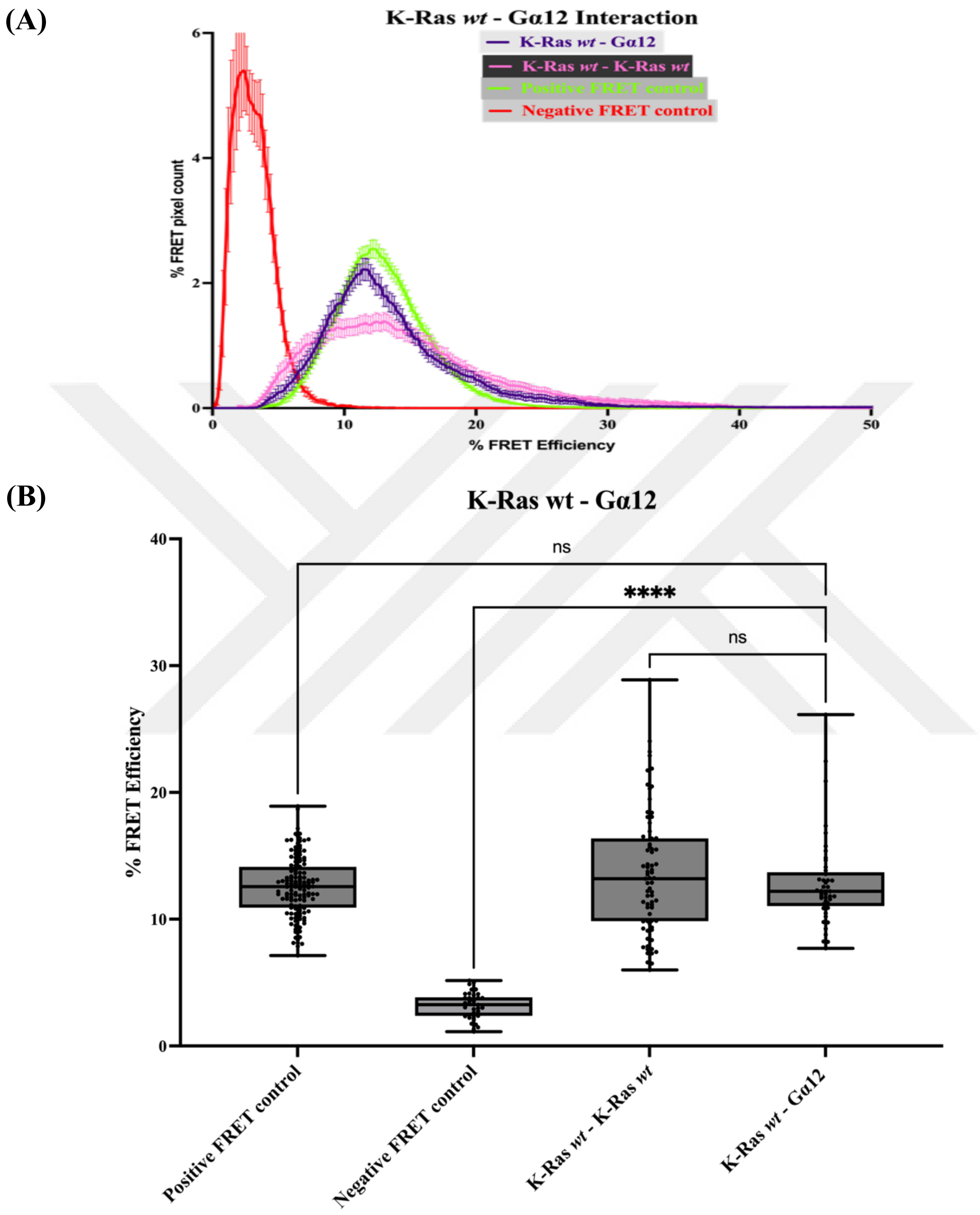

Figure 3.36: K-Ras *wt* – Gα12 interaction FRET efficiency in line graph and box plot. (A) FRET efficiency in the line graph, FRET efficiency mean±SEM values distribution in the range. (B) FRET efficiency in the box plot, all cells mean FRET Efficiency. T-test statistical analysis was performed, significance level $p<0.05$.

Gα12 interaction with K-Ras *onc* was also tested in identical conditions of the FRET technique, and the FRET signal was obtained in the FRET channel, indicating the interaction between these two proteins in Figure 3.37.

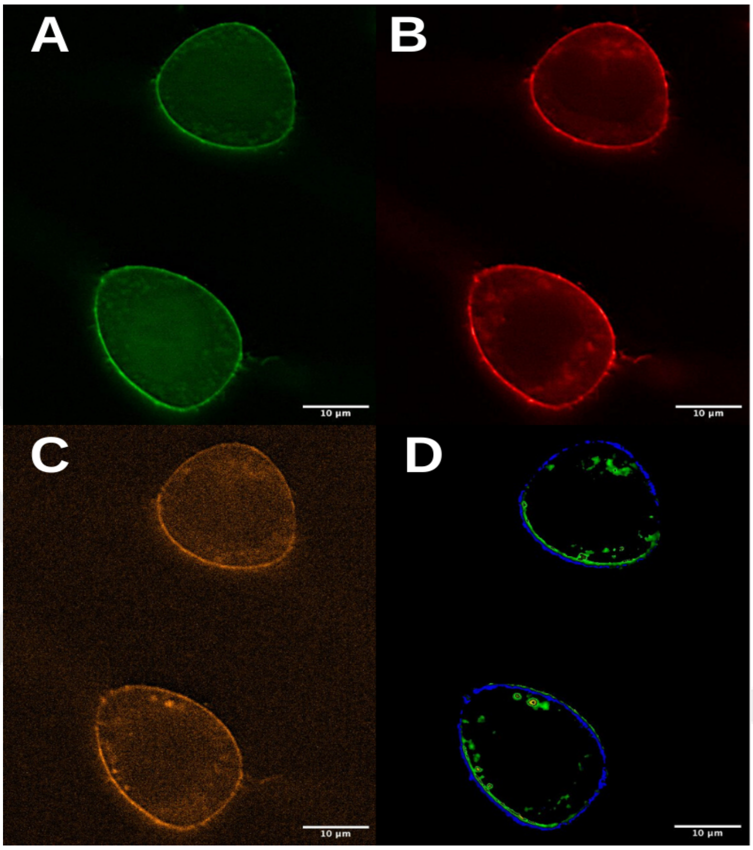

Figure 3.37: Confocal FRET images of K-Ras *onc* mCherry – Gα12 EGFP in live N2-a cells, 63X magnification, 10 µm scale line. (A) Image of the EGFP channel. (B) Image of the mCherry channel. (C) Image of the FRET channel. (D) Image of the FRET efficiency in color scale.

Compared to the K-Ras *wt* – Gα12 interaction, the line graph of K-Ras *onc* – Gα12 is slightly shifted to the left side of the graph and seems to have similar dynamics compared to the K-Ras *wt* – Gα12 interaction according to Figure 3.38A. According to the mean values of FRET efficiencies of the FRET pair in Figure 3.38B, the K-Ras *onc* – Gα12 interaction is slightly lower than the K-Ras *onc* - K-

Ras *onc* interaction. However, overall, it is significantly higher than negative FRET control and proves there is interaction between these two proteins.

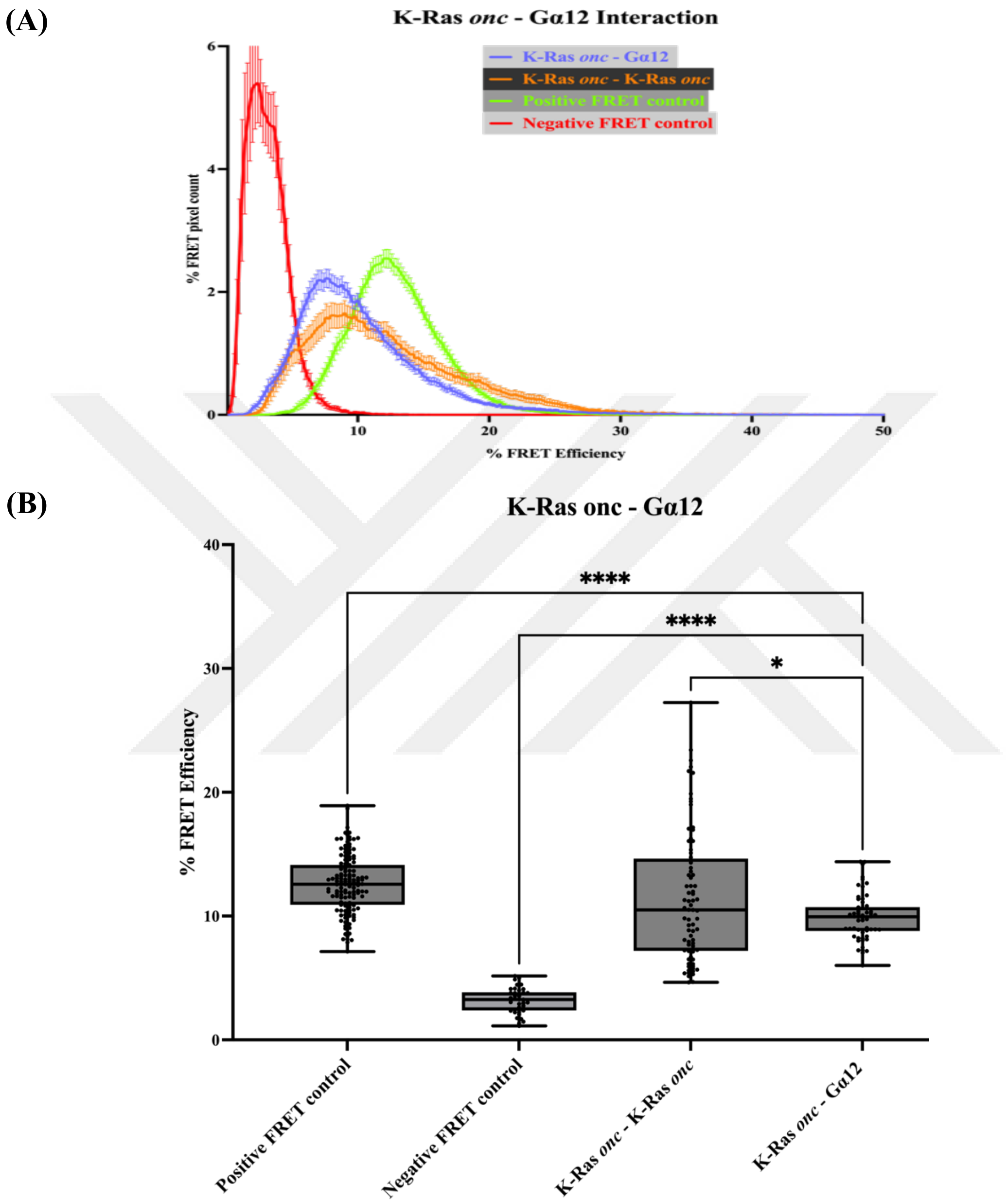

Figure 3.38: K-Ras *onc* – Gα12 interaction FRET efficiency in line graph and box plot. (A) FRET efficiency in the line graph, FRET efficiency mean±SEM values distribution in the range. (B) FRET efficiency in the box plot, all cells mean FRET Efficiency. T-test statistical analysis was performed, significance level $p<0.05$.

3.11 Interaction of K-Ras *wt*/K-Ras *onc* – Gα13 Proteins heterodimerization detection with FRET technique & analysis

The last Gα protein that was tested with K-Ras *wt* interaction was Gα13. Like other Gα protein FRET studies, Gα13 was tagged with EGFP at its 215th position and used as a donor, while K-Ras *wt* was tagged at the 62nd position with mCherry and used as an acceptor. According to confocal microscopy images in Figure 3.39, the signal was obtained in the FRET channel, showing the interaction between proteins.

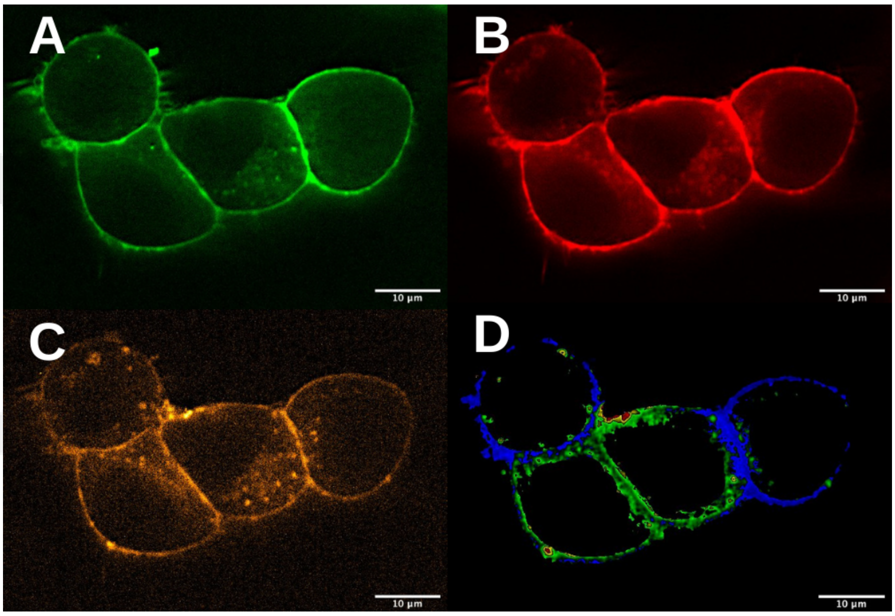

Figure 3.39: Confocal FRET images of K-Ras *wt* mCherry – Gα13 EGFP in live N2-a cells, 63X magnification, 10 µm scale line. (A) Image of the EGFP channel. (B) Image of the mCherry channel. (C) Image of the FRET channel. (D) Image of the FRET efficiency in color scale.

After FRET efficiency calculations interaction between K-Ras *wt* and Gα13 protein, the line graph shows the K-Ras *wt* - Gα13 interaction has a similar distribution in terms of efficiency and range with K-Ras *wt* – K-Ras *wt* but a little lower percentage shown below in Figure 3.40A. FRET efficiency mean value of K-Ras *wt* - Gα13 interaction has no significant difference from positive control. However, it is significantly higher than negative FRET control, according to Figure 3.40B, indicating an interaction between these two proteins.

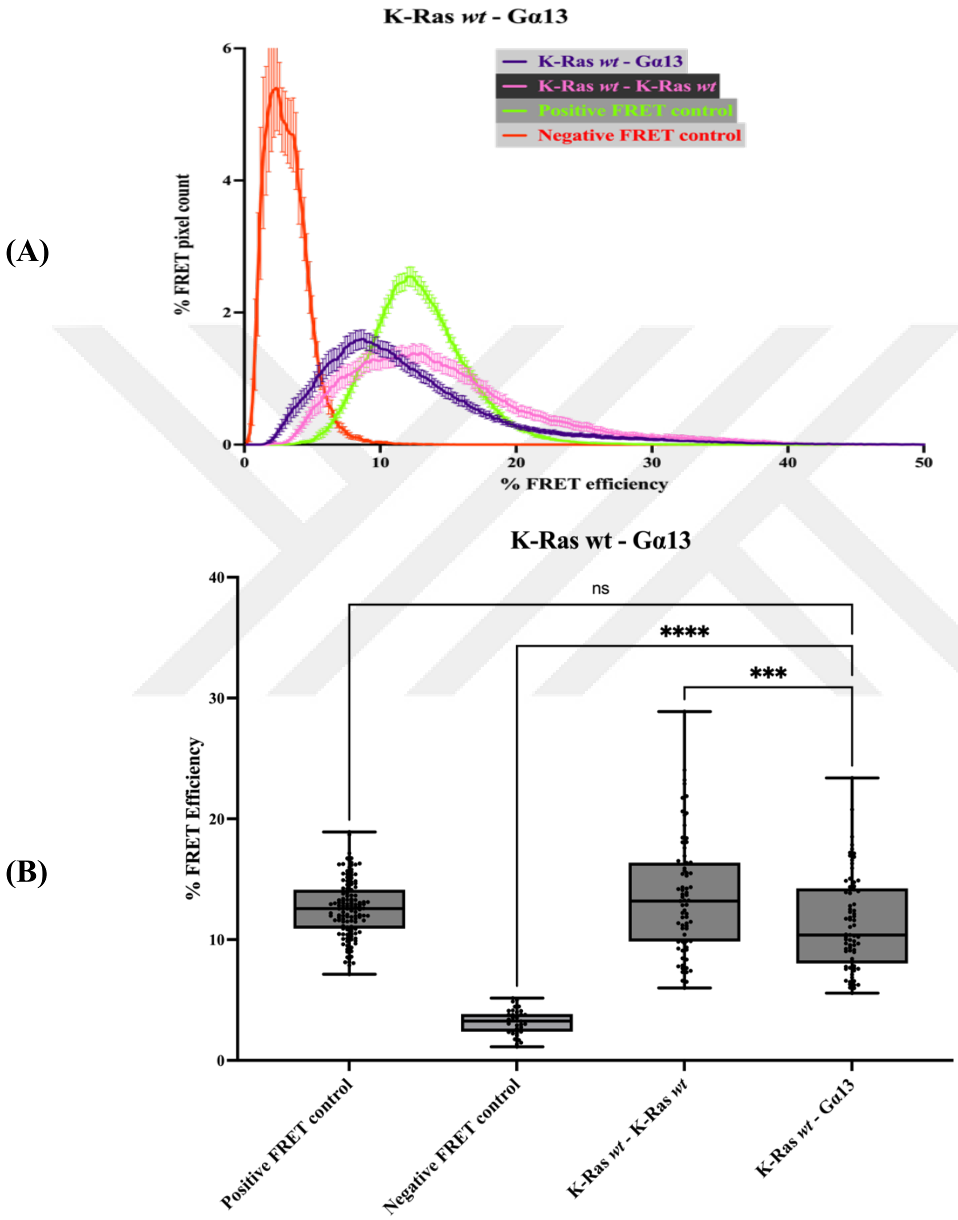

Figure 3.40: K-Ras *wt* – Gα13 interaction FRET efficiency in line graph and box plot. (A) FRET efficiency in the line graph, FRET efficiency mean±SEM values distribution in the range. (B) FRET efficiency in the box plot, all cells mean FRET Efficiency. T-test statistical analysis was performed, significance level p<0.05.

Similar to other Gα proteins, Gα13 protein interaction with K-Ras *onc* protein was tested in the same conditions. After live imaging under confocal microscopy, as shown in Figure 3.41, the interaction between these two proteins was detected based on the FRET channel signal and FRET efficiency frame.

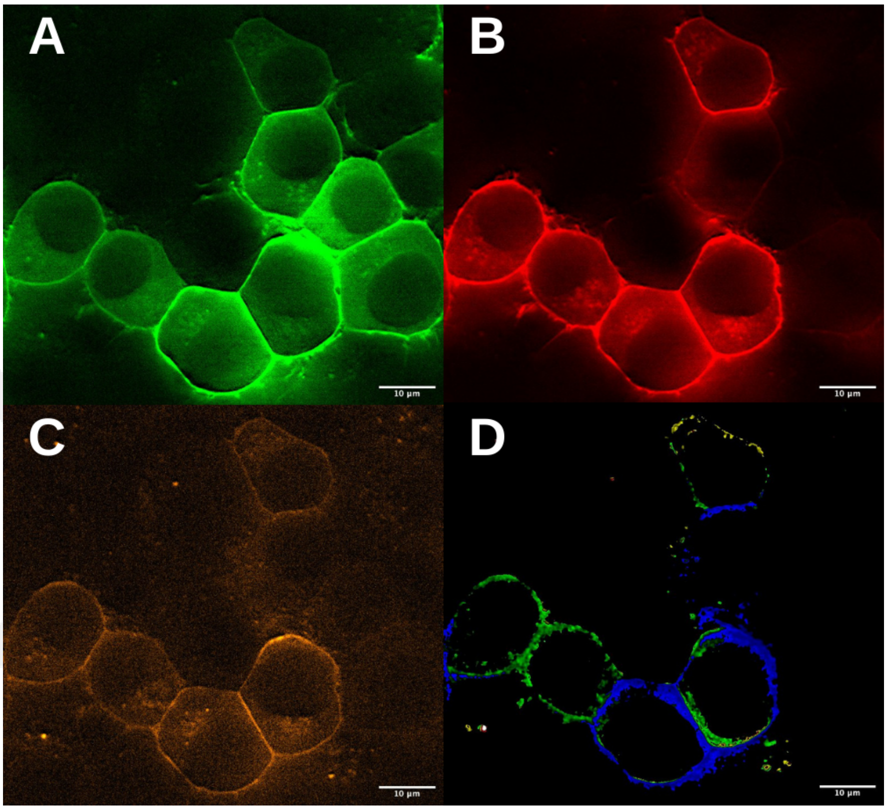

Figure 3.41: Confocal FRET images of K-Ras *onc* mCherry – Gα13 EGFP in live N2-a cells, 63X magnification, 10 μm scale line. (A) Image of the EGFP channel. (B) Image of the mCherry channel. (C) Image of the FRET channel. (D) Image of the FRET efficiency in color scale.

Cells' FRET efficiency distribution graph in Figure 3.42A shows the overlap between K-Ras *onc* - Gα13 and K-Ras *onc* homodimerization. In Figure 3.42B, mean values of FRET efficiencies of K-Ras *onc* - Gα13 interaction show no significant difference between K-Ras *onc*- K-Ras *onc* and K-Ras *wt* - Gα13 interactions in addition to positive FRET control.

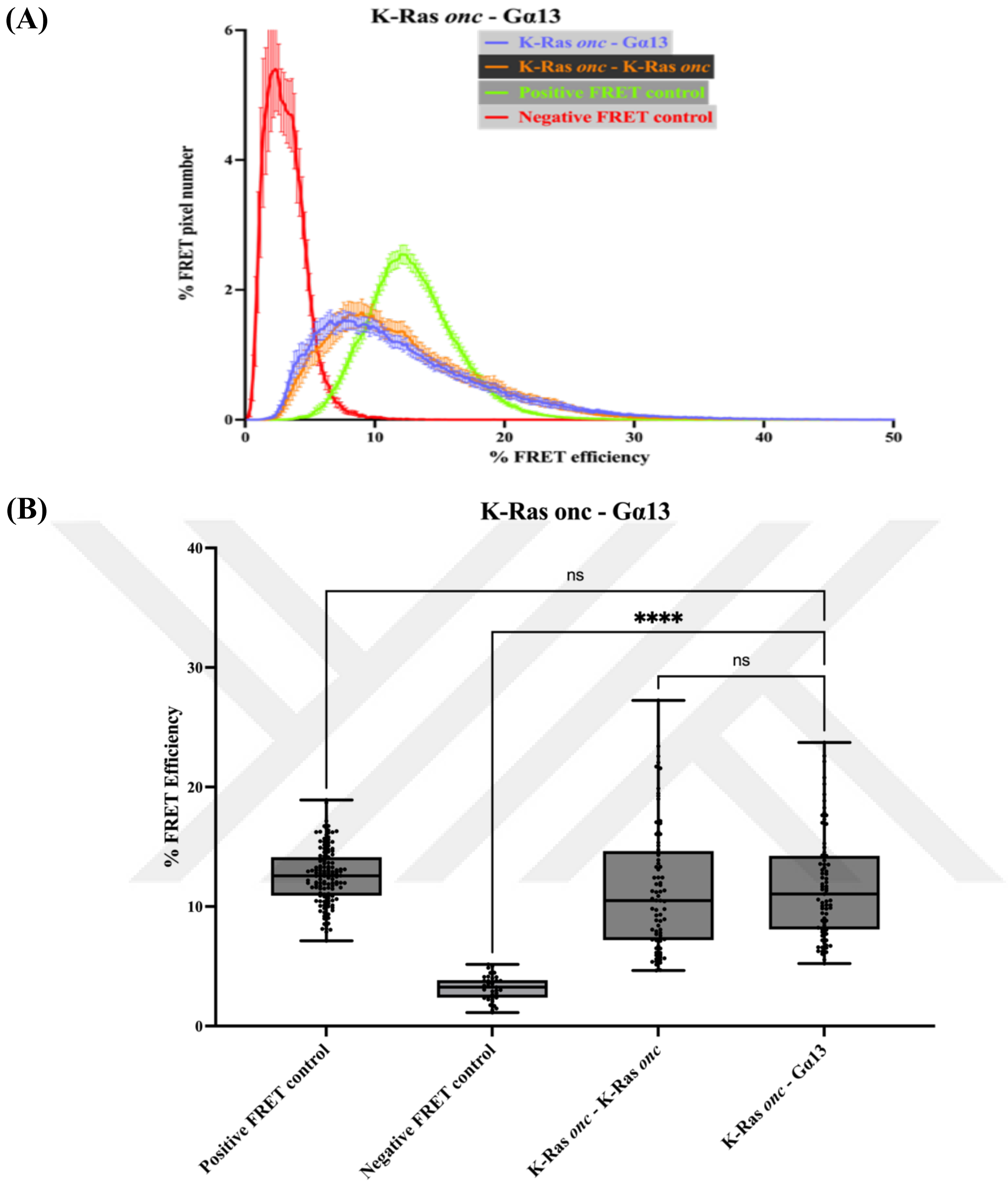

Figure 3.42: K-Ras *onc* – Gα13 interaction FRET efficiency in line graph and box plot. (A) FRET efficiency in line graph, FRET efficiency mean±SEM values distribution in the range. (B) FRET efficiency in box plot, all cells mean FRET Efficiency. T-test statistical analysis was performed, significance level $p<0.05$.

3.12 Site-Directed Mutagenesis on Dimerization Interfaces of K-Ras & Gα Proteins Interaction

According to the literature, firstly, K-Ras *wt* and K-Ras *onc* are mutated with site-directed mutagenesis technique in their homo-dimerization α-interface hot spot amino acids, Lysine 101 and Arginine 102 were mutated to negatively charged Aspartic acid 101 and Glutamic acid 102 amino acid. After these charge reversal mutations on K-Ras, disruption of the dimerization of K-Ras and K-Ras is reported. Figure 3.43 shows successful mutations on indicated amino acids.

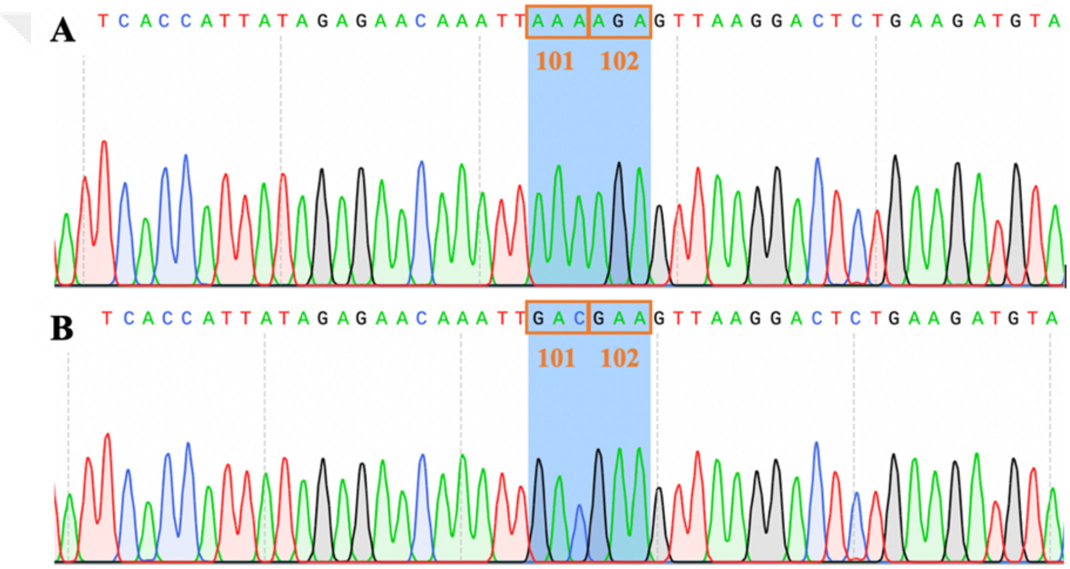

Figure 3.43: Sanger sequencing results of K-Ras & K-Ras K101D&R102E. (A) K-Ras K101&R102 sequence. (B) K-Ras K101D&R102E sequence.

After K-Ras charge reversal mutations, to study the K-Ras and Gα proteins dimerization, the corresponding amino acids on Gα proteins α-interface were mutated. According to K-Ras and Gα proteins' structure modeling and alignment, their G-domains overlap due to high structural homology. In their structural and multiple protein sequence alignment, amino acids that may play a role in the dimerization of K-Ras and Gα proteins were systematically mutated with the site-directed mutation method considering amino acid charges and polarities to mimic K-

Ras homodimerization α-interface. According to alignments, corresponding amino acids were decided on Gα proteins that correspond to the K-Ras homodimerization hot spots, 101st and 102nd amino acids.

Figure 3.44 shows multiple protein alignment sequences of K-Ras (NCBI RefSeq: NP_004976.2), Gαs (NCBI RefSeq: NP_000507.1), Gαi1 (NCBI RefSeq: NP_002060.4), Gα11 (NCBI RefSeq: NP_002058.2), Gα12 (NCBI RefSeq: NP_031379.2), Gα13 (NCBI RefSeq: NP_006563.2). The K-Ras α-interface dimerization region is picked to understand corresponding conserved amino acids in Gα protein.

```
K-Ras  72  MRTGEGFLCVFAINN------------TKSFEDIHHYREQIKRVKDSEDVPMVLVGNKCDLPSRTVDTKQAQDLARSYG  138
Gαs   238  FNDVTAIIFVVASSSYNMVIREDNQTNRLQEALNLFKSIWNNRWLRTISVILFLNKQDLLAEKVLAGkSKIEDYFPEFA  328
Gαi   215  FEGVTAIIFCVALSDYDLVLAEDEEMNRMHESMKLFDSICNNKWFTDTSIILFLNKKDLFEEKIKK--SPLTICYPEYA  291
Gα11  220  FENVTSIMFLVALSEYDQVLVESDNENRMEESKALFRTIITYPWFQNSSVILFLNKKDLLEDKILY--SHLVDYFPEFD  296
Gα12  242  FDGITSILFMVSSSEYDQVLMEDRRTNRLVESMNIFETIVNNKLFFNVSIILFLNKMDLLVEKVKTV--SIKKHFPDFR  318
Gα13  237  FDSVTSILFLVSSSEFDQVLMEDRLTNRLTESLNIFETIVNNRVFSNVSIILFLNKTDLLEEKVQIV--SIKDYFLEFE  313
```

Figure 3.44: Multiple Sequence Alignment of K-Ras, Gαs, Gαi, Gα11, Gα12, Gα13 regarding K-Ras dimerization interface.

Once multiple sequence alignment was conducted, 3D structures obtained from PDB of Gα proteins and K-Ras were aligned if the multiple protein sequence alignments matched structurally.

K-Ras and Gαs structural alignment yielded N279 & R280 residues on Gαs that correspond to K101 & R102 residues on K-Ras. Since both residues at this position are arginine, mutation of only the first residue on Gαs to lysine was enough to mimic the reported K-Ras dimerization interface. Figure 3.45 shows the protein structure alignment of K-Ras and Gαs proteins.

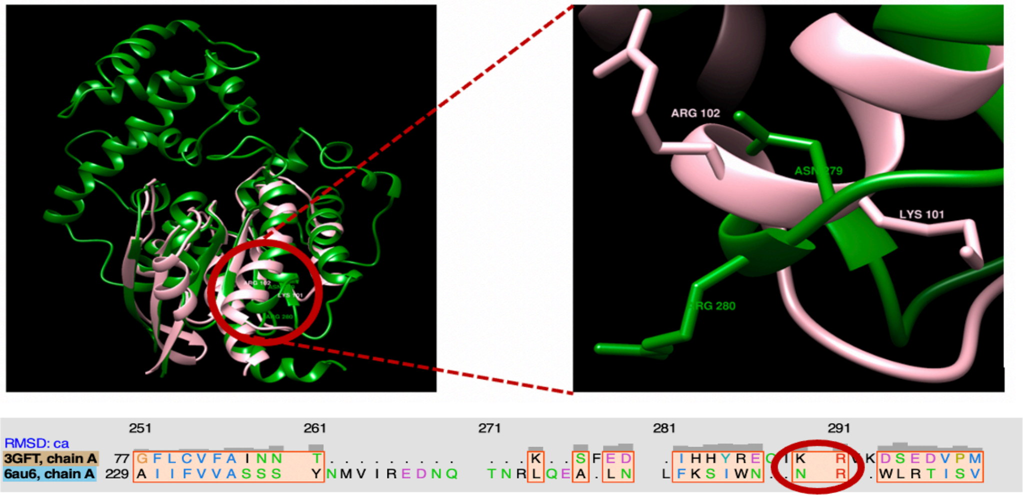

Figure 3.45: K-Ras and Gαs structural alignment and corresponding residues on K-Ras dimerization interface.

In the context of K-Ras and Gαi1 alignment, Gαi1 has residues N256 & K257 for K-Ras dimerization hot spots, and they are mutated to lysine and arginine amino acids in the same residue to imitate K-Ras dimerization interface. Figure 3.46 shows the structural alignment of K-Ras and Gαi1.

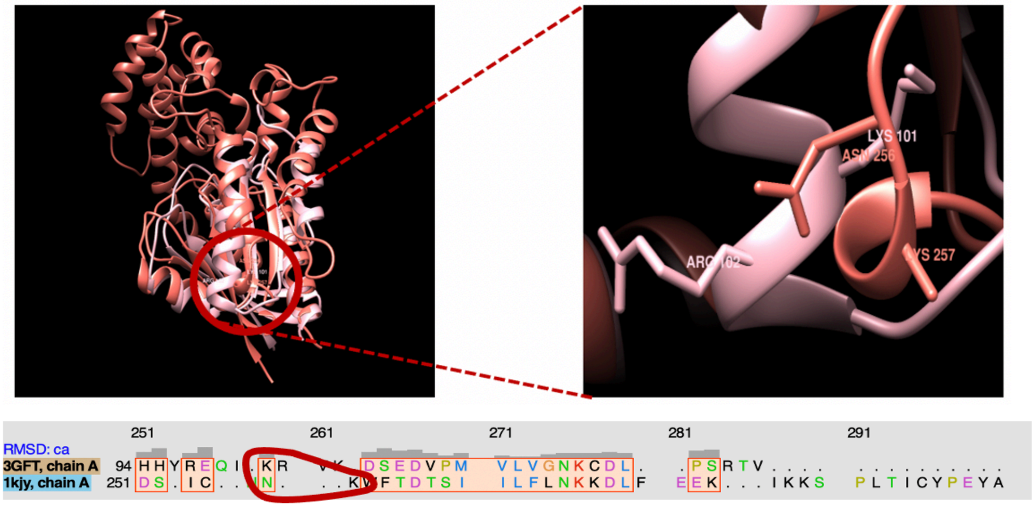

Figure 3.46: K-Ras and Gαi1 structural alignment and corresponding residues on K-Ras dimerization interface.

According to K-Ras and Gα11 alignment, corresponding amino acids on K-Ras K101 & R102 are Y261 & P262 Gα11. These tyrosine and proline residues were mutated to lysine and arginine residues to mimic the K-Ras dimerization interface. Figure 3.47 shows 3D protein structures of K-Ras and Gα11 alignment.

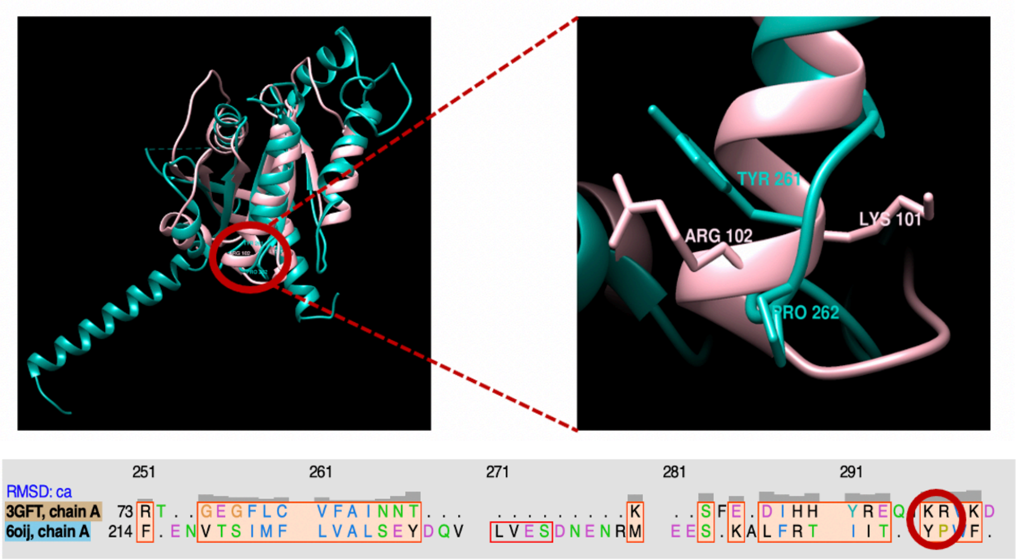

Figure 3.47: K-Ras and Gα11 structural alignment and corresponding residues on K-Ras dimerization interface.

For K-Ras and Gα12 alignment, corresponding amino acids for K-Ras dimerization hot spots K101 & R102 are N283 & K284 residues on Gα12 protein. Therefore, mutating these residues on Gα12 to lysine and arginine was done to mimic the region. Figure 3.48 shows K-Ras and Gα12 alignment in 3D protein structures.

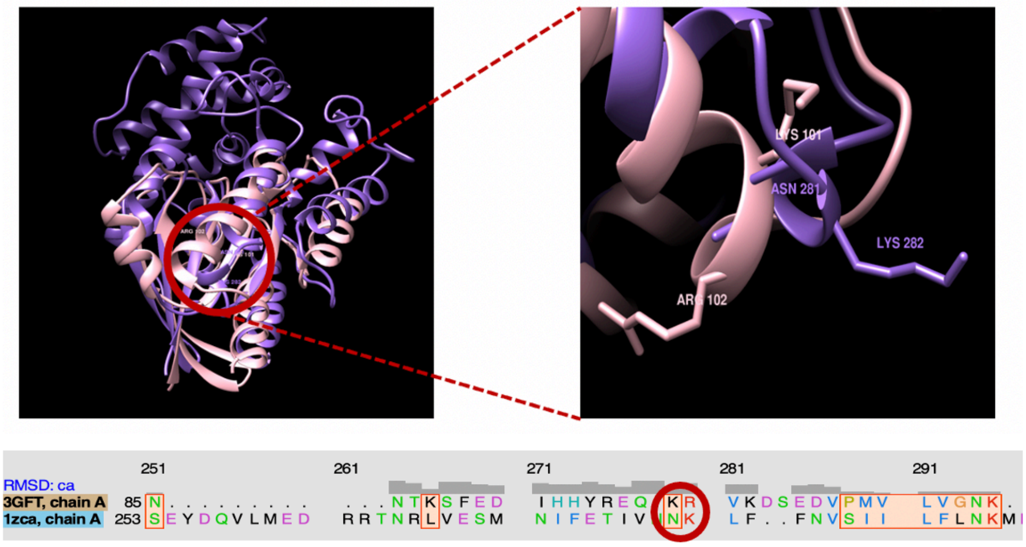

Figure 3.48: K-Ras and Gα12 structural alignment and corresponding residues on K-Ras dimerization interface.

Finally, Gα13 N278 & R279 correspondings to amino acids K101 & R102 on K-Ras. Since they have R residues in common as second amino acids, only the first amino acid, N278, is mutated into a lysine residue to mimic the K-Ras dimerization interface. Figure 3.49 shows the alignment of protein structures K-Ras and Gα13.

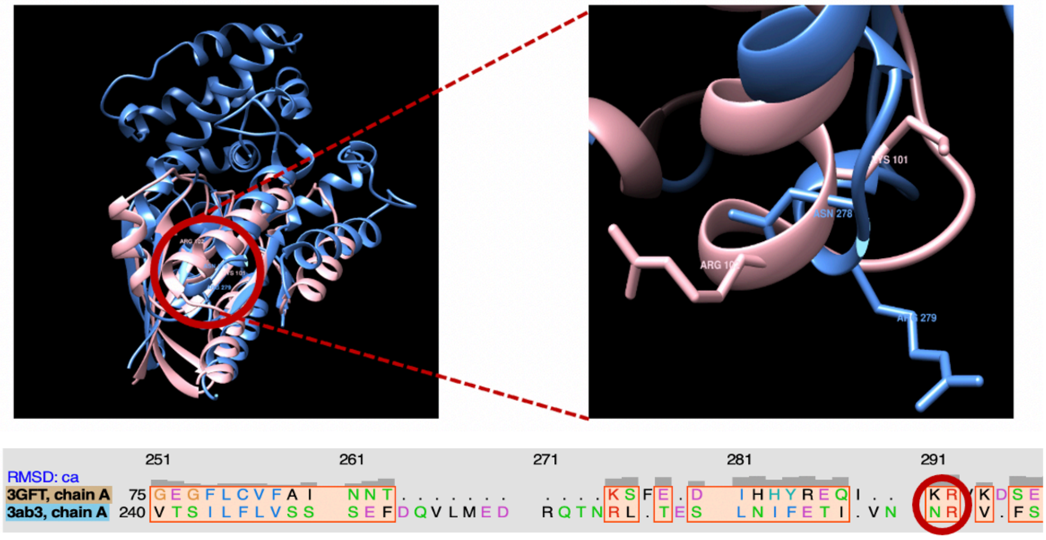

Figure 3.49: K-Ras and Gα13 structural alignment and corresponding residues on K-Ras dimerization interface.

After multiple sequence alignments and the structural alignments of K-Ras and Gα proteins, Gαi, Gα11, and Gα13 were picked for further interaction studies. Following this decision, the residues corresponding to K-Ras dimerization interface were mutated to study Gα11 - K-Ras interaction dynamics. Table 3.1 shows constructs and their desired residues before and after site-directed mutagenesis. Some residues in Gα proteins are common in hot spots amino acid of K-Ras R102, so they were not mutated.

Table 3.1: Desired residues and mutation on constructs to understand K-Ras and Gα proteins interaction closeness.

Constructs	**Corresponding region**	**Desired mutation on site after SDM**
K-Ras	K101 & R102	K101D & R102E
GNAI	N256 & K257	N256K & K257R
GNA11	Y261 & P262	Y261K&P262R
GNA13	N278 & R279	N278K

After applying Site-Directed Mutagenesis on Gαi, Gα11, and Gα13, all constructs were confirmed by sequencing to prove inserted mutations. In Figure 3.50, sequence results are shown.

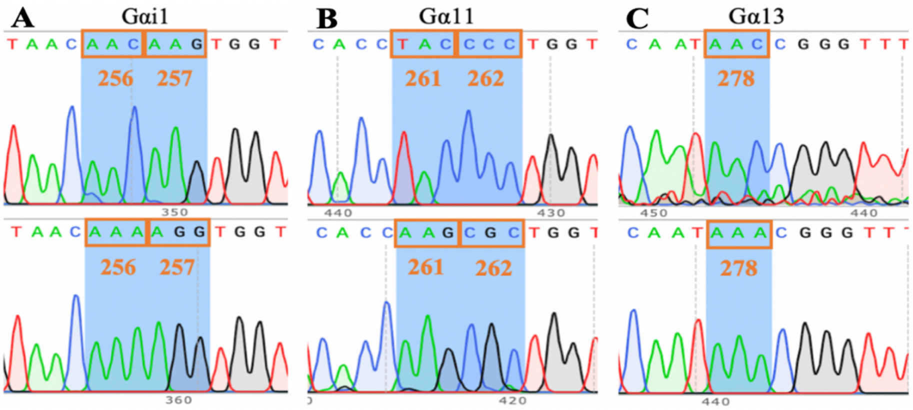

Figure 3.50: Sanger sequencing results of mutated Gαi, Gα11, and Gα13. (A) Gαi N256K & K257R sequence. (B) Gα11 Y261K&P262R sequence. (C) Gα13 N278K sequence.

3.13 Localization Detection of EGFP/mCherry labeled proteins in live cells using a confocal microscope after Site-Directed Mutagenesis

3.13.1 Visualization of EGFP/mCherry labeled K-Ras *wt* & K-Ras *onc* proteins in N2-a cells after Site-Directed Mutagenesis

After the site-directed mutagenesis on K-Ras *wt* and K-Ras *onc* proteins to obtain K101D&R102E mutations, 62nd position tagged with EGFP and mCherry constructs were transiently transfected to N2-a cells and imaged to see its localization using confocal microscope below shown in Figure 3.51.

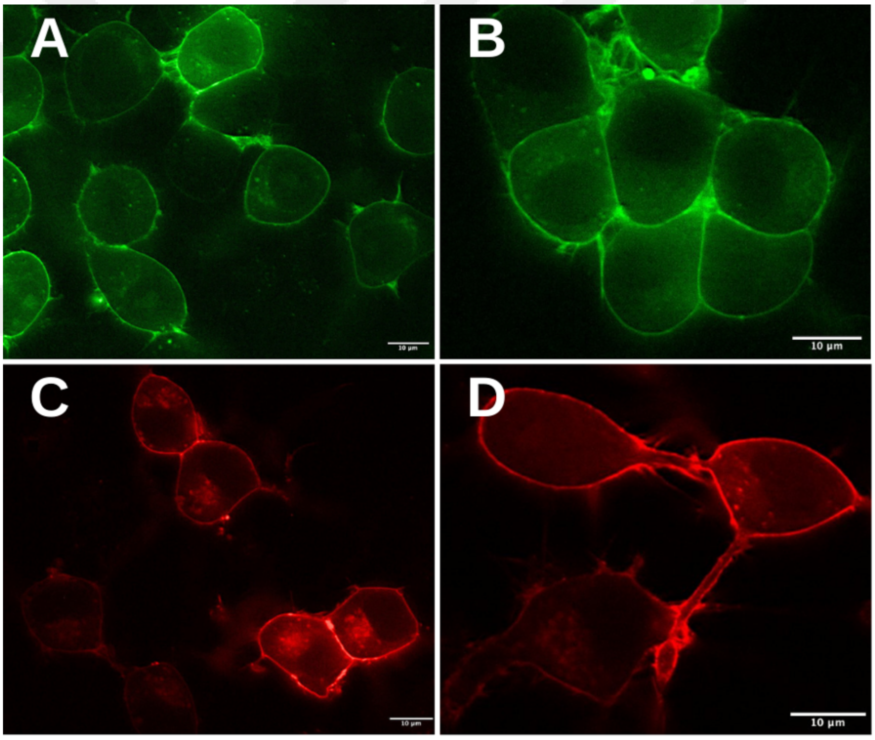

Figure 3.51: Confocal images of K-Ras *wt* & K-Ras *onc* 62nd EGFP/mCherry K101D&R102E in live N2-a cells, 63X magnification, 10 µm scale line. (A) Image of the of K-Ras *wt* 62nd EGFP K101D&R102E in EGFP channel. (B) Image of the of K-Ras *onc* 62nd K101D&R102E EGFP in EGFP channel. (C) Image of the of K-Ras *wt* 62nd mCherry K101D&R102E in mCherry channel. (D) Image of the of K-Ras *onc* 62nd mCherry K101D&R102E in mCherry channel.

3.13.2 Visualization of EGFP labeled Gα Proteins in N2-a cells after Site-Directed Mutagenesis

In this study, Gαi, Gα11, and Gα13 were chosen for site-directed mutagenesis experiments to mimic the dimerization interface on the K-Ras protein. In Figure 3.52, the 121st position EGFP tagged Gαi N256K & K257R, 246th position EGFP tagged Gα11 Y261K&P262R, and 215th position tagged Gα13 N278K were mutated. Proteins were imaged using a confocal microscope for the proper trafficking in live cell.

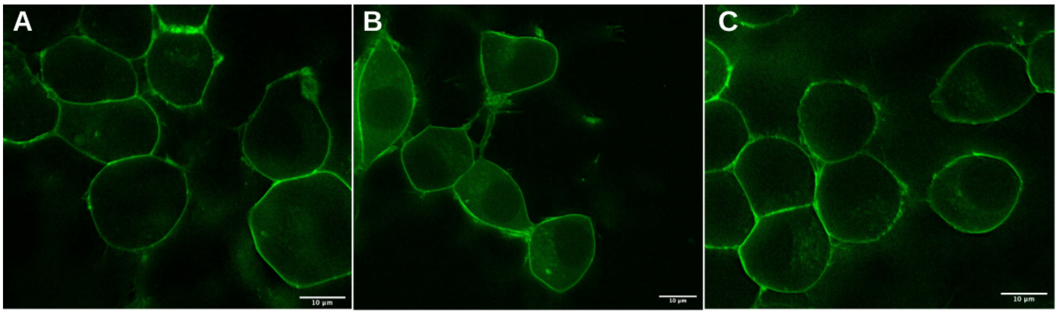

Figure 3.52: Confocal images of mutated Gαi, Gα11, and Gα13 in live N2-a cells, 63X magnification, 10 µm scale line. (A) Image of the of Gαi 121st EGFP N256K & K257R in EGFP channel. (B) Image of the of Gα11 246th EGFP Y261K&P262R in EGFP channel. (C) Image of the of Gα13 215th EGFP N278K in EGFP channel.

3.14 Interaction of K-Ras *wt*/K-Ras *onc* in terms of homo/hetero-dimerization detection & analysis

As mentioned, K-Ras has different dimerization interfaces, the α-interface or the β-interface. In this study, K-Ras dimerization was examined through its α-interface. Literature suggests that charge reversal mutations on K101 and R102 residues of K-Ras α-interface decrease the dimerization of K-Ras proteins by interfering with this interface (Muratcioglu, 2020).

In this study, the FRET technique was used to demonstrate the interaction efficiency of K-Ras dimerization. Firstly, K-Ras *wt* - K-Ras *wt* (non-oncogenic homolog) K101D&R102E constructs were transfected to study dimerization. Figure 3.53 shows that both EGFP and mCherry signals are visible on the channels, but the FRET signal seems more faded compared to K-Ras *wt* - K-Ras *wt* interaction's FRET signal as in Figure 3.18, and so does the FRET efficiency image.

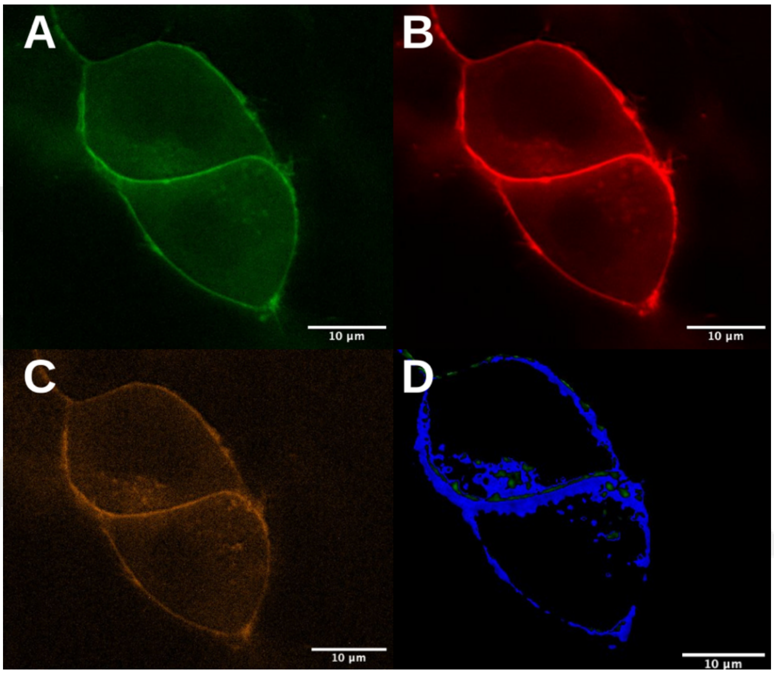

Figure 3.53: Confocal FRET images of K-Ras *wt* mCherry - K-Ras *wt* EGFP K101D&R102E in live N2-a cells, 63X magnification, 10 µm scale line. (A) Image of the EGFP channel. (B) Image of the mCherry channel. (C) Image of the FRET channel. (D) Image of the FRET efficiency in color scale.

After observing dimerization decrease in K-Ras *wt* - K-Ras *wt* K101D&R102E pair, K-Ras *wt* K101D&R102E - K-Ras *wt* K101D&R102E pair was transfected to N2-a cell for FRET studies. As a result, no signal was obtained in the FRET channel in Figure 3.54, which implied interference with the interface caused a decrease in the dimerization thus, observed FRET efficiency.

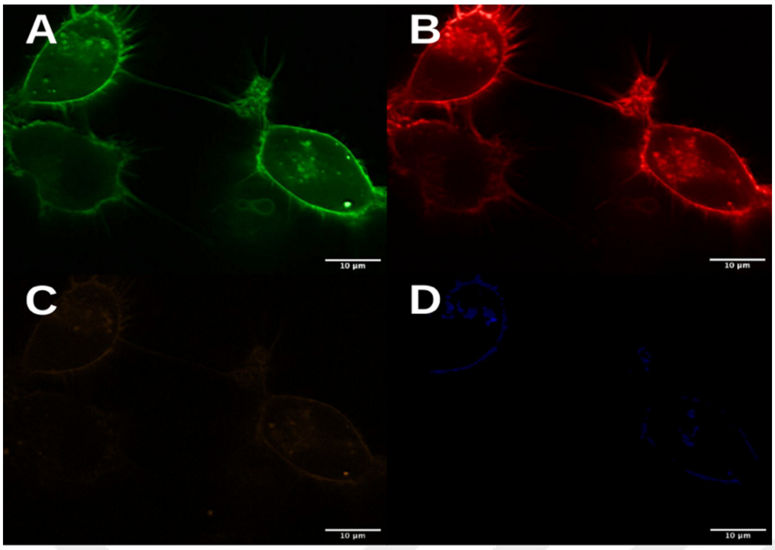

Figure 3.54: Confocal FRET images of K-Ras *wt* K101D&R102E mCherry - K-Ras *wt* EGFP K101D&R102E in live N2-a cells, 63X magnification, 10 µm scale line. (A) Image of the EGFP channel. (B) Image of the mCherry channel. (C) Image of the FRET channel. (D) Image of the FRET efficiency in color scale.

Then, FRET results of "K-Ras *wt* - K-Ras *wt* K101D&R102E" and "K-Ras *wt* K101D&R102E - K-Ras *wt* K101D&R102E" were compared with "K-Ras *wt* - K-Ras *wt*" changes in distribution of FRET efficiency of the cells according to pixel counts was observed as shown in Figure 3.55A. K-Ras *wt* - K-Ras *wt* K101D&R102E pair was less dynamic and less efficient in dimerization compared to K-Ras *wt* - K-Ras *wt*. Moreover, K-Ras *wt* K101D&R102E - K-Ras *wt* K101D&R102E distribution is shifted towards the negative control. Mean values of K-Ras *wt* interactions, including their mutants, were represented by box plots to compare the changes in dimerization efficiencies in Figure 3.55B. As it can be seen from the figure, "K-Ras *wt* - K-Ras *wt*", "K-Ras *wt* - K-Ras *wt* K101D&R102E" "K-Ras *wt* - K-Ras *wt* K101D&R102E", "K-Ras *wt* K101D&R102E - K-Ras *wt* K101D&R102E" respectively showed a significant decrease in mean FRET efficiencies, and there is no significant difference between negative control and K-Ras *wt* K101D&R102E - K-Ras *wt* K101D&R102E dimer.

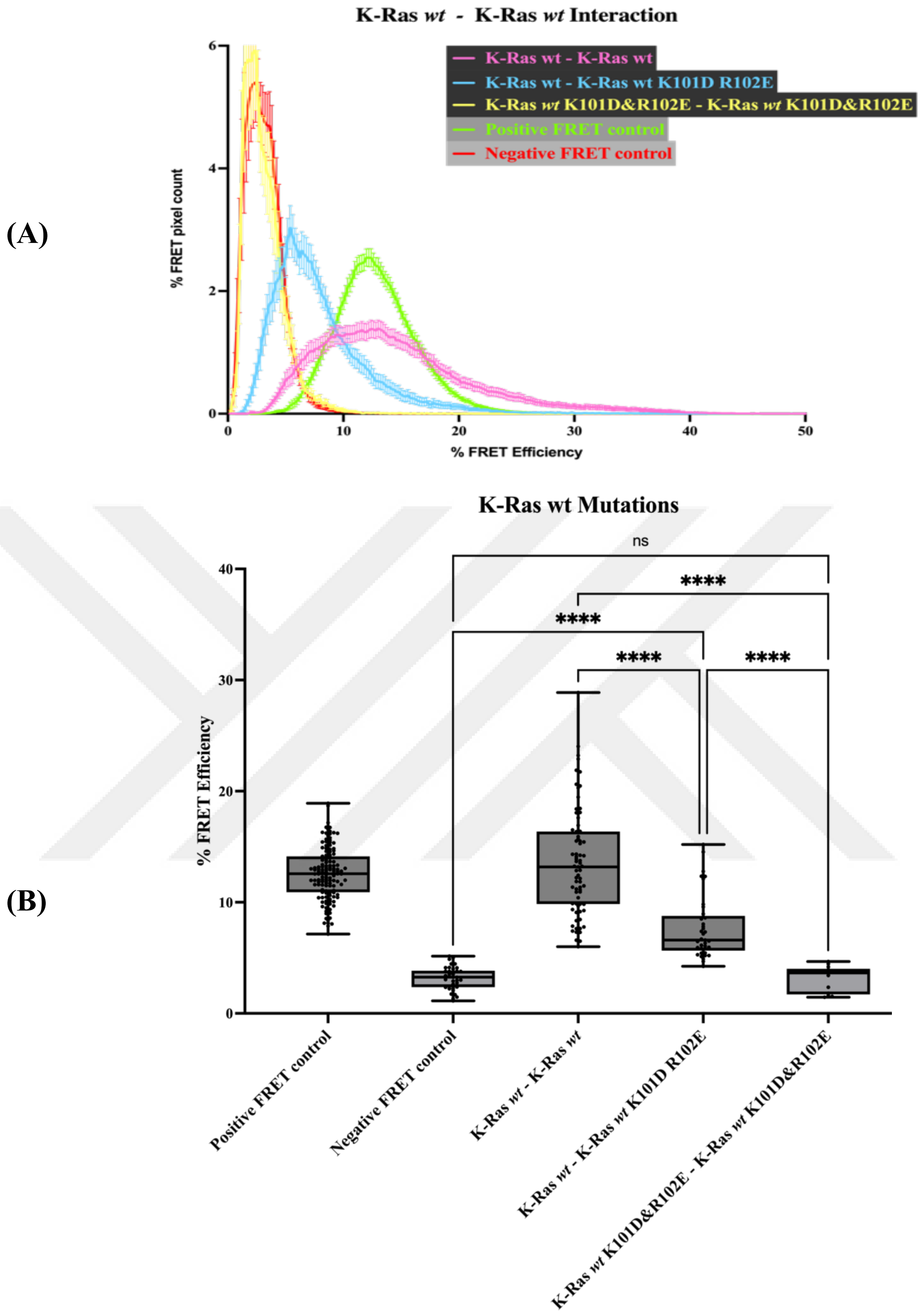

Figure 3.55: K-Ras *wt* - K-Ras *wt* and their dimerization interface mutated forms interaction FRET efficiency in line graph and box plot. (A) FRET efficiency in the line graph, FRET efficiency mean±SEM values distribution in the range. (B) FRET efficiency in the box plot, all cells mean FRET Efficiency. T-test statistical analysis was performed, significance level $p<0.05$.

After K-Ras *wt* was studied in its dimerization interface mutated form, K-Ras *onc* homolog also mutated on the dimerization interface, and FRET was measured under the same conditions. In Figure 3.56, the K-Ras *onc* - K-Ras *onc* K101D&R102E pair was co-expressed, and the FRET signal was collected. As a result, this pair had less FRET signal in the FRET channel compared to the K-Ras *onc* - K-Ras *onc* pair.

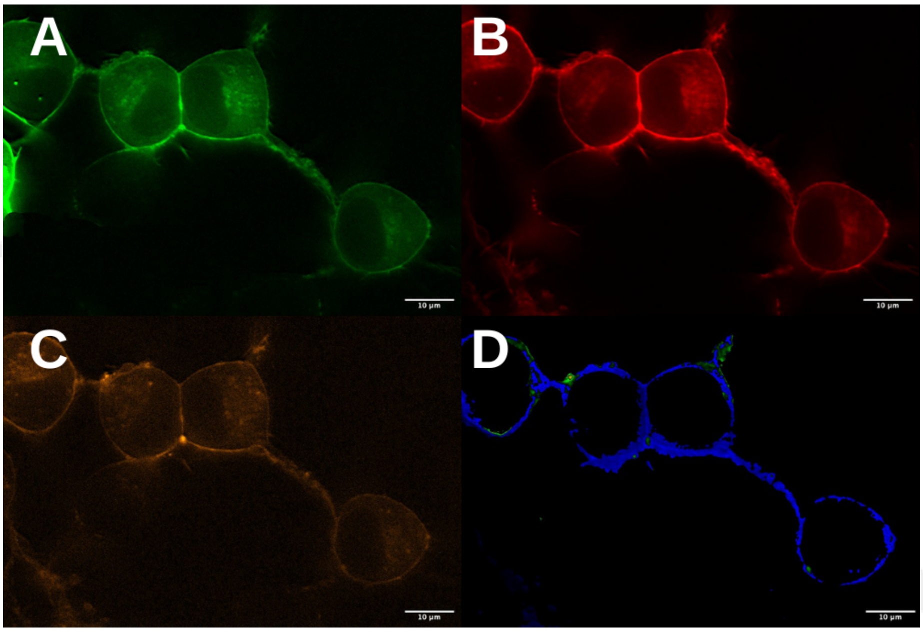

Figure 3.56: Confocal FRET images of K-Ras *onc* mCherry - K-Ras *onc* EGFP K101D&R102E in live N2-a cells, 63X magnification, 10 µm scale line. (A) Image of the EGFP channel. (B) Image of the mCherry channel. (C) Image of the FRET channel. (D) Image of the FRET efficiency in color scale.

Then, K-Ras *onc* K101D&R102E - K-Ras *onc* K101D&R102E pair were studied for the interaction, and no FRET signal was detected in the FRET channel while EGFP and mCherry signals were present in Figure 3.57.

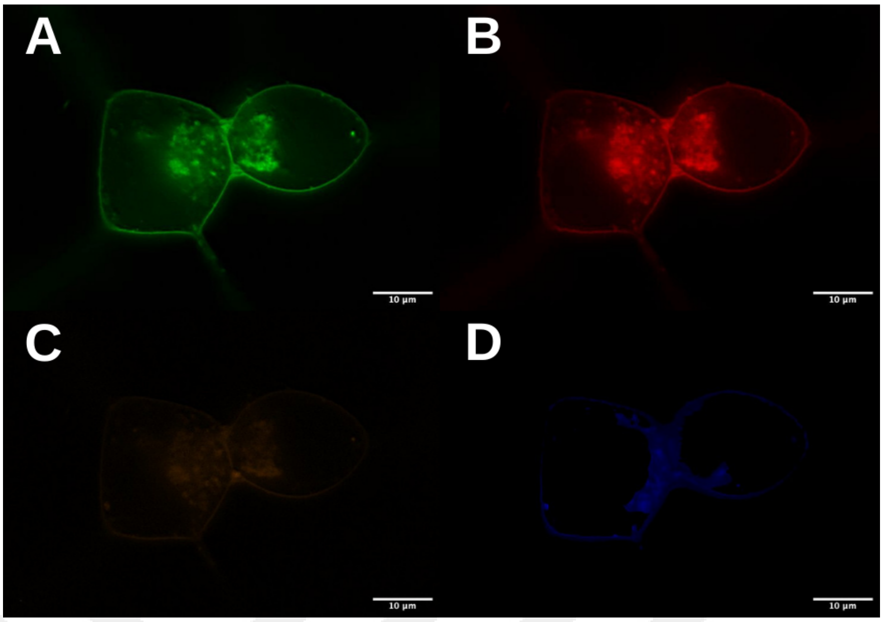

Figure 3.57: Confocal FRET images of K-Ras *onc* mCherry K101D&R102E - K-Ras *onc* EGFP K101D&R102E in live N2-a cells, 63X magnification, 10 µm scale line. (A) Image of the EGFP channel. (B) Image of the mCherry channel. (C) Image of the FRET channel. (D) Image of the FRET efficiency in color scale.

All FRET efficiency calculations were compared with K-Ras *onc* - K-Ras *onc* interaction in Figure 3.58A. Similar to K-Ras *wt* mutation interactions, K-Ras *onc* mutations were shifted to negative control region on the graph in the order of K-Ras *onc* - K-Ras *onc* K101D&R102E to K-Ras *onc* K101D&R102E - K-Ras *onc* K101D&R102E pair. They had less efficient FRET and less dynamic interaction than K-Ras *onc* - K-Ras *onc* distribution. The mean values of FRET efficiencies for the K-Ras *onc* mutant interactions were put in box plots and given in Figure 3.58B. From K-Ras *onc* - K-Ras *onc* to K-Ras *onc* - K-Ras *onc* K101D&R102E and K-Ras *onc* K101D&R102E - K-Ras *onc* K101D&R102E pairs, FRET efficiency means were decreased significantly, which suggests mutations at this region interfere with the dimerization. Moreover, K-Ras *onc* K101D&R102E - K-Ras *onc* K101D&R102E interaction is not significantly different than the negative FRET control.

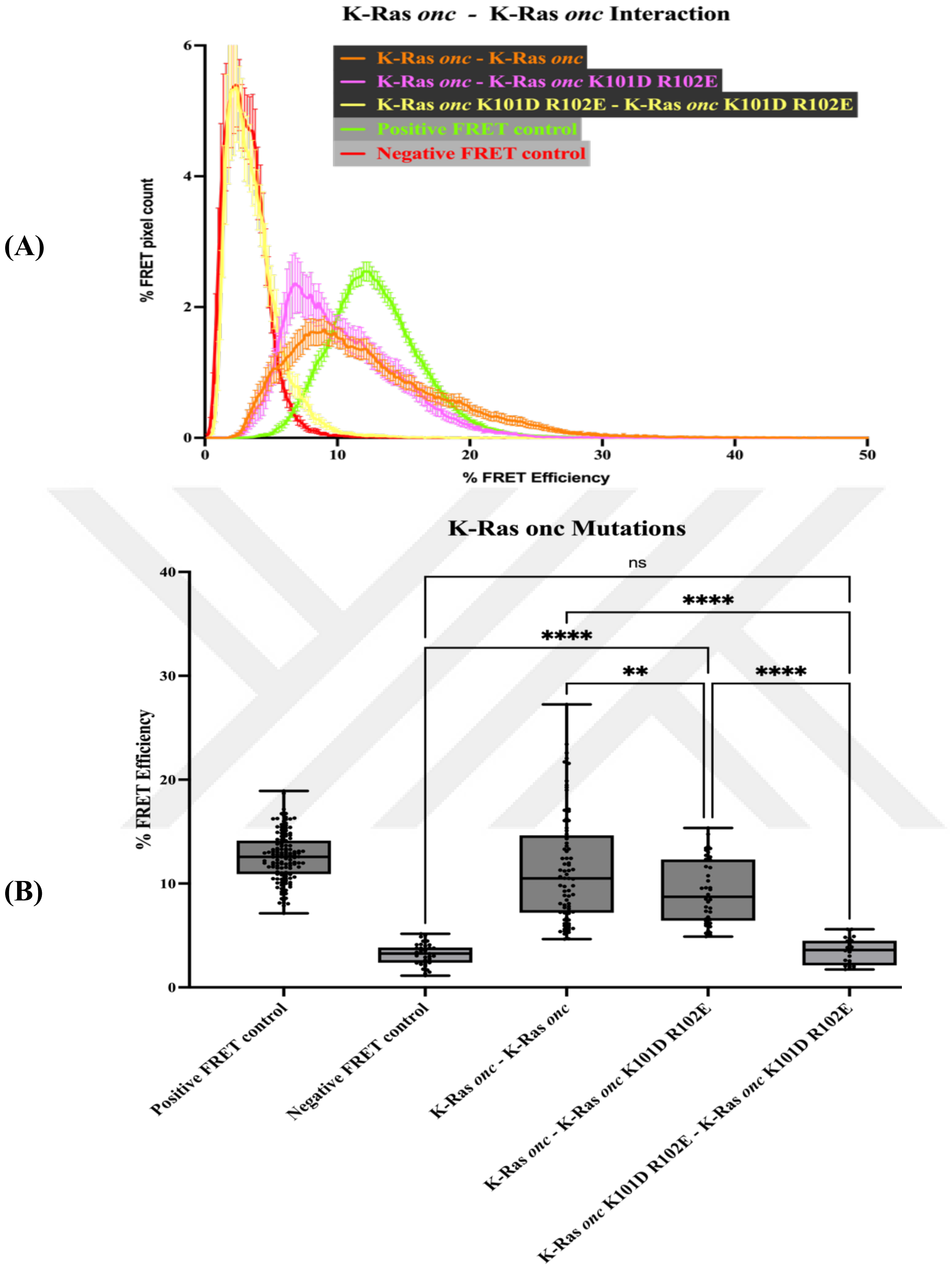

Figure 3.58: K-Ras *onc* –K-Ras *onc* and their dimerization interface mutated forms interaction FRET efficiency in line graph and box plot. (A) FRET efficiency in the line graph, FRET efficiency mean±SEM values distribution in the range. (B) FRET efficiency in the box plot, all cells mean FRET Efficiency. T-test statistical analysis was performed, significance level $p<0.05$.

To check if there are any differences between K-Ras *wt* and K-Ras *onc* mutations in FRET efficiencies, interaction ranges, and distribution were compared with the line graph in Figure 3.59A. K-Ras *wt* - K-Ras *wt* K101D&R102E and K-Ras *onc* - K-Ras *onc* K101D&R102E pairs show similar ranges and K-Ras *wt* K101D&R102E - K-Ras *wt* K101D&R102E and K-Ras *onc* K101D&R102E - K-Ras *onc* K101D&R102E interactions overlap with negative FRET control efficiency. Then, these distributions were compared in their cell's efficiency mean values to see differences in Figure 3.59B. After employing the One-Way ANOVA test, there was no significant difference between K-Ras *wt* - K-Ras *wt* K101D&R102E and K-Ras *onc* - K-Ras *onc* K101D&R102E. Moreover, K-Ras *wt* K101D&R102E - K-Ras *wt* K101D&R102E and K-Ras *onc* K101D&R102E - K-Ras *onc* K101D&R102E interactions do not have any significant difference between each other.

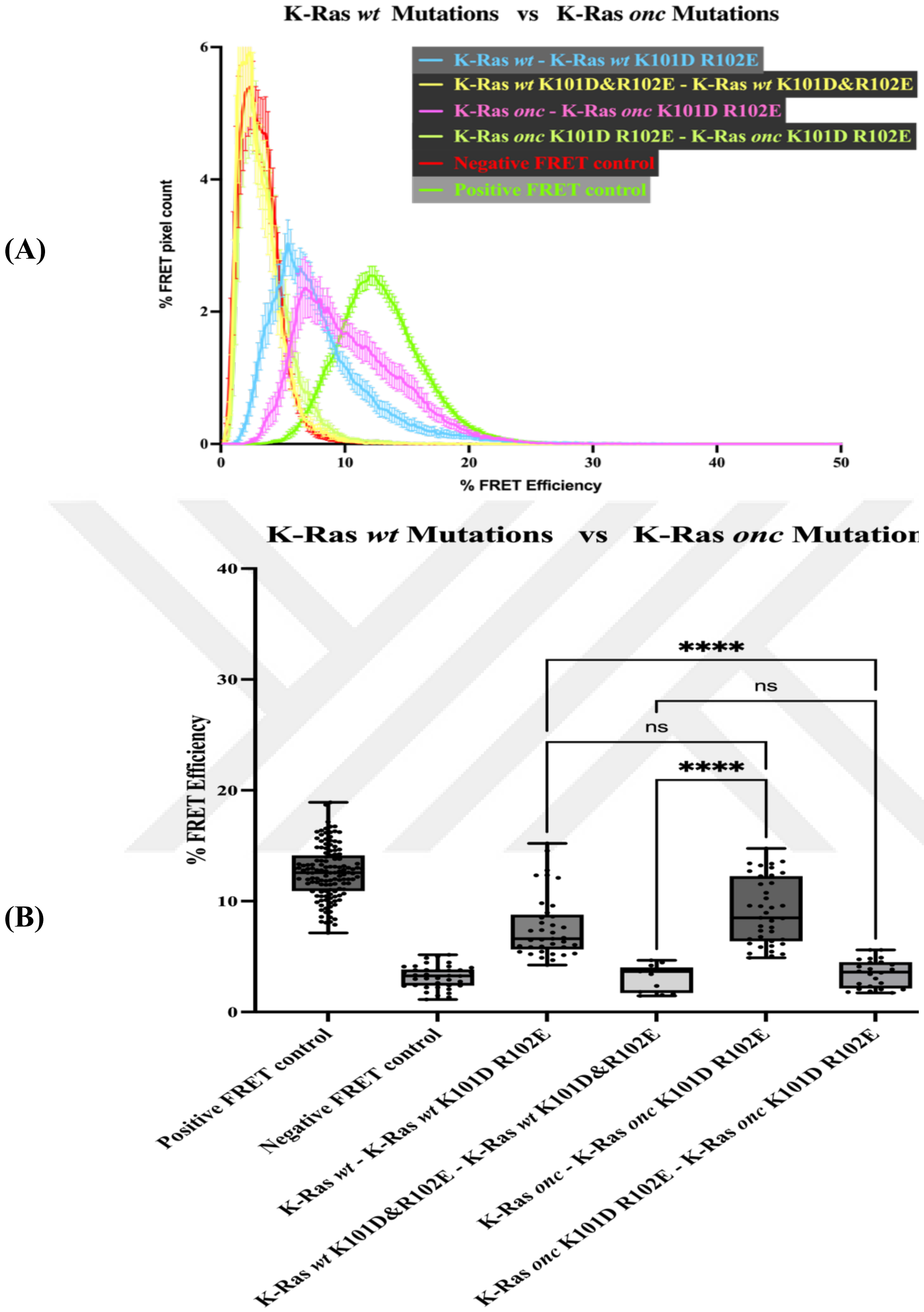

Figure 3.59: K-Ras *wt* –K-Ras *wt* vs K-Ras *onc* –K-Ras *onc* and their dimerization interface mutated forms interaction FRET efficiency in line graph and box plot. (A) FRET efficiency in the line graph, FRET efficiency mean±SEM values distribution in the range. (B) FRET efficiency in the box plot, all cells mean FRET Efficiency. T-test statistical analysis was performed, significance level $p<0.05$.

3.15 Interaction of K-Ras *wt*/K-Ras *onc* – Gαi1 Proteins and their mutated forms in terms of heterodimerization detection & analysis

After interfering with K-Ras – K-Ras dimerization in the dimerization interface, Gαi protein interaction with K-Ras was examined regarding Gαi G-domain changes.

Firstly, EGFP tagged Gαi N256K & K257R contrast that mimics K-Ras K101&R102 residues interaction with mCherry tagged K-Ras *wt* were examined with FRET technique in live cells under confocal microscope in Figure 3.60. Compared to the K-Ras *wt* – Gαi interaction in Figure 3.27, higher FRET signal was observed in the FRET channel under these conditions. Moreover, its FRET efficiency frame pixel distribution is at higher levels according to the 5 Ramps color code.

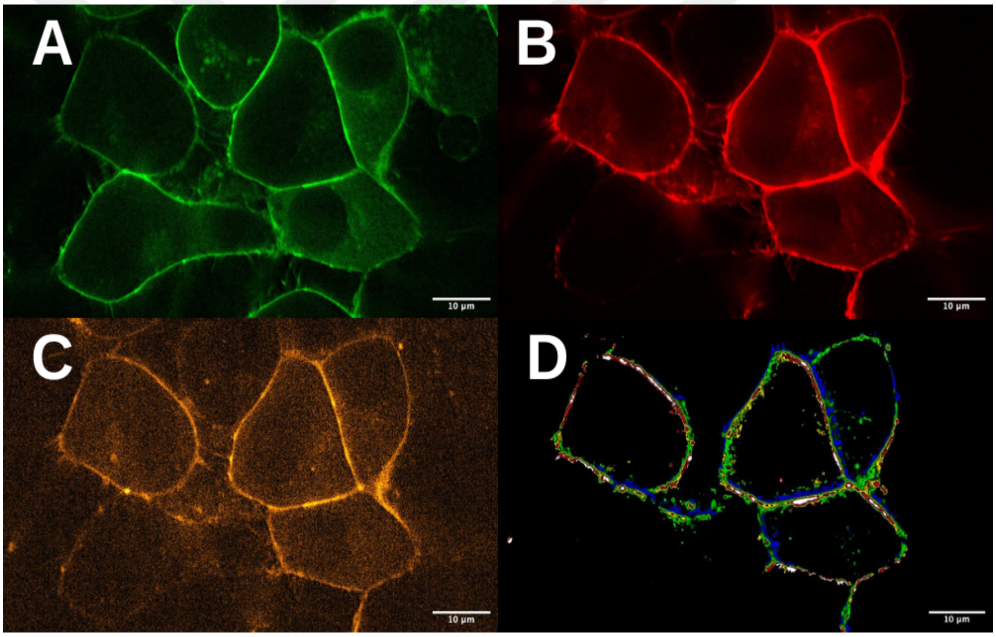

Figure 3.60: Confocal images of K-Ras *wt* – Gαi N256K & K257R in live N2-a cells, 63X magnification, 10 μm scale line. (A) Image of the EGFP channel. (B) Image of the mCherry channel. (C) Image of the FRET channel. (D) Image of the FRET efficiency in color scale.

Once examination of K-Ras *wt* – Gαi N256K & K257R interaction was completed, mCherry tagged K-Ras *wt* K101D&R102E– EGFP tagged Gαi N256K & K257R interaction was assessed in FRET technique under the same conditions. As a result, no FRET signal was detected in the FRET channel in Figure 3.61.

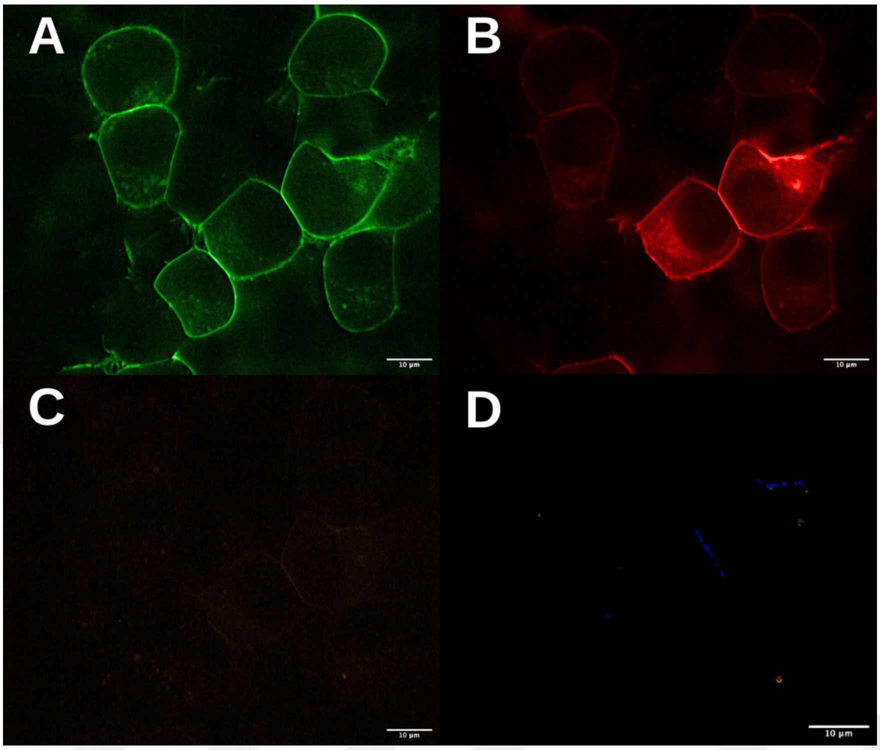

Figure 3.61: Confocal images of K-Ras *wt* K101D&R102E – Gαi N256K & K257R in live N2-a cells, 63X magnification, 10 µm scale line. (A) Image of the EGFP channel. (B) Image of the mCherry channel. (C) Image of the FRET channel. (D) Image of the FRET efficiency in color scale.

These two new interactions FRET efficiency distributions were compared with K-Ras *wt* - K-Ras *wt* and K-Ras *wt* – Gαi interaction visually in Figure 3.62A. K-Ras *wt* – Gαi N256K & K257R interaction has more dynamic interactions and wide distribution than all other interactions, which varies from 10% to 40% efficiency. Moreover, K-Ras *wt* K101D&R K-Ras *wt* – Gαi N256K & K257R102E– Gαi N256K & K257R interaction overlap with negative FRET control. In their mean values of FRET efficiencies in Figure 3.62B, the mean FRET efficiency of K-Ras *wt* – Gαi N256K & K257R interaction is significantly higher than K-Ras *wt* – K-Ras *wt*, K-Ras *wt* – Gαi and K-Ras *wt* K101D&R102E– Gαi N256K & K257R interactions.

Also, K-Ras *wt* K101D&R102E– Gαi N256K & K257R has no significant difference from negative FRET control.

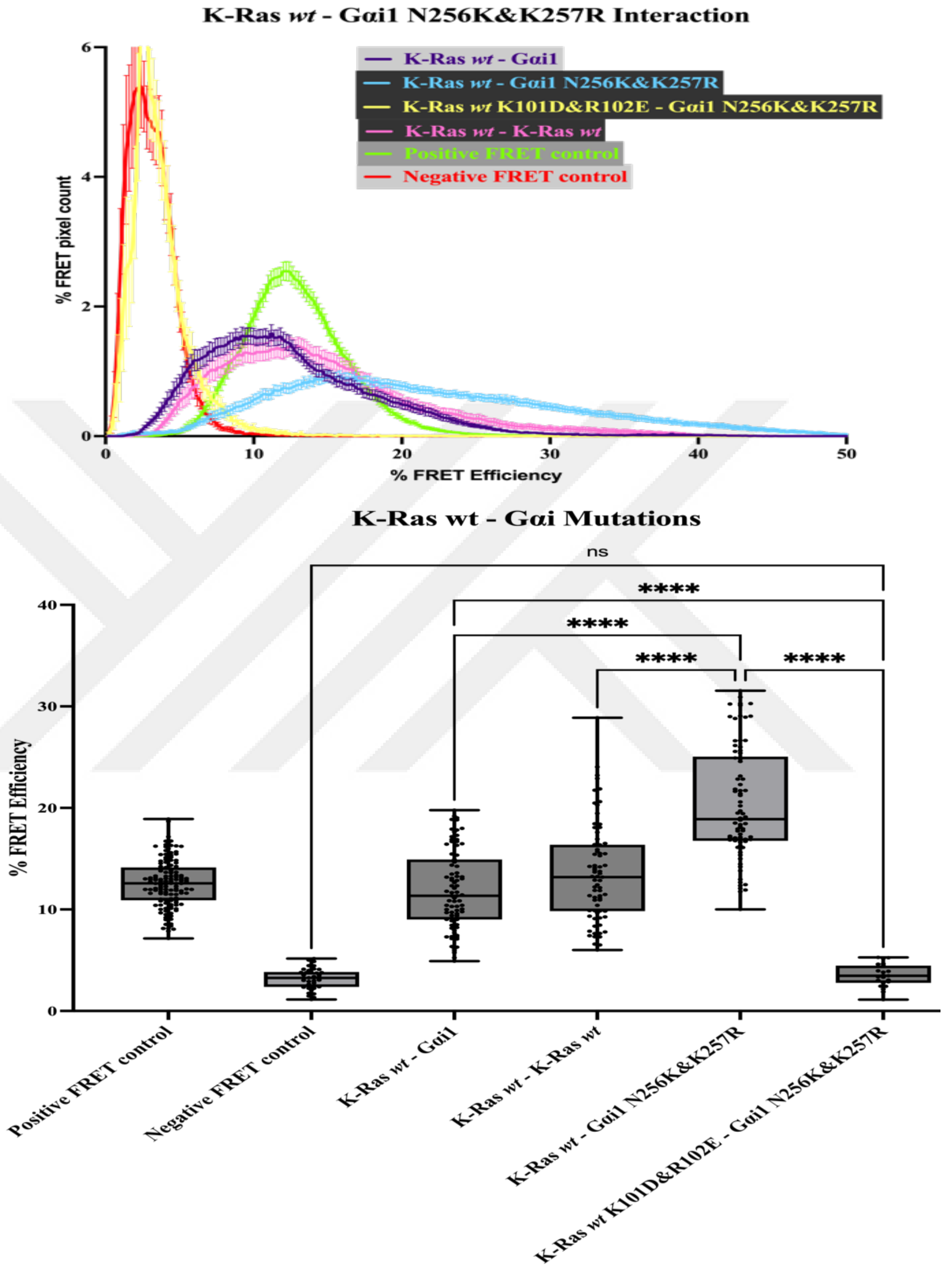

Figure 3.62: K-Ras *wt* – Gαi and K-Ras dimerization interface mutated & mimicked forms interaction FRET efficiency in line graph and box plot. (A) FRET efficiency in the line graph, FRET efficiency mean±SEM values distribution in the range. (B) FRET efficiency in the box plot, all cells mean FRET Efficiency. T-test statistical analysis was performed, significance level $p<0.05$.

The G-domain effect of K-Ras – Gαi interaction was also tested with the K-Ras *onc* homolog with the same mutations and conditions. As a result, in K-Ras *onc*– Gαi N256K & K257R, in Figure 3.63, more FRET signal was obtained compared to K-Ras *onc* - K-Ras *onc* in Figure 3.20. Moreover, in the FRET frame, pixel intensity is dense according to the color code.

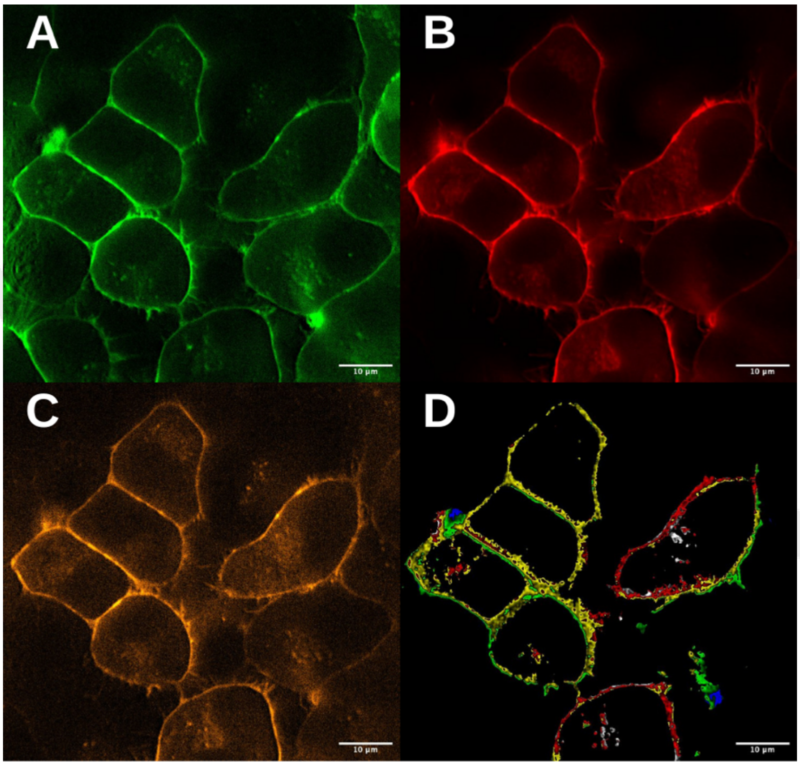

Figure 3.63: Confocal images of K-Ras *onc* – Gαi N256K & K257R in live N2-a cells, 63X magnification, 10 μm scale line. (A) Image of the EGFP channel. (B) Image of the mCherry channel. (C) Image of the FRET channel. (D) Image of the FRET efficiency in color scale.

In Figure 3.64: K-Ras *onc* K101D&R102E– Gαi N256K & K257R interaction was analyzed under a confocal microscope, and no FRET signal was observed in the FRET channel.

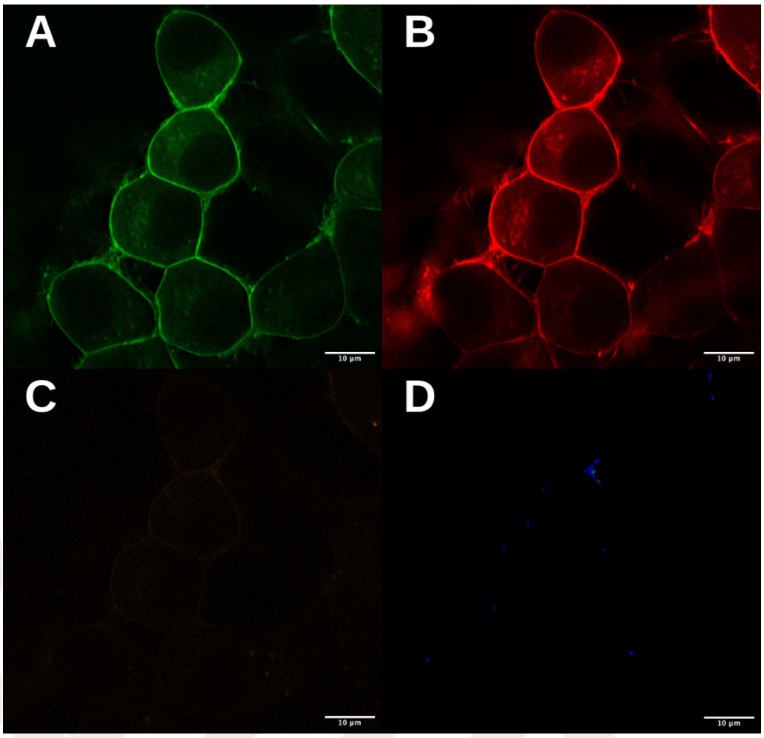

Figure 3.64: Confocal images of K-Ras *onc* K101D&R102E – Gαi N256K & K257R in live N2-a cells, 63X magnification, 10 µm scale line. (A) Image of the EGFP channel. (B) Image of the mCherry channel. (C) Image of the FRET channel. (D) Image of the FRET efficiency in color scale.

K-Ras *onc* – Gαi N256K & K257R interaction has a wide distribution and higher level in the FRET efficiency compared to K-Ras *onc* - K-Ras *onc* and K-Ras *onc* – Gαi interactions in Figure 3.65. In addition, K-Ras *onc* – Gαi N256K & K257R FRET efficiency distribution varies from 10% to 40%. also, K-Ras *onc* K101D&R102E – Gαi N256K & K257R interaction has same trend as negative control. Once these mutated pairs are compared in their FRET efficiency mean values, it is seen that K-Ras *onc* – Gαi N256K & K257R interaction is significantly higher from all other interactions and no significant difference between negative FRET control and K-Ras *onc* K101D&R102E – Gαi N256K & K257R pairs.

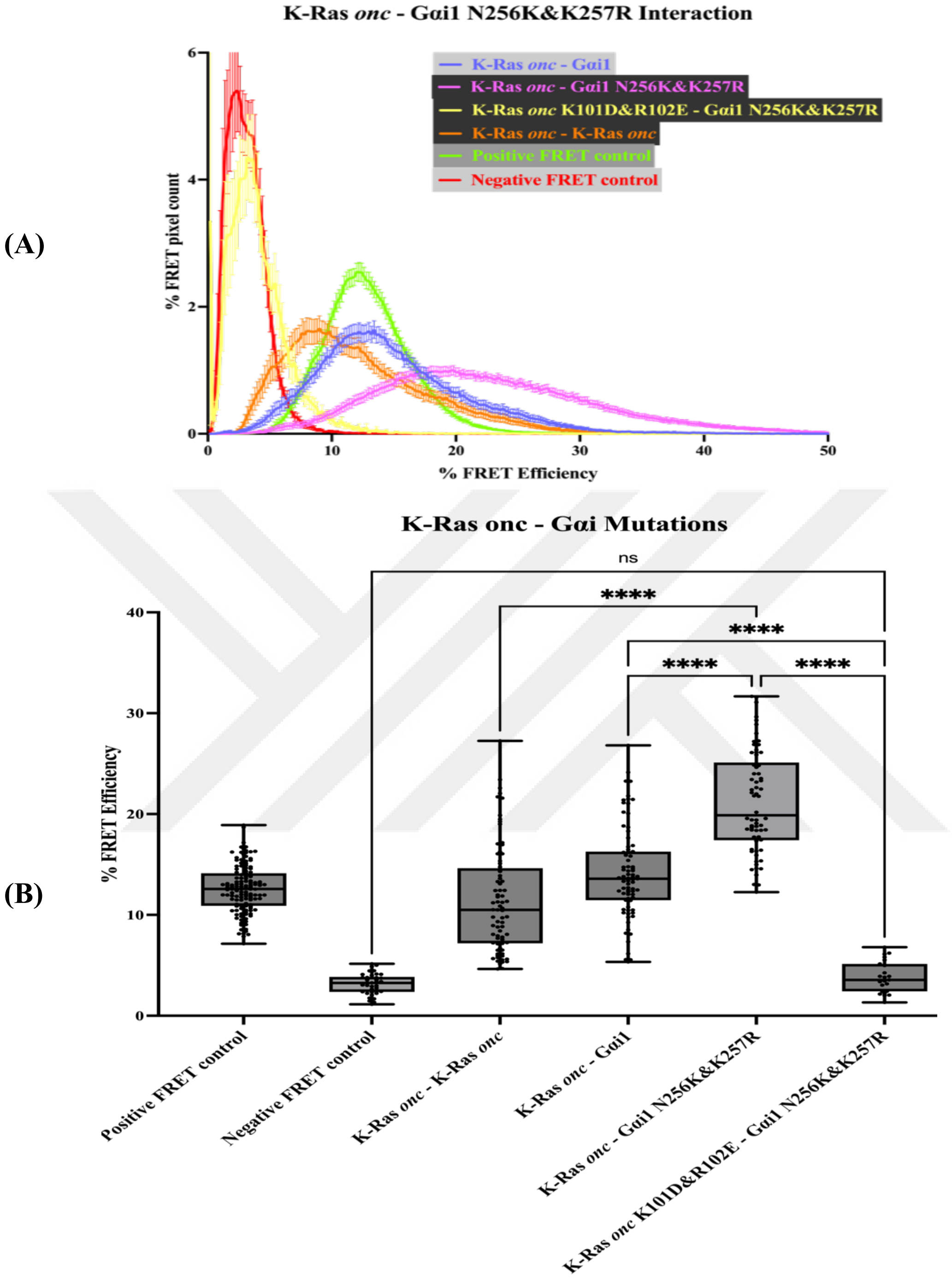

Figure 3.65: K-Ras *onc* – Gαi and K-Ras dimerization interface mutated & mimicked forms interaction FRET efficiency in line graph and box plot. (A) FRET efficiency in the line graph, FRET efficiency mean±SEM values distribution in the range. (B) FRET efficiency in the box plot, all cells mean FRET Efficiency. T-test statistical analysis was performed, significance level $p<0.05$.

3.16 Interaction of K-Ras *wt*/K-Ras *onc* – Gα11 Proteins and their mutated forms in terms of heterodimerization detection & analysis

After Gαi interactions with K-Ras *wt*, Gα11, and its mutated form were examined for interaction with K-Ras *wt.* EGFP tagged at 246th position Gα11 with Y261K&P262R mimic mutation was co-transfected with 62nd position mCherry tagged K-Ras *wt*. K-Ras *wt* - Gα11 Y261K&P262R interaction was assessed in the FRET technique in Figure 3.66. No signal was detected in the FRET channel from this interaction.

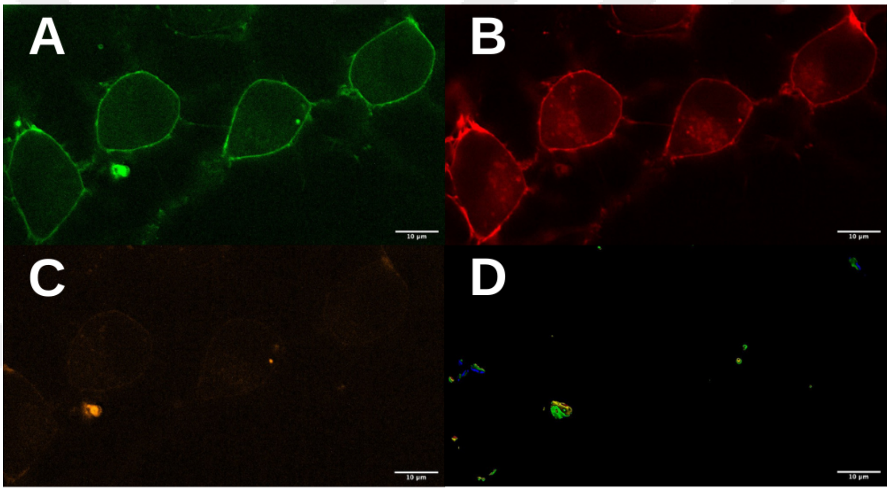

Figure 3.66: Confocal images of K-Ras *wt* – Gα11 Y261K&P262R in live N2-a cells, 63X magnification, 10 μm scale line. (A) Image of the EGFP channel. (B) Image of the mCherry channel. (C) Image of the FRET channel. (D) Image of the FRET efficiency in color scale.

Then, in figure 3.67, K-Ras *wt* K101D&R102E and Gα11 Y261K&P262R interaction was examined and similar to other Gα11 studies, no signal was detected in FRET channel.

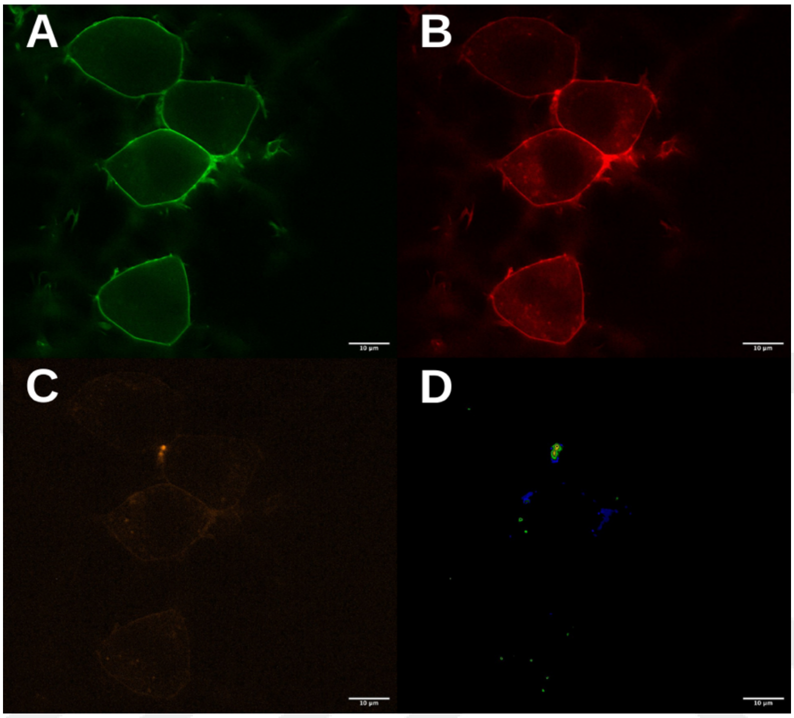

Figure 3.67: Confocal images of K-Ras *wt* K101D&R102E – Gα11 Y261K&P262R in live N2-a cells, 63X magnification, 10 µm scale line. (A) Image of the EGFP channel. (B) Image of the mCherry channel. (C) Image of the FRET channel. (D) Image of the FRET efficiency in color scale.

K-Ras *wt* - Gα11 Y261K&P262R and K-Ras *wt* K101D&R102E - Gα11 Y261K&P262R FRET efficiency distribution was presented in the line graph of K-Ras *wt* - K-Ras *wt* and K-Ras *wt* - Gα11 distributions, and these mutated interactions overlap with negative FRET control in Figure 3.68A. Mean values of FRET efficiencies were tested for K-Ras *wt* - Gα11 Y261K&P262R and K-Ras *wt* K101D&R102E - Gα11 Y261K&P262R interactions, and no significant differences were found in them from negative FRET control.

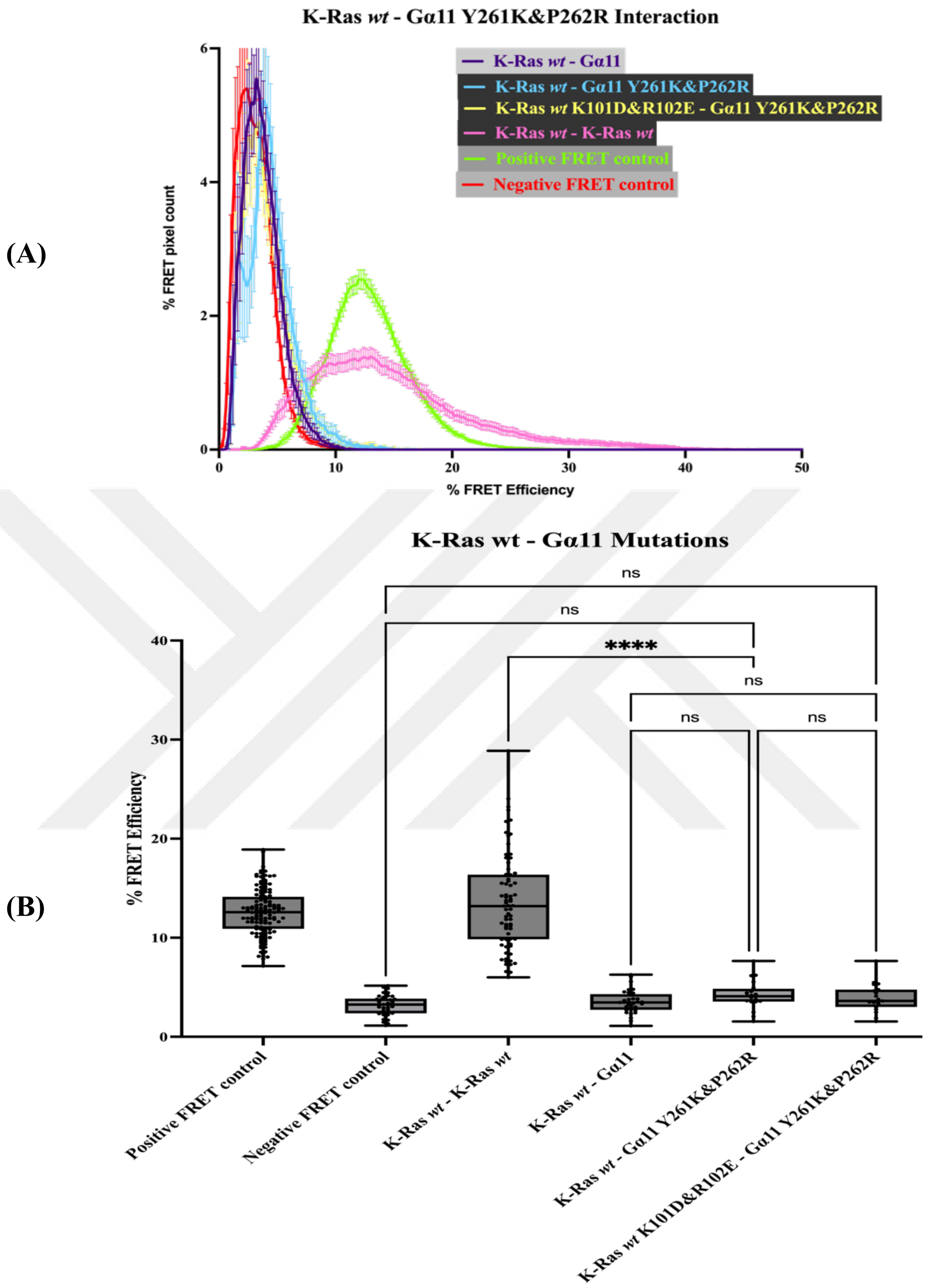

Figure 3.68: K-Ras *wt* – Gα11 and K-Ras dimerization interface mutated & mimicked forms interaction FRET efficiency in line graph and box plot. (A) FRET efficiency in the line graph, FRET efficiency mean±SEM values distribution in the range. (B) FRET efficiency in the box plot, all cells mean FRET Efficiency. T-test statistical analysis was performed, significance level $p<0.05$.

Gα11 Y261K&P262R mutation also evaluated its interaction with K-Ras *onc* protein in the same FRET technique conditions. Similar to interaction with K-Ras *wt,* K-Ras *onc* - Gα11 Y261K&P262R did not give a signal in the FRET channel in Figure 3.69.

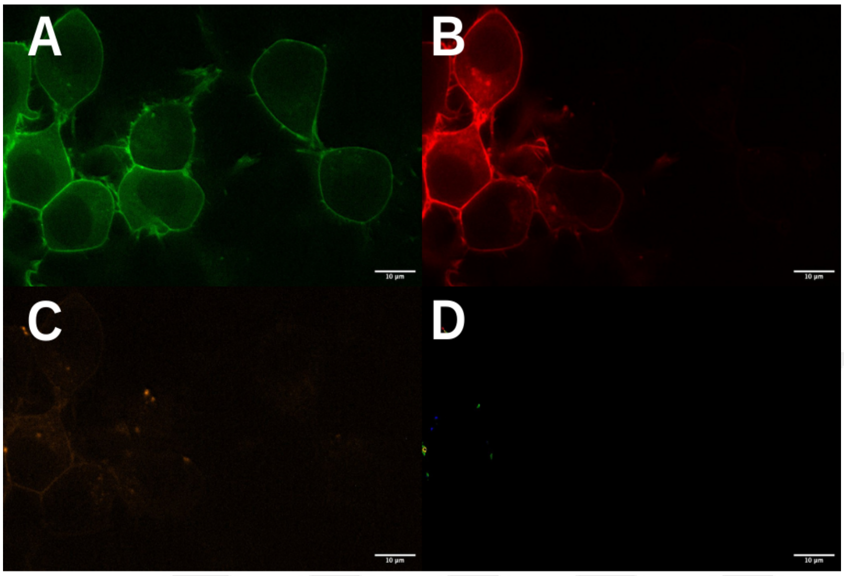

Figure 3.69: Confocal images of K-Ras *onc* – Gα11 Y261K&P262R in live N2-a cells, 63X magnification, 10 µm scale line. (A) Image of the EGFP channel. (B) Image of the mCherry channel. (C) Image of the FRET channel. (D) Image of the FRET efficiency in color scale.

In addition, FRET studies of K-Ras *onc* K101D&R102E - Gα11 Y261K&P262R interaction gave no signal in the FRET channel even though both proteins were co-expressed, as seen in relative channels in Figure 3.70.

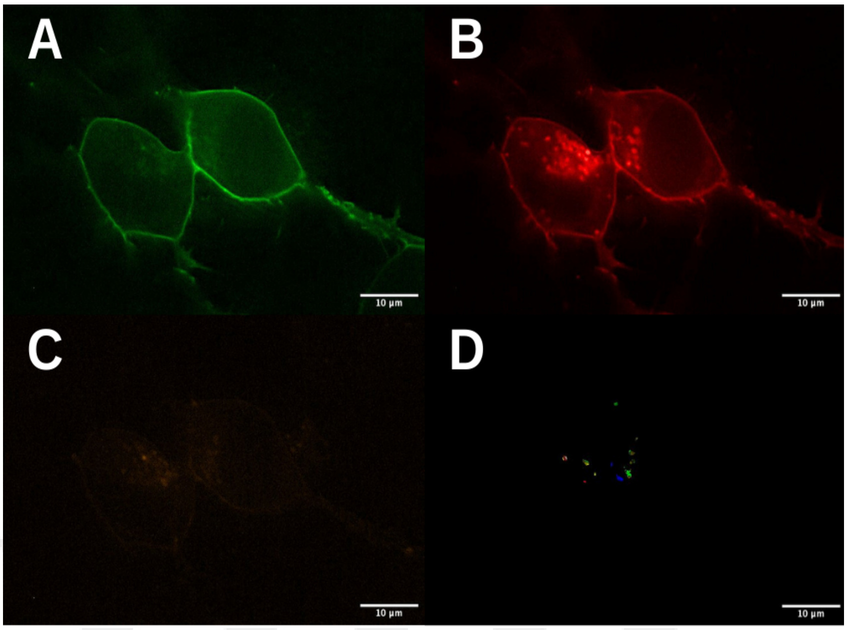

Figure 3.70: Confocal images of K-Ras *onc* K101D&R102E –Gα11 Y261K&P262R in live N2-a cells, 63X magnification, 10 µm scale line. (A) Image of the EGFP channel. (B) Image of the mCherry channel. (C) Image of the FRET channel. (D) Image of the FRET efficiency in color scale.

In Figure 3.71A, all Gα11 interactions, K-Ras *onc* - Gα11, K-Ras *onc* - Gα11 Y261K&P262R, and K-Ras *onc* K101D&R102E - Gα11 Y261K&P262R gave lower than 5% FRET efficiency as in the case for negative FRET control signal distribution. According to One Way ANOVA statistical analysis, there was no significant difference between K-Ras *onc* - Gα11, K-Ras *onc* - Gα11 Y261K&P262R, and K-Ras *onc* K101D&R102E - Gα11 Y261K&P262R interactions FRET efficiency mean values from negative FRET control according to Figure 3.71B.

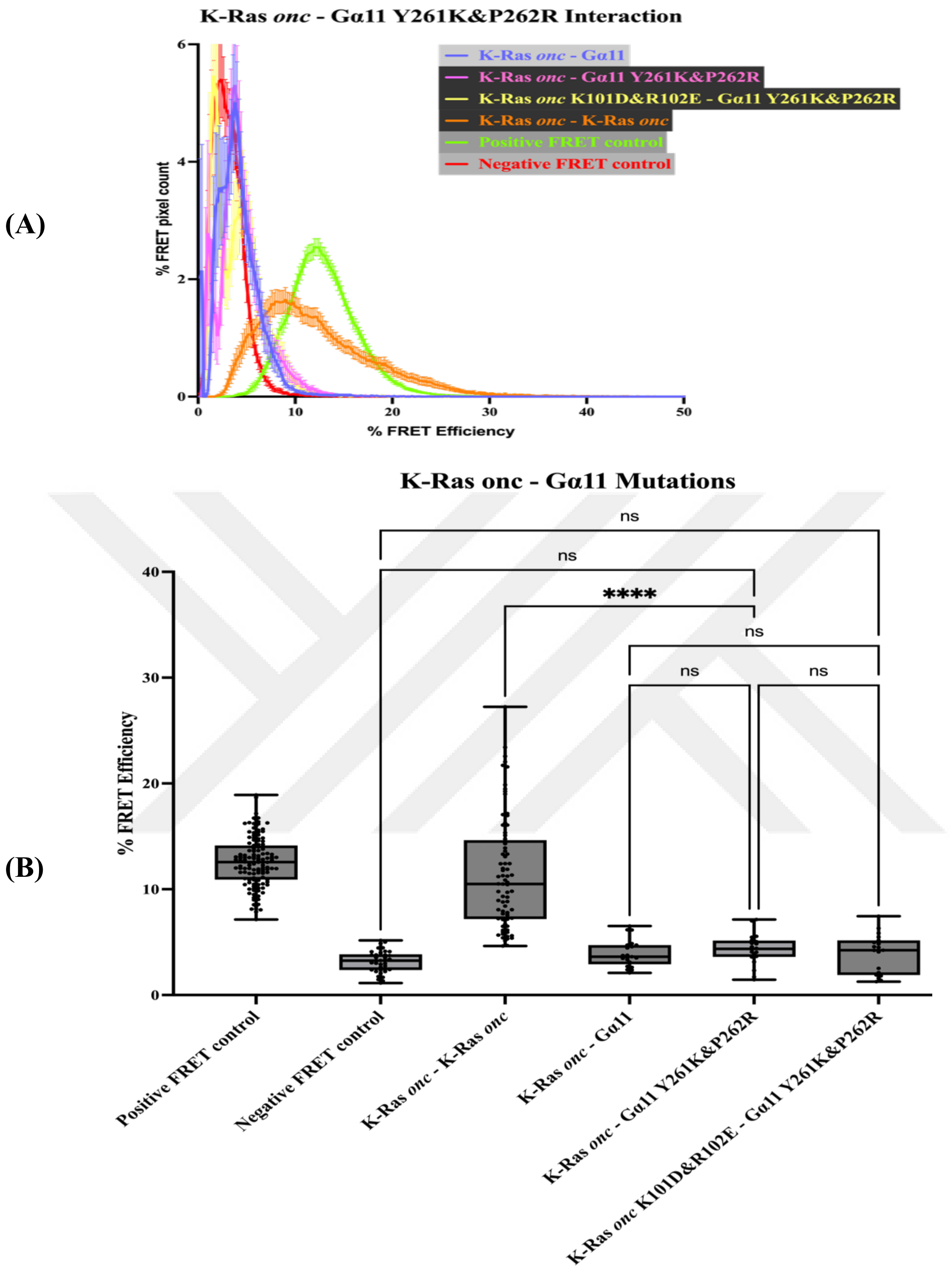

Figure 3.71: K-Ras *onc* – Gαi and K-Ras dimerization interface mutated & mimicked forms interaction FRET efficiency in line graph and box plot. (A) FRET efficiency in line graph, FRET efficiency mean±SEM values distribution in the range. (B) FRET efficiency in box plot, all cells mean FRET Efficiency. T-test statistical analysis was performed, significance level p<0.05.

3.17 Interaction of K-Ras *wt*/K-Ras *onc* – Gα13 Proteins and their mutated forms in terms of heterodimerization detection & analysis

The last protein studied for G-domain importance for K-Ras interaction was Gα13. To mimic K-Ras dimerization interface hotspot residues, 215th position EGFP tagged Gα13 N278K co-transfected to N2-a cells with 62nd position mCherry tagged K-Ras *wt.* Figure 3.72 shows an increased FRET signal compared to the K-Ras *wt* - Gα13 interaction in Figure 3.41. Moreover, pixel count in FRET efficiency seemed to increase in number.

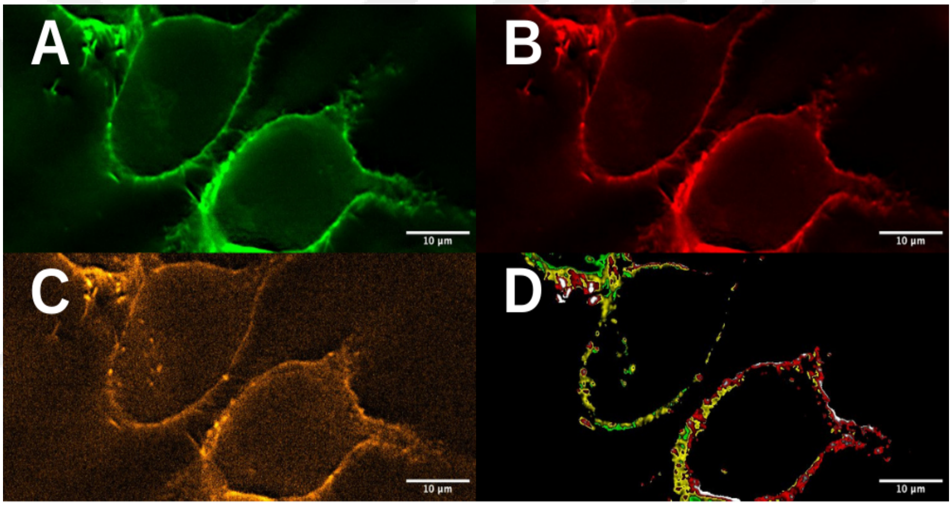

Figure 3.72: Confocal images of K-Ras *wt* -Gα13 N278K in live N2-a cells, 63X magnification, 10 μm scale line. (A) Image of the EGFP channel. (B) Image of the mCherry channel. (C) Image of the FRET channel. (D) Image of the FRET efficiency in color scale.

Then, the dimerization interface interfered with 62nd position mCherry tagged K-Ras *wt* K101D&R102E was expressed with same EGFP tagged Gα13 N278K protein to examine the interaction with FRET technique. According to Figure 3.73, the FRET signal was not observed in the FRET channel.

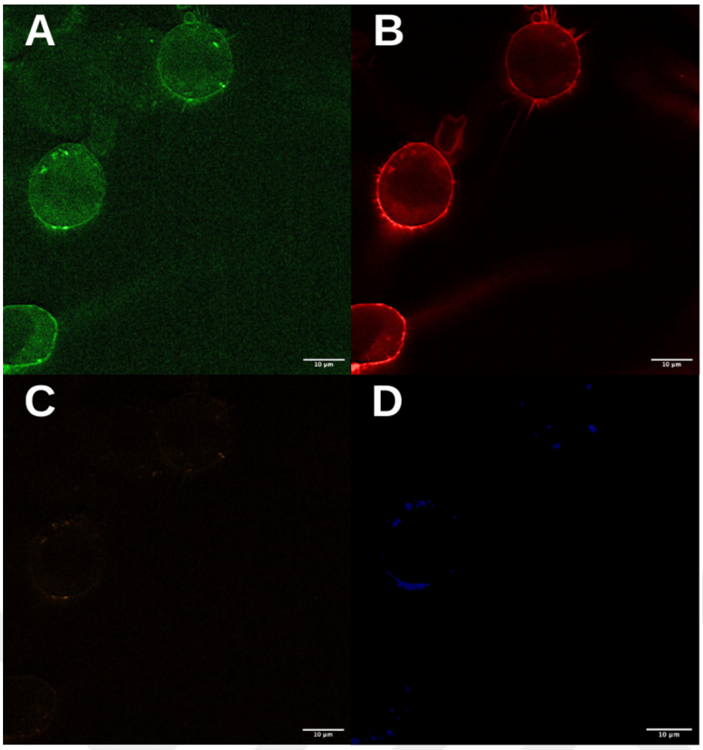

Figure 3.73: Confocal images of K-Ras *wt* K101D&R102E-Gα13 N278K in live N2-a cells, 63X magnification, 10 µm scale line. (A) Image of the EGFP channel. (B) Image of the mCherry channel. (C) Image of the FRET channel. (D) Image of the FRET efficiency in color scale.

When all FRET efficiency distributions of K-Ras *wt* - Gα13 and their mutants were merged in the line graph in Figure 3.74A, it is seen that the K-Ras *wt* - Gα13 N278K pair has very dynamic interaction varying from 10% to 40%. On the other hand, K-Ras *wt* K101D&R102E - Gα13 N278K interaction has the same trend as negative FRET control. According to the cell's FRET efficiency mean values of interaction in Figure 3.74B, K-Ras *wt* - Gα13 N278K has significantly higher FRET efficiency compared to K-Ras *wt*- K-Ras *wt,* K-Ras *wt* - Gα13 and K-Ras *wt* K101D&R102E - Gα13 N278K. Also, there is no significant difference between K-Ras *wt* K101D&R102E - Gα13 N278K and negative FRET control.

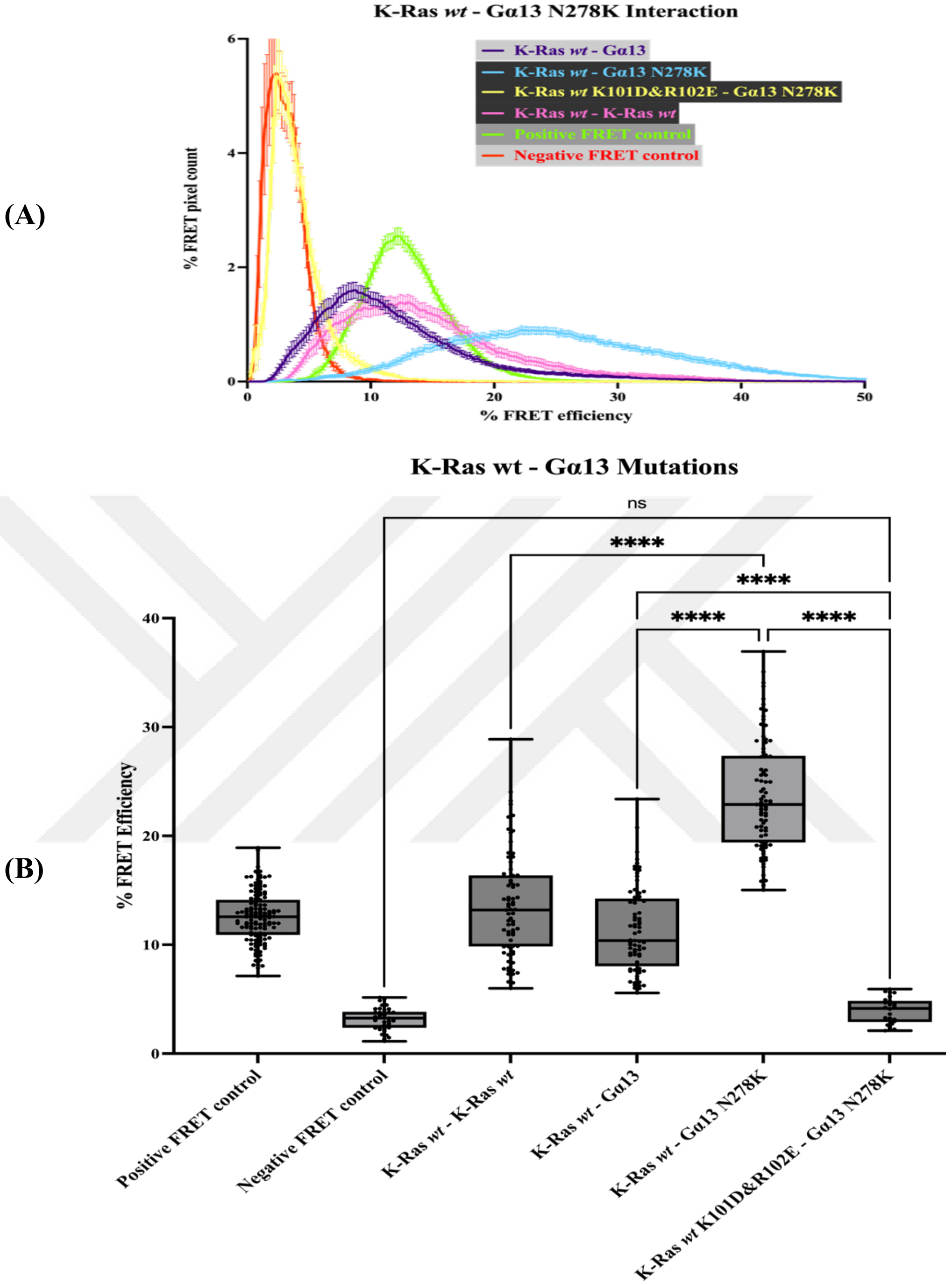

Figure 3.74: K-Ras *wt* – Gα13 and K-Ras dimerization interface mutated & mimicked forms interaction FRET efficiency in line graph and box plot. (A) FRET efficiency in the line graph, FRET efficiency mean±SEM values distribution in the range. (B) FRET efficiency in the box plot, all cells mean FRET Efficiency. T-test statistical analysis was performed, significance level $p<0.05$.

Gα13 mimic mutations were also tested with K-Ras *onc* protein to see the effect on the interaction under the same FRET conditions. In Figure 3.75, the FRET channel of K-Ras *onc* - Gα13 N278K has a higher signal compared to K-Ras *onc* - K-Ras *onc* in Figure 3.20. Also, a denser pixel count in the FRET efficiency frame is observed.

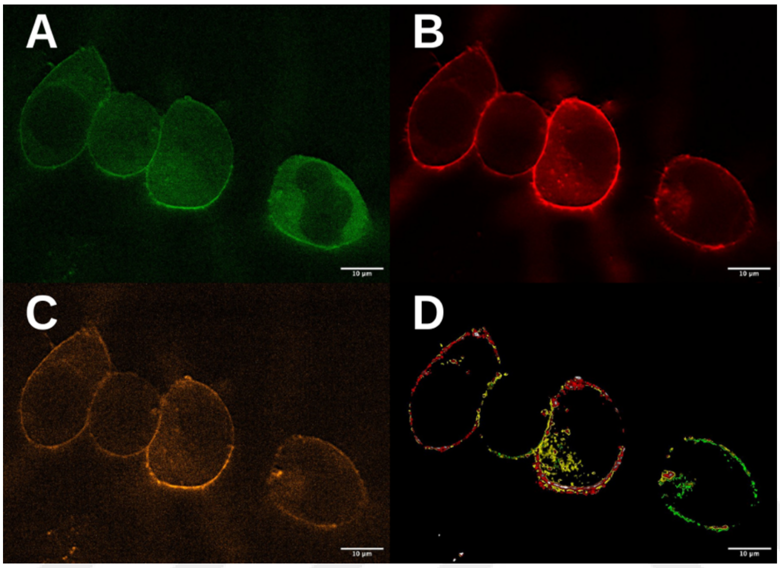

Figure 3.75: Confocal images of K-Ras *onc* -Gα13 N278K in live N2-a cells, 63X magnification, 10 µm scale line. (A) Image of the EGFP channel. (B) Image of the mCherry channel. (C) Image of the FRET channel. (D) Image of the FRET efficiency in color scale.

Then, Gα13 N278K, was tested for interaction with K-Ras *onc* K101D&R102E. Similar to the negative FRET control a relatively low FRET signal was detected in the FRET channel as represented in Figure 3.76.

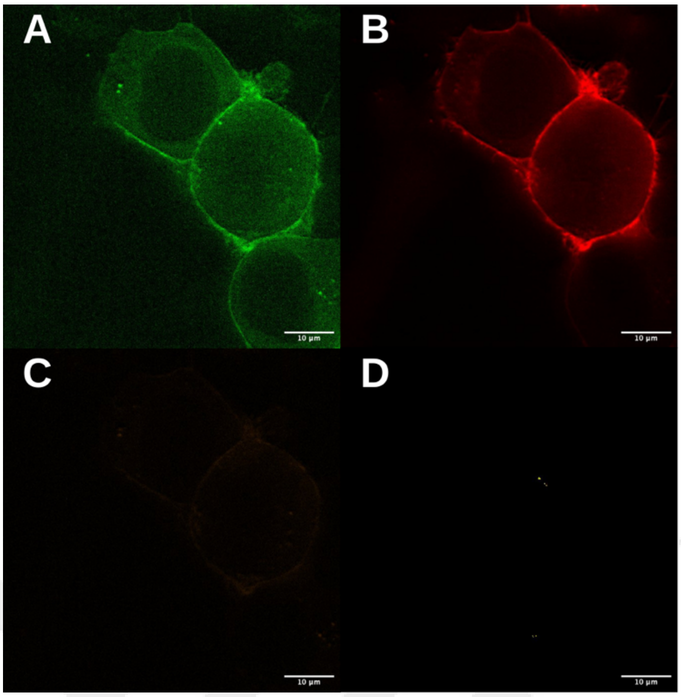

Figure 3.76: Confocal images of K-Ras *onc* K101D&R102E-Gα13 N278K in live N2-a cells, 63X magnification, 10 µm scale line. (A) Image of the EGFP channel. (B) Image of the mCherry channel. (C) Image of the FRET channel. (D) Image of the FRET efficiency in color scale.

Similar to K-Ras *wt* - Gα13 N278K interaction FRET efficiency distribution in Figure 3.74, K-Ras *onc* - Gα13 N278K has the same trend that shows dynamic interaction and wide range in the distribution in Figure 3.77A. Also, K-Ras *onc* K101D&R102E - Gα13 N278K interaction efficiency resulted in a similar plot as negative FRET control efficiency. After the statistical analysis, One Way ANOVA results show that the FRET efficiency mean of K-Ras *onc* - Gα13 N278K interaction resulted in a significantly higher value, and K-Ras *onc* K101D&R102E - Gα13 N278K gave similar FRET distribution with the negative FRET pair, data was plotted as in Figure 3.77B.

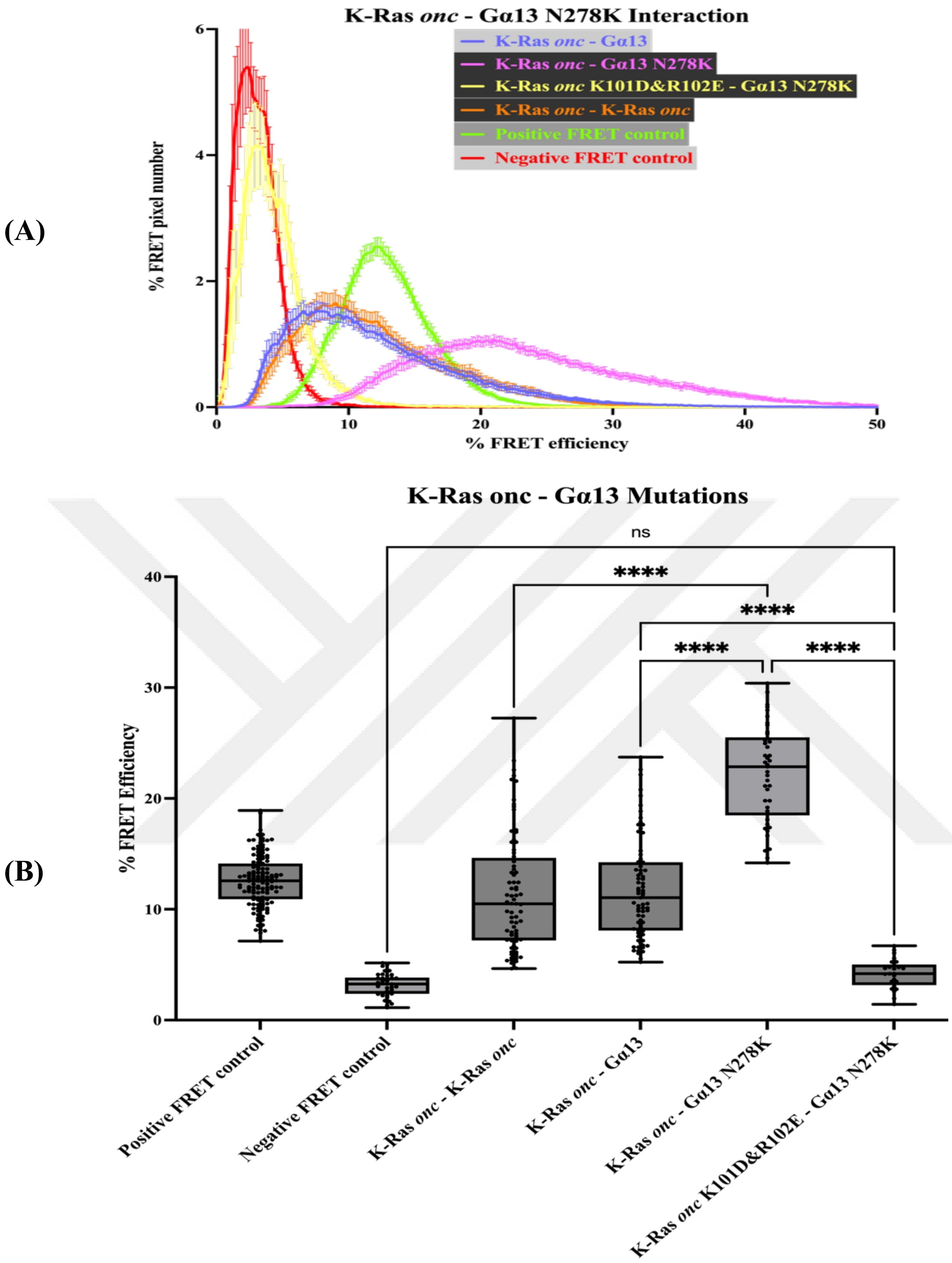

Figure 3.77: K-Ras *onc* – Gα13 and K-Ras dimerization interface mutated & mimicked forms interaction FRET efficiency in line graph and box plot. (A) FRET efficiency in the line graph, FRET efficiency mean±SEM values distribution in the range. (B) FRET efficiency in the box plot, all cells mean FRET Efficiency. T-test statistical analysis was performed, significance level $p<0.05$.

3.18 Protein expression levels of dimerized proteins via Western Blot

3.18.1 BSA protein concentration standard curve

The concentrations of BSA protein ranging from 0 µg/mL to 2000 µg/mL were assessed in Bradford Assay and absorbance was measured at 595 nm. Then, the standard curve was plotted as absorbance values against BSA concentrations to quantify unknown protein concentrations (Figure 3.78).

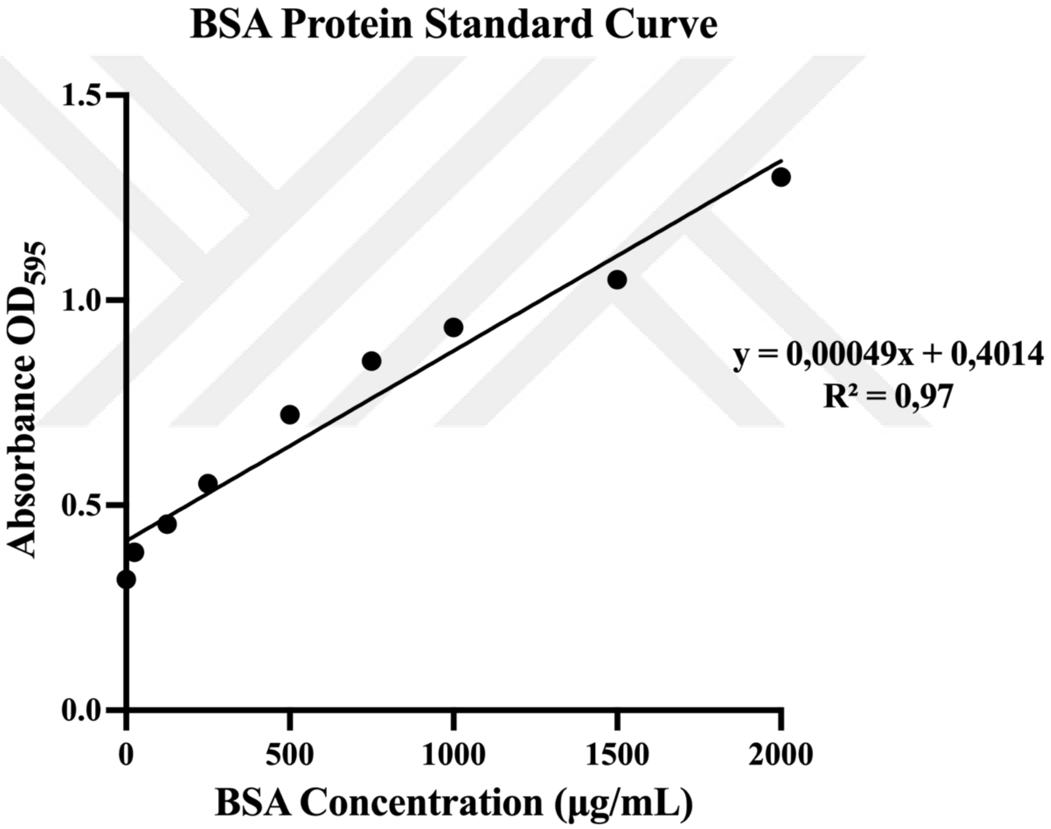

Figure 3.78: BSA Protein Standard Curve

3.18.2 K-Ras *wt*/K-Ras *onc* homo-dimerization, K-Ras *wt*/K-Ras *onc* - Gα Proteins hetero-dimerization and mutated K-Ras *wt*/K-Ras *onc* - Gα Proteins hetero-dimerization protein expression

Figure 3.79 shows the protein expression levels using anti-K-Ras and anti-GAPDH in FRET studies. Western Blot studies were done to show all constructs were expressed in same amount. As a result, presence of K-Ras and its expression levels in FRET studies were observed. Their expression levels were approximately same when comparing GAPDH home-keeping protein expression levels in each blot.

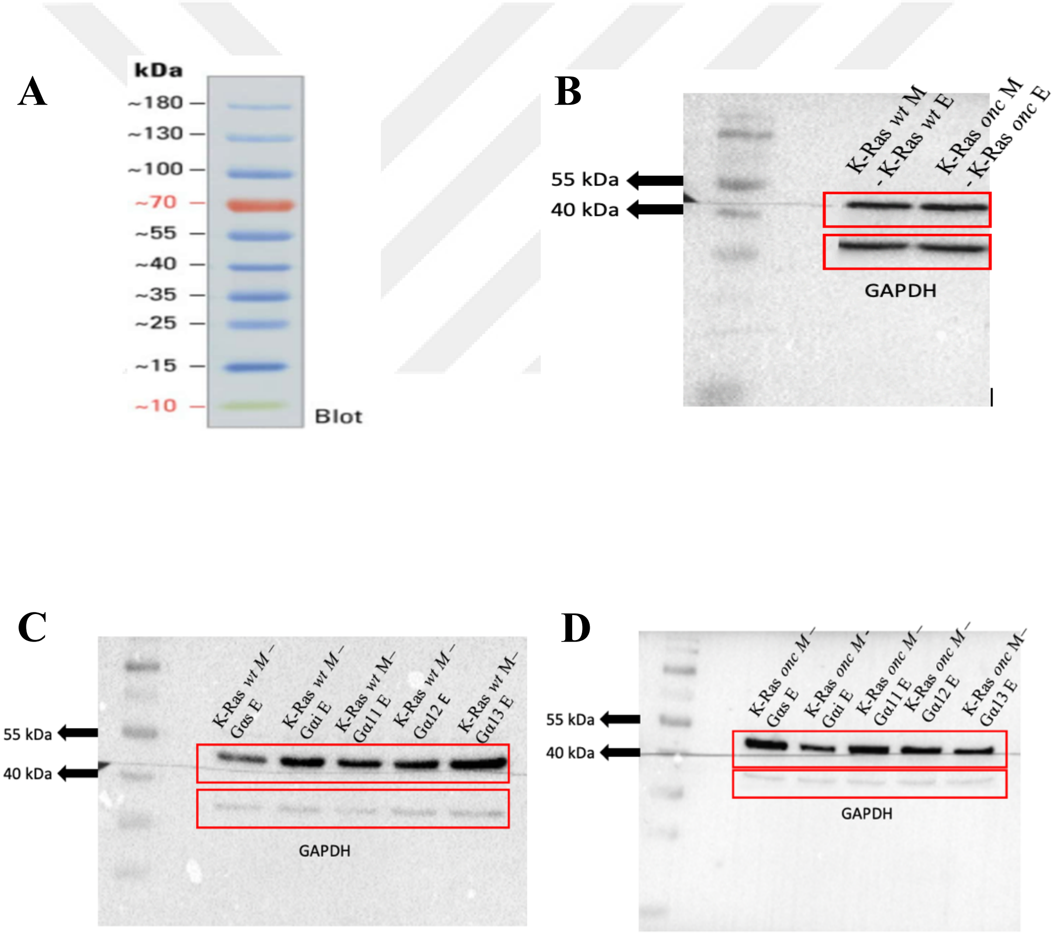

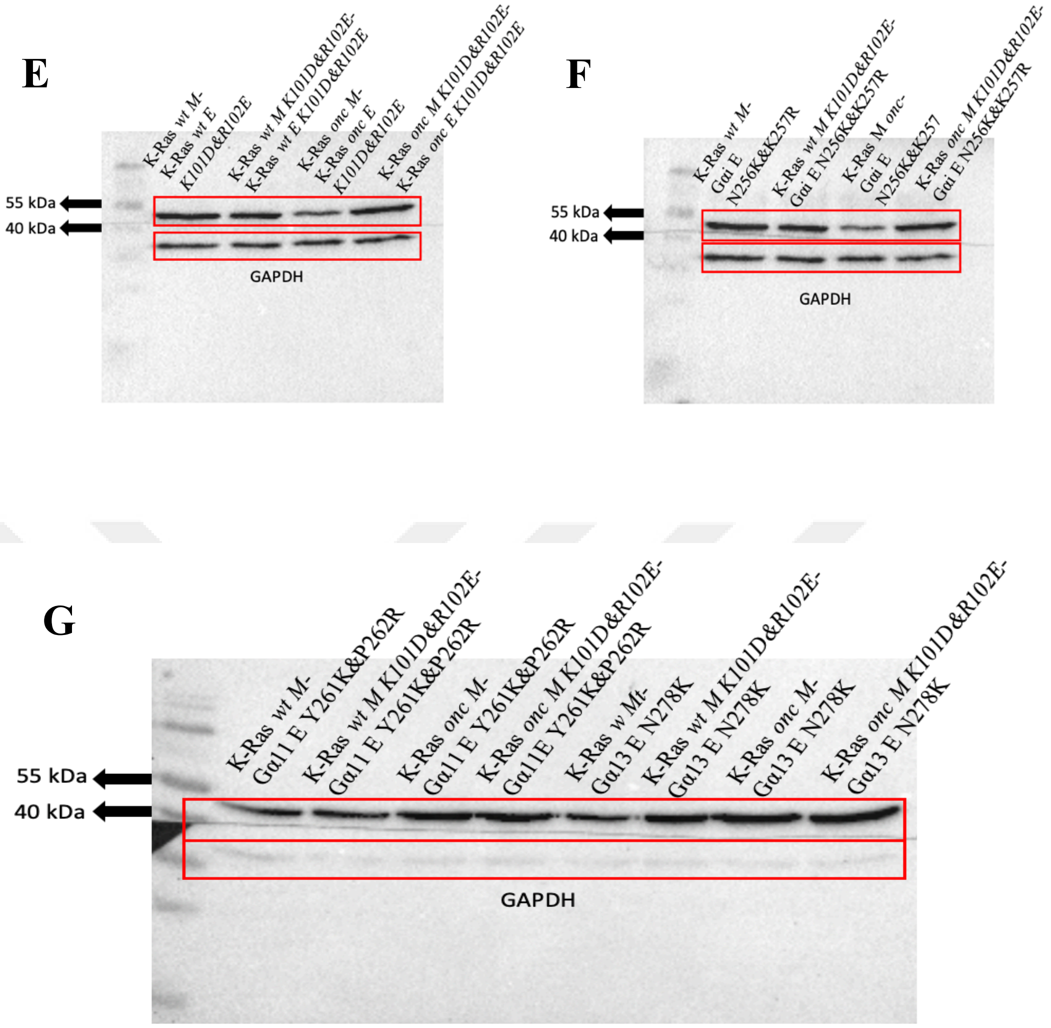

Figure 3.79: Western Blot images of proteins used in FRET studies. (A) 180 kDa Protein Ladder. (B) K-Ras *wt/onc* homodimerization. (C) K-Ras *wt* - Gα proteins heterodimerization. (D) K-Ras *onc* - Gα proteins heterodimerization. (E) K-Ras *wt/onc* mutated dimerization interface. (F) K-Ras *wt/onc* – Gαi mimicked & mutated dimerization interface. (G) K-Ras *wt/onc* – Gα11/ Gα13 mimicked & mutated dimerization interface.

CHAPTER 4

DISCUSSION

In this study, the role of G-Domain on K-Ras and Gα Proteins dimerization was analyzed in live neuronal cells using a confocal microscope and comparing FRET measurements. The interaction studies were carried out following the presentation of EGFP and mCherry tagged K-Ras and EGFP tagged Gα Protein expression on the plasma membrane. Firstly, the previously reported K-Ras – K-Ras homodimerization, was validated with the FRET technique using both K-Ras wild-type or K-Ras oncogenic homodimers. According to the literature K-Ras dimerizes through its G-Domain on the cell membrane (Nan *et al*., 2015). Moreover, our results show that there is no significant difference in dimerization efficiencies between K-Ras wild-type and K-Ras oncogenic. The difference between K-Ras oncogenic and K-Ras wild-type is the 12th amino acid mutation, which is glycine to aspartic acid (G12D) on oncogenic homolog that causes constitutive activation of the protein. Since the dimerization interface is away from this mutation site, it does not affect the dimerization efficiency of the protein. Therefore, K-Ras wild-type and K-Ras oncogenic have the same average dimerization efficiency, meaning a similar distance between the proteins.

Then, possible interactions of various Gα Proteins with K-Ras *wt/onc* was tested. Our results showed that Gαs, Gαi, Gα12, and Gα13 could dimerize with K-Ras on the plasma membrane in live cells. On the other hand, interaction studies between Gα11 – K-Ras demonstrated no significant difference in FRET efficiency from negative FRET control. This result suggests Gα11 – K-Ras may not interact under these conditions or the labeling sites were not suitable for the detection of possible interaction. As the labeling site was decided according to the structural alignment of all Gα proteins the latter possibility is unlikely thus we conclude these proteins are not interacting under our experimental conditions.

To understand the importance of α-interface dimerization of K-Ras, some amino acid residues were mutated to disrupt the dimerization interface. These critical residues on the α-interface play a vital role in K-Ras dimerization. Charge reversal mutations were applied on 101st and 102nd amino acids on K-Ras to test the importance of these hot spots. After application, K101D&R102E mutations were obtained in both K-Ras *wt* and K-Ras *onc* proteins. As a result, K-Ras – K-Ras K101D&R102E interaction had a significant decrease in FRET efficiency compared to K-Ras – K-Ras interaction, and the proteins, although relatively weaker, still dimerize in the presence of a mutation in one of the proteins. This implies that the α-interface has a role in K-Ras dimerization. This result was previously shown in the literature, and we showed that under our experimental conditions, the two residues in the interface is enough to disrupt the interaction measured by FRET. In addition to the literature, our results showed that the same effect can be seen in the oncogenic G12D mutant version of K-Ras.

Both K-Ras and Gα proteins share G-domain in their structures, literature and our results showed that two residues that affect homodimerization α-interface are located in the G-domain which may play an important role in the interaction of these proteins. In this study, Gα proteins were aligned according to their structures and coding sequences with K-Ras protein, and residues were found on Gα proteins, which corresponded to K-Ras α-interface hot spots amino acids, K101 and R102. Gαi had N256 and K257 residues, and Gα13 had N278 and R279 residues corresponding to K-Ras. Therefore, to mimic K101&R102 amino acids on the α-interface of K-Ras, on Gαi, N256, and K257 residues were mutated to N256K and K257R, and on Gα13, only N278 was mutated to N278K since the second residue was already R279 which was same amino acid on R102 of K-Ras. The interactions between K-Ras *wt*/*onc* - Gαi N256K&K257R and K-Ras *wt*/*onc* – Gα13 N278K were tested. Results showed increased efficiency in the interaction compared to K-Ras *wt*/*onc* – Gαi or K-Ras *wt*/*onc* – Gα13 interaction and created a more favorable binding environment to K-Ras. Moreover, K-Ras *wt*/*onc* - Gαi N256K&K257R and K-Ras *wt*/*onc* – Gα13 N278K heterodimerization efficiency values distribute in a high range, which may show a more variable interaction between protein pairs, or this can be due to tetramer or oligomer formation in addition to the dimerization of proteins and causes high interaction points in some regions and relatively low interaction in some other regions that create varying efficiency distribution. Protein interaction dynamics change according to interaction states such as dimerization, tetramerization, or oligomerization and occur in different efficiencies. For example, in positive FRET control, FRET efficiency distribution is narrow since two fluorophores are linked and all FRET pairs in the cell transfer approximately the same energy on the plasma membrane. However, in higher-order interactions, fluorophore positions change and cause different efficiencies during these interactions. Our results indicate that mimicking K-Ras α-interface dimerization hot-spots on Gα proteins increases the interaction efficiency of K-Ras – Gαi and K-Ras – Gα13 proteins and create higher-order dynamic interactions on the plasma membrane.

Then, dimerization α-interface disrupted K-Ras interactions were tested with K-Ras α-interface mimicking mutations on Gα proteins. As a result, K-Ras *wt*/*onc* K101D&R102E - Gαi N256K&K257R and K-Ras *wt*/*onc* K101D&R102E – Gα13 N278K interaction had no significant difference from negative FRET control. Therefore, disrupting dimerization interface on K-Ras impairs interaction with Gαi and Gα13 as observed with dimerization-mimicking mutants. Moreover, these mimicking mutations on Gαi and Gα13 are not enough to rescue and recover when the interference mutations are present on the K-Ras dimerization interface, causing impairment in the interaction.

Mimicking studies were also carried out with the Gα11 protein. FRET results suggested that K-Ras *wt*/*onc* - Gα11 do not interact with each other. When the residues corresponding to the α-interface on Gα11 compared with K-Ras it has the most divergent sequence compared to all tested Gα proteins. To test if changing some of these residues to K-Ras similar residues could rescue dimerization we mutated

Gα11 to mimic the K-Ras dimerization interface after modeling studies. K101 and R102 amino acids on the K-Ras dimerization interface correspond to Y261 and P262 residues on Gα11. However, when Y261 and P262 residues were mutated to Y261K and P262R to mimic the K-Ras dimerization interface, the interaction efficiency did not increase between K-Ras *wt*/*onc* - Gα11 Y261K&P262R compared to K-Ras *wt*/*onc* - Gα11 interaction. There may be several reasons for these results. Firstly, these corresponding residues Y261 and P262 on Gα11 are less conserved than other Gα proteins and mutating only these residues may not be enough to mimic the K-Ras dimerization interface. Moreover, structural conformation changes after mutations on Gα11 may create a less favorable interaction environment with K-Ras due to the electrostatic properties of the amino acids around. K-Ras *wt*/*onc* K101D&R102E protein was also tested with Gα11 Y261K&P262R mimicking protein for interaction, and results were the same with negative control.

CHAPTER 5

CONCLUSION AND FUTURE STUDIES

5.1 Conclusion

K-Ras *wt* - K-Ras *wt* and K-Ras *onc* - K-Ras *onc* homodimerize on the cell membrane in live cells. Moreover, there is no difference between K-Ras wild-type and oncogenic homologs in their mean dimerization efficiencies.

FRET results indicated that K-Ras *wt/onc* heterodimerizes with Gαs, Gαi, Gα12, and Gα13 on the cell membrane in live cells. However, the interaction between K-Ras *wt/onc* – Gα11 does not occur under the same conditions.

K-Ras α-interface dimerization hot spot residues play an important role in this interaction. K101&R102 residues are essential for the homodimerization of K-Ras *wt/onc*, and once they are mutated to opposite charges, the interaction efficiencies decrease and dimerization is impaired. Moreover, being a wild-type or oncogenic form of K-Ras also does not change these interactions' mean efficiency after mutations.

When K-Ras homo-dimerization α-interface is mimicked on Gαi and Gα13, the interaction efficiency of K-Ras *wt/onc* – Gαi and K-Ras *wt/onc* – Gα13 significantly increased and showed a wider distribution in the dimer distances. However, when K-Ras dimerization disrupting mutations K101D&R102E are present, the interactions are impaired.

K-Ras α-interface dimerization mimicking mutations on Gα11 does not promote an interaction between K-Ras and Gα11.

To conclude, G-Domain has a role in K-Ras-K-Ras homo-dimerization as well as K-Ras-Gα hetero-dimerization.

5.2 Future Studies

Besides these labeling positions on proteins, different residues can be picked for FRET studies. Moreover, other residues in the α-dimerization interface or other dimerization interfaces on K-Ras or Gα proteins can be studied to understand these interactions better.

Since mimicking mutations on Gα11 is not enough to promote interaction with K-Ras, additional mutations or other interfaces can be examined.

In this study, only Gαi, Gα11, and Gα13 are assessed for dimerization interface manipulations; therefore, other Gα proteins, such as Gα12 and Gαs, can be considered.

K-Ras and Gα proteins and their manipulated interaction effects on protein expression and protein modification levels in common downstream pathways can be studied.

REFERENCES

Albani, A., Theodoropoulou, M., & Reincke, M. (2018). Genetics of Cushing's disease. *Clinical Endocrinology*, *88*(1), 3–12. https://doi.org/https://doi.org/10.1111/cen.13457

Aran, V. (2021). K-RAS4A: Lead or Supporting Role in Cancer Biology? *Frontiers in Molecular Biosciences*, *8*. https://doi.org/10.3389/fmolb.2021.729830

Bajar, B. T., Wang, E. S., Zhang, S., Lin, M. Z., & Chu, J. (2016). A Guide to Fluorescent Protein FRET Pairs. *Sensors*, *16*(9). https://doi.org/10.3390/s16091488

Berney, C., & Danuser, G. (2003). FRET or No FRET: A Quantitative Comparison. *Biophysical Journal*, *84*(6), 3992–4010. https://doi.org/https://doi.org/10.1016/S0006-3495(03)75126-1

Blanden, M. J., Suazo, K. F., Hildebrandt, E. R., Hardgrove, D. S., Patel, M., Saunders, W. P., Distefano, M. D., Schmidt, W. K., & Hougland, J. L. (2017). Efficient farnesylation of an extended C-terminal C(x)3X sequence motif expands the scope of the prenylated proteome. *The Journal of Biological Chemistry*, *293*, 2770–2785. https://api.semanticscholar.org/CorpusID:3613661

Blumer, J. B., & Tall, G. G. (2012). G Protein $α$ i/o/z. In S. Choi (Ed.), *Encyclopedia of Signaling Molecules* (pp. 710–722). Springer New York. https://doi.org/10.1007/978-1-4419-0461-4_648

Bondar, A., & Lazar, J. (2013). Dissociated G$α$GTP and G$β$$γ$ Protein Subunits Are the Major Activated Form of Heterotrimeric Gi/o Proteins*. *The Journal of Biological Chemistry*, *289*, 1271–1281. https://api.semanticscholar.org/CorpusID:23833295

Boutin, J. A. (1997). Myristoylation. *Cellular Signalling*, *9*(1), 15–35. https://doi.org/https://doi.org/10.1016/S0898-6568(96)00100-3

Busquets-Hernández, C., & Triola, G. (2021). Palmitoylation as a Key Regulator of

Ras Localization and Function. *Frontiers in Molecular Biosciences*, *8*. https://doi.org/10.3389/fmolb.2021.659861

Canon, J. R., Rex, K. L., Saiki, A. Y., Mohr, C., Cooke, K. S., Bagal, D., Gaida, K., Holt, T., Knutson, C. G., Koppada, N., Lanman, B. A., Werner, J., Rapaport, A. S., Miguel, T. S., Ortiz, R., Ortiz, R., Osgood, T., Sun, J. R., Zhu, X., … Lipford, J. R. (2019). The clinical KRAS(G12C) inhibitor AMG 510 drives anti-tumour immunity. *Nature*, *575*, 217–223. https://api.semanticscholar.org/CorpusID:204969251

Castellano, E., & Downward, J. (2011). RAS Interaction with PI3K: More Than Just Another Effector Pathway. *Genes \& Cancer*, *2*(3), 261–274. https://doi.org/10.1177/1947601911408079

Chen, M., Peters, A., Huang, T., & Nan, X. (2016). Ras Dimer Formation as a New Signaling Mechanism and Potential Cancer Therapeutic Target. *Mini Reviews in Medicinal Chemistry*, *16*(5), 391—403. https://doi.org/10.2174/1389557515666151001152212

Chen, Y. E., Mauldin, J. P., Day, R. N., & Periasamy, A. (2007). Characterization of spectral FRET imaging microscopy for monitoring nuclear protein interactions. *Journal of Microscopy*, *228*(2), 139–152. https://doi.org/https://doi.org/10.1111/j.1365-2818.2007.01838.x

Chung, K. Y. (2013). Structural Aspects of GPCR-G Protein Coupling. *Toxicological Research*, *29*, 149–155. https://api.semanticscholar.org/CorpusID:24710604

Cooper, J. M., Bodemann, B. O., & White, M. A. (2013). Chapter Six - The RalGEF/Ral Pathway: Evaluating an Intervention Opportunity for Ras Cancers. In F. Tamanoi & C. J. Der (Eds.), *Inhibitors of the Ras superfamily G-proteins, Part B* (Vol. 34, pp. 137–156). Academic Press. https://doi.org/https://doi.org/10.1016/B978-0-12-420146-0.00006-8

Dhanasekaran, N., & Dermott, J. M. (1996). Signaling by the G12 class of G proteins. *Cellular Signalling*, *8*(4), 235–245.

https://doi.org/https://doi.org/10.1016/0898-6568(96)00048-4

Dickson, E. J., Falkenburger, B. H., & Hille, B. (2013). Quantitative properties and receptor reserve of the IP3 and calcium branch of Gq-coupled receptor signaling. *Journal of General Physiology*, *141*(5), 521–535. https://doi.org/10.1085/jgp.201210886

EVIDENT. (2024a). *Fluorescence Resonance Energy Transfer (FRET) Microscopy*. https://www.olympus-lifescience.com/en/microscope-resource/primer/techniques/fluorescence/fret/fretintro/

EVIDENT. (2024b). *Introduction to Confocal Microscopy*. https://www.olympus-lifescience.com/en/microscope-resource/primer/techniques/confocal/confocalintro/

Falkenburger, B. H., Dickson, E. J., & Hille, B. (2013). Quantitative properties and receptor reserve of the DAG and PKC branch of Gq-coupled receptor signaling. *Journal of General Physiology*, *141*(5), 537–555. https://doi.org/10.1085/jgp.201210887

Fivaz, M., & Meyer, T. (2005). Reversible intracellular translocation of KRas but not HRas in hippocampal neurons regulated by Ca2+/calmodulin. *Journal of Cell Biology*, *170*(3), 429–441. https://doi.org/10.1083/jcb.200409157

Galbiati, F., Guzzi, F., Magee, A. I., Milligan, G., & Parenti, M. (1994). N-terminal fatty acylation of the α-subunit of the G-protein Gi1: only the myristoylated protein is a substrate for palmitoylation. *Biochemical Journal*, *303*(3), 697–700. https://doi.org/10.1042/bj3030697

Gasper, R., & Wittinghofer, F. (2020). The Ras switch in structural and historical perspective. *Biological Chemistry*, *401*(1), 143–163. https://doi.org/doi:10.1515/hsz-2019-0330

Geiser, M., Cébe, R., Drewello, D., & Schmitz, R. (2001). Integration of PCR Fragments at Any Specific Site within Cloning Vectors without the Use of Restriction Enzymes and DNA Ligase. *BioTechniques*, *31*(1), 88–92.

https://doi.org/10.2144/01311st05

Gimple, R. C., & Wang, X. (2019). RAS: Striking at the Core of the Oncogenic Circuitry. *Frontiers in Oncology*, *9*. https://doi.org/10.3389/fonc.2019.00965

Golan, T., Khvalevsky, E. Z., Hubert, A., Gabai, R. M., Hen, N., Segal, A., Domb, A. J., Harari, G., David, E. Ben, Raskin, S. P., Goldes, Y., Goldin, E., Eliakim, R., Lahav, M., Kopleman, Y., Dancour, A., Shemi, A., & Galun, E. (2015). RNAi therapy targeting KRAS in combination with chemotherapy for locally advanced pancreatic cancer patients. *Oncotarget*, *6*, 24560–24570. https://api.semanticscholar.org/CorpusID:15285441

Goricanec, D., Stehle, R., Egloff, P., Grigoriu, S., Plückthun, A., Wagner, G., & Hagn, F. (2016). Conformational dynamics of a G-protein α subunit is tightly regulated by nucleotide binding. *Proceedings of the National Academy of Sciences*, *113*(26), E3629–E3638. https://doi.org/10.1073/pnas.1604125113

Guan, G., Cannon, R. D., Coates, D. E., & Mei, L. (2023). Effect of the Rho-Kinase/ROCK Signaling Pathway on Cytoskeleton Components. *Genes*, *14*(2). https://doi.org/10.3390/genes14020272

Güldenhaupt, J., Rudack, T., Bachler, P. S., Mann, D., Triola, G., Waldmann, H., Kötting, C., & Gerwert, K. (2012). N-Ras forms dimers at POPC membranes. *Biophysical Journal*, *103 7*, 1585–1593. https://api.semanticscholar.org/CorpusID:29890051

Hanahan, D., & Weinberg, R. A. (2011). Hallmarks of Cancer: The Next Generation. *Cell*, *144*, 646–674. https://api.semanticscholar.org/CorpusID:13011249

Henis, Y. I., Hancock, J. F., & Prior, I. A. (2009). Ras acylation, compartmentalization and signaling nanoclusters (Review). *Molecular Membrane Biology*, *26*(1–2), 80–92. https://doi.org/10.1080/09687680802649582

Hurowitz, E. H., Melnyk, J. M., Chen, Y.-J., Kouros-Mehr, H., Simon, M. I., & Shizuya, H. (2000). Genomic Characterization of the Human Heterotrimeric G

Protein α, β, and γ Subunit Genes. *DNA Research*, *7*(2), 111–120. https://doi.org/10.1093/dnares/7.2.111

Inouye, K., Mizutani, S., Koide, H., & Kaziro, Y. (2000). Formation of the Ras Dimer Is Essential for Raf-1 Activation*. *The Journal of Biological Chemistry*, *275*, 3737–3740. https://api.semanticscholar.org/CorpusID:1092786

Ishikawa, Y., & Homcy, C. J. (1997). The Adenylyl Cyclases as Integrators of Transmembrane Signal Transduction. *Circulation Research*, *80*(3), 297–304. https://doi.org/10.1161/01.RES.80.3.297

Issahaku, A. R., Aljoundi, A., & Soliman, M. E. S. (2022). Establishing the mutational effect on the binding susceptibility of AMG510 to KRAS switch II binding pocket: Computational insights. *Informatics in Medicine Unlocked*, *30*, 100952. https://doi.org/https://doi.org/10.1016/j.imu.2022.100952

Kamato, D., Thach, L., Bernard, R., Chan, V., Zheng, W., Kaur, H., Brimble, M., Osman, N., & Little, P. J. (2015). Structure, Function, Pharmacology, and Therapeutic Potential of the G Protein, GÎ±/q,11. *Frontiers in Cardiovascular Medicine*, *2*. https://doi.org/10.3389/fcvm.2015.00014

Kaur, G., Verma, S. K., Singh, D., & Singh, N. K. (2023). Role of G-Proteins and GPCRs in Cardiovascular Pathologies. *Bioengineering (Basel, Switzerland)*, *10*(1). https://doi.org/10.3390/bioengineering10010076

Kazi, A., Xiang, S., Yang, H., Chen, L., Kennedy, P., Ayaz, M., Fletcher, S., Cummings, C., Lawrence, H. R., Beato, F., Kang, Y., Kim, M. P., Delitto, A., Underwood, P. W., Fleming, J. B., Trevino, J. G., Hamilton, A. D., & Sebti, S. M. (2019). Dual Farnesyl and Geranylgeranyl Transferase Inhibitor Thwarts Mutant KRAS-Driven Patient-Derived Pancreatic Tumors. *Clinical Cancer Research*, *25*(19), 5984–5996. https://doi.org/10.1158/1078-0432.CCR-18-3399

Ke, X., Zhang, Q., Zhu, P., He, H., Yuan, J., & Ao, Q. (2023). GNA13 is a new marker for germinal center-derived B cell lymphomas. *Nano TransMed*, *2*(2), 100002. https://doi.org/https://doi.org/10.1016/j.ntm.2023.100002

Kim, T. H., Yang, Y. M., Han, C. Y., Koo, J. H., Oh, H., Kim, S. S., You, B. H., Choi, Y. H., Park, T.-S., Lee, C. H., Kurose, H., Noureddin, M., Seki, E., Wan, Y.-J. Y., Choi, C. S., & Kim, S. G. (2018). Gα12 ablation exacerbates liver steatosis and obesity by suppressing USP22/SIRT1-regulated mitochondrial respiration. *The Journal of Clinical Investigation*, *128*(12), 5587–5602. https://doi.org/10.1172/JCI97831

Kleuss, C., & Krause, E. (2003). G\&\#x3b1;$_s$ is palmitoylated at the N\&\#x2010;terminal glycine. *The EMBO Journal*, *22*(4), 826–832. https://doi.org/https://doi.org/10.1093/emboj/cdg095

Kramer, H. E. A., & Fischer, P. (2011). The Scientific Work of Theodor Förster: A Brief Sketch of his Life and Personality. *ChemPhysChem*, *12*(3), 555–558. https://doi.org/https://doi.org/10.1002/cphc.201000733

Lacal, J. C. (2001). GTPase. In M. Schwab (Ed.), *Encyclopedic Reference of Cancer* (pp. 375–378). Springer Berlin Heidelberg. https://doi.org/10.1007/3-540-30683-8_688

Lambert, J. M., Lambert, Q. T., Reuther, G. W., Malliri, A., Siderovski, D., Sondek, J., Collard, J. G., & Der, C. J. (2002). Tiam1 mediates Ras activation of Rac by a PI(3)K-independent mechanism. *Nature Cell Biology*, *4*, 621–625. https://api.semanticscholar.org/CorpusID:21639425

Levine, M. A. (1999). Clinical Implications of Genetic Defects in G Proteins: Oncogenic Mutations in Gαs as the Molecular Basis for the McCune-Albright Syndrome. *Archives of Medical Research*, *30*(6), 522–531. https://doi.org/https://doi.org/10.1016/S0188-4409(99)00075-2

Ligeti, E., Welti, S., & Scheffzek, K. (2012). Inhibition and Termination of Physiological Responses by GTPase Activating Proteins. *Physiological Reviews*, *92*(1), 237–272. https://doi.org/10.1152/physrev.00045.2010

Lin, T., Scott, B. L., Hoppe, A. D., & Chakravarty, S. (2018). FRETting about the affinity of bimolecular protein–protein interactions. *Protein Science*, *27*(10), 1850–1856. https://doi.org/https://doi.org/10.1002/pro.3482

Liu, P., Wang, Y., & Li, X. (2019). Targeting the untargetable KRAS in cancer therapy. *Acta Pharmaceutica Sinica B*, *9*(5), 871–879. https://doi.org/https://doi.org/10.1016/j.apsb.2019.03.002

Liu, R., Chen, Y., Liu, G., Li, C., Song, Y., Cao, Z., Li, W., Hu, J., Lu, C., & Liu, Y. (2020). PI3K/AKT pathway as a key link modulates the multidrug resistance of cancers. *Cell Death \& Disease*, *11*. https://api.semanticscholar.org/CorpusID:221918666

Louche, A., Salcedo, S. P., & Bigot, S. (2017). Protein--Protein Interactions: Pull-Down Assays. In L. Journet & E. Cascales (Eds.), *Bacterial Protein Secretion Systems: Methods and Protocols* (pp. 247–255). Springer New York. https://doi.org/10.1007/978-1-4939-7033-9_20

Marrari, Y., Crouthamel, M., Irannejad, R., & Wedegaertner, P. B. (2007). Assembly and Trafficking of Heterotrimeric G Proteins. *Biochemistry*, *46*(26), 7665–7677. https://doi.org/10.1021/bi700338m

McCudden, C. R., Hains, M. D., Kimple, R. J., Siderovski, D., & Willard, F. S. (2005). G-protein signaling: back to the future. *Cellular and Molecular Life Sciences*, *62*, 551–577. https://api.semanticscholar.org/CorpusID:15149105

Mehla, J., Caufield, J. H., Sakhawalkar, N., & Uetz, P. (2017). Chapter Seventeen - A Comparison of Two-Hybrid Approaches for Detecting Protein–Protein Interactions. In A. K. Shukla (Ed.), *Proteomics in Biology, Part B* (Vol. 586, pp. 333–358). Academic Press. https://doi.org/https://doi.org/10.1016/bs.mie.2016.10.020

Menyhárd, D. K., Pálfy, G., Orgován, Z., Vida, I., Keserű, G. M., & Perczel, A. (2020). Structural impact of GTP binding on downstream KRAS signaling. *Chem. Sci.*, *11*(34), 9272–9289. https://doi.org/10.1039/D0SC03441J

Michaelson, D., Ali, W., Chiu, V. K., Bergo, M., Silletti, J., Wright, L., Young, S. G., & Philips, M. (2005). Postprenylation CAAX Processing Is Required for Proper Localization of Ras but Not Rho GTPases. *Molecular Biology of the Cell*, *16*(4), 1606–1616. https://doi.org/10.1091/mbc.e04-11-0960

Milligan, G., & Kostenis, E. (2006). Heterotrimeric G-proteins: a short history. *British Journal of Pharmacology*, *147*(S1), S46–S55. https://doi.org/https://doi.org/10.1038/sj.bjp.0706405

Moore, A. R., & Malek, S. (2021). The promise and peril of KRAS G12C inhibitors. *Cancer Cell*, *39 8*, 1059–1061. https://api.semanticscholar.org/CorpusID:236976975

Morrison, D. K. (2012). MAP kinase pathways. *Cold Spring Harbor Perspectives in Biology*, *4 11*. https://api.semanticscholar.org/CorpusID:21416321

Muir, A. M., Gardner, J. F., van Jaarsveld, R. H., de Lange, I. M., van der Smagt, J., Wilson, G. N., Dubbs, H. A., Goldberg, E. M., Zitano, L., Bupp, C. P., Martínez, J. E., Srour, M., Accogli, A., Alhakeem, A., Meltzer, M. R., Gropman, A. L., Brewer, C., Caswell, R. C., Montgomery, T., … Mefford, H. C. (2021). Variants in GNAI1 Cause a Syndrome Associated with Variable Features including Developmental Delay, Seizures and Hypotonia. *Genetics in Medicine : Official Journal of the American College of Medical Genetics*, *23*, 881–887. https://api.semanticscholar.org/CorpusID:231664213

Muratcioglu, S., Aydin, C., Odabasi, E., Ozdemir, E. S., Firat-Karalar, E. N., Jang, H., Tsai, C.-J., Nussinov, R., Kavakli, I. H., Gursoy, A., & Keskin, O. (2020). Oncogenic K-Ras4B Dimerization Enhances Downstream Mitogen-activated Protein Kinase Signaling. *Journal of Molecular Biology*, *432*(4), 1199–1215. https://doi.org/https://doi.org/10.1016/j.jmb.2020.01.002

Nam, J. C., Bhatt, P. S., Kim, S.-I., & Kang, H.-G. (2023). Co-immunoprecipitation for Assessing Protein--Protein Interactions in Agrobacterium-Mediated Transient Expression System in Nicotiana benthamiana. In S. Mukhtar (Ed.), *Protein-Protein Interactions: Methods and Protocols* (pp. 101–110). Springer US. https://doi.org/10.1007/978-1-0716-3327-4_9

Nan, X., Tamgüney, T. M., Collisson, E. A., Lin, L.-J., Pitt, C., Galeas, J., Lewis, S., Gray, J. W., McCormick, F., & Chu, S. (2015). Ras-GTP dimers activate the Mitogen-Activated Protein Kinase (MAPK) pathway. *Proceedings of the*

National Academy of Sciences, *112*(26), 7996–8001. https://doi.org/10.1073/pnas.1509123112

Nussinov, R., Tsai, C.-J., Chakrabarti, M., & Jang, H. (2016). A New View of Ras Isoforms in Cancers. *Cancer Research*, *76 1*, 18–23. https://api.semanticscholar.org/CorpusID:1644978

O'Hayre, M., Inoue, A., Kufareva, I., Wang, Z., Mikelis, C. M., Drummond, R. A., Avino, S., Finkel, K., Kalim, K. W., Dipasquale, G., Guo, F., Aoki, J., Zheng, Y., Lionakis, M. S., Molinolo, A. A., & Gutkind, J. S. (2015). Inactivating Mutations in GNA13 and RHOA in Burkitt's Lymphoma and Diffuse Large B cell Lymphoma: A Tumor Suppressor Function for the G$α$13/RhoA Axis in B Cells. *Oncogene*, *35*, 3771–3780. https://api.semanticscholar.org/CorpusID:13785813

Oldham, W. M., & Hamm, H. E. (2008). Heterotrimeric G protein activation by G-protein-coupled receptors. *Nature Reviews Molecular Cell Biology*, *9*, 60–71. https://api.semanticscholar.org/CorpusID:24267759

Origene. (2024). *KRAS*. https://www.origene.com/research-areas/kras

Pantsar, T. (2020). The current understanding of KRAS protein structure and dynamics. *Computational and Structural Biotechnology Journal*, *18*, 189–198. https://api.semanticscholar.org/CorpusID:210936144

Peterson, D. A. (2010). Confocal Microscopy. In K. Kompoliti & L. V. Metman (Eds.), *Encyclopedia of Movement Disorders* (pp. 250–252). Academic Press. https://doi.org/https://doi.org/10.1016/B978-0-12-374105-9.00230-6

Prior, I. A., Lewis, P. D., & Mattos, C. (2012). A Comprehensive Survey of Ras Mutations in Cancer. *Cancer Research*, *72*(10), 2457–2467. https://doi.org/10.1158/0008-5472.CAN-11-2612

Quilliam, L. A., Rebhun, J. F., & Castro, A. F. (2002). *A growing family of guanine nucleotide exchange factors is responsible for activation of ras-family GTPases* (Vol. 71, pp. 391–444). Academic Press.

https://doi.org/https://doi.org/10.1016/S0079-6603(02)71047-7

Rasheed, S. A. K., Subramanyan, L. V., Lim, W. K., Udayappan, U. K., Wang, M., & Casey, P. J. (2021). The emerging roles of G$α$12/13 proteins on the hallmarks of cancer in solid tumors. *Oncogene*, *41*, 147–158. https://api.semanticscholar.org/CorpusID:239460624

Rebenku, I., Lloyd, C. B., Szöllősi, J., & Vereb, G. (2023). Pixel-by-pixel autofluorescence corrected FRET in fluorescence microscopy improves accuracy for samples with spatially varied autofluorescence to signal ratio. *Scientific Reports*, *13*. https://api.semanticscholar.org/CorpusID:257023701

Richards, A. L., Eckhardt, M., & Krogan, N. J. (2021). Mass spectrometry-based protein–protein interaction networks for the study of human diseases. *Molecular Systems Biology*, *17*(1), e8792. https://doi.org/https://doi.org/10.15252/msb.20188792

Sadana, R., & Dessauer, C. W. (2008). Physiological Roles for G Protein-Regulated Adenylyl Cyclase Isoforms: Insights from Knockout and Overexpression Studies. *Neurosignals*, *17*(1), 5–22. https://doi.org/10.1159/000166277

Schmick, M., Vartak, N., Papke, B., Kovacevic, M., Truxius, D. C., Rossmannek, L., & Bastiaens, P. I. H. (2014). KRas Localizes to the Plasma Membrane by Spatial Cycles of Solubilization, Trapping and Vesicular Transport. *Cell*, *157*, 459–471. https://api.semanticscholar.org/CorpusID:15223703

Sekar, R. B., & Periasamy, A. (2003). Fluorescence resonance energy transfer (FRET) microscopy imaging of live cell protein localizations. *Journal of Cell Biology*, *160*(5), 629–633. https://doi.org/10.1083/jcb.200210140

Sharma, A., Kumar, G., Sharma, S., Walia, K., Chouhan, P., Mandal, B., & Tuli, A. (2021). Chapter 11 - Methods for binding analysis of small GTP-binding proteins with their effectors. In A. K. Shukla (Ed.), *Biomolecular Interactions Part A* (Vol. 166, pp. 235–250). Academic Press. https://doi.org/https://doi.org/10.1016/bs.mcb.2021.06.003

Shi, S., Zheng, L., Ren, Y., & Wang, Z. (2023). Impacts of Mutations in the P-Loop on Conformational Alterations of KRAS Investigated with Gaussian Accelerated Molecular Dynamics Simulations. *Molecules*, *28*(7). https://doi.org/10.3390/molecules28072886

Sigmon, J., & Larcom, L. L. (1996). The effect of ethidium bromide on mobility of DNA fragments in agarose gel electrophoresis. *ELECTROPHORESIS*, *17*(10), 1524–1527. https://doi.org/https://doi.org/10.1002/elps.1150171003

Silva-Rodríguez, P., Fernández-Díaz, D., Bande, M., Pardo, M., Loidi, L., & Blanco-Teijeiro, M. J. (2022). GNAQ and GNA11 Genes: A Comprehensive Review on Oncogenesis, Prognosis and Therapeutic Opportunities in Uveal Melanoma. *Cancers*, *14*(13). https://doi.org/10.3390/cancers14133066

Simanshu, D. K., Nissley, D. V, & McCormick, F. (2017). RAS Proteins and Their Regulators in Human Disease. *Cell*, *170*, 17–33. https://api.semanticscholar.org/CorpusID:206564753

Song, G., Ouyang, G., & Bao, S. (2005). The activation of Akt/PKB signaling pathway and cell survival. *Journal of Cellular and Molecular Medicine*, *9*(1), 59–71. https://doi.org/10.1111/j.1582-4934.2005.tb00337.x

Song, S., Cong, W., Zhou, S., Shi, Y., Dai, W., Zhang, H., Wang, X., He, B., & Zhang, Q. (2019). Small GTPases: Structure, biological function and its interaction with nanoparticles. *Asian Journal of Pharmaceutical Sciences*, *14*(1), 30–39. https://doi.org/https://doi.org/10.1016/j.ajps.2018.06.004

Soriano, O., Alcón-Pérez, M., Vicente-Manzanares, M., & Castellano, E. (2021). The Crossroads between RAS and RHO Signaling Pathways in Cellular Transformation, Motility and Contraction. *Genes*, *12*(6). https://doi.org/10.3390/genes12060819

Spiegel, A. M. (1987). Signal transduction by guanine nucleotide binding proteins. *Molecular and Cellular Endocrinology*, *49*(1), 1–16. https://doi.org/https://doi.org/10.1016/0303-7207(87)90058-X

Stolze, B., Reinhart, S., Bulllinger, L., Fröhling, S., & Scholl, C. (2015). Comparative analysis of KRAS codon 12, 13, 18, 61, and 117 mutations using human MCF10A isogenic cell lines. *Scientific Reports*, *5*. https://api.semanticscholar.org/CorpusID:16239374

Suzuki, N., Hajicek, N., & Kozasa, T. (2009). Regulation and Physiological Functions of G12/13-Mediated Signaling Pathways. *Neurosignals*, *17*(1), 55–70. https://doi.org/10.1159/000186690

Takai, Y., Sasaki, T., & Matozaki, T. (2001). Small GTP-Binding Proteins. *Physiological Reviews*, *81*(1), 153–208. https://doi.org/10.1152/physrev.2001.81.1.153

Taussig, R., Iñiguez-Lluhi, J. A., & Gilman, A. G. (1993). Inhibition of Adenylyl Cyclase by $G_{i\&\#x3b1;}$ *Science*, *261*(5118), 218–221. https://doi.org/10.1126/science.8327893

Ternet, C., Junk, P., Sevrin, T., Catozzi, S., Oliviero, G., Wynne, K., & Kiel, C. (2022). Analysis of context-specific KRAS-effectors (sub)complexes in Caco-2 cells. *BioRxiv*. https://doi.org/10.1101/2022.08.15.503960

Terrell, E. M., & Morrison, D. K. (2019). Ras-Mediated Activation of the Raf Family Kinases. *Cold Spring Harbor Perspectives in Medicine*, *9 1*. https://api.semanticscholar.org/CorpusID:29815002

Tsutsumi, R., Fukata, Y., Noritake, J., Iwanaga, T., Perez, F., & Fukata, M. (2008). Identification of G Protein \$α\$ Subunit-Palmitoylating Enzyme. *Molecular and Cellular Biology*, *29*, 435–447. https://api.semanticscholar.org/CorpusID:24738314

Turan, S., & Bastepe, M. (2013). The GNAS Complex Locus and Human Diseases Associated with Loss-of-Function Mutations or Epimutations within This Imprinted Gene. *Hormone Research in Paediatrics*, *80*(4), 229–241. https://doi.org/10.1159/000355384

University of Gothenburg. (2024). *Fluorescence Resonance Energy Transfer*.

https://www.gu.se/en/core-facilities/fluorescence-resonance-energy-transfer

Vatansever, S., Erman, B., & Gümüş, Z. H. (2017). Oncogenic G12D mutation alters local conformations and dynamics of K-Ras. *Scientific Reports*, *9*. https://api.semanticscholar.org/CorpusID:199543138

Wang, D., Wang, Q., Wang, Y., Chen, P., Lu, X., Jia, F., Sun, Y., Sun, T., Zhang, L., Che, F., He, J., Lian, L., Morano, G., Shen, M., Ren, M., Dong, S. S., Zhao, J. J., & Zhang, K. (2022). Targeting oncogenic KRAS with molecular brush-conjugated antisense oligonucleotides. *Proceedings of the National Academy of Sciences*, *119*(29), e2113180119. https://doi.org/10.1073/pnas.2113180119

Wang, W., Yuan, T., Qian, M., Yan, F., Yang, L., He, Q., Yang, B., Lu, J., & Zhu, H. (2020). Post-translational modification of KRAS: potential targets for cancer therapy. *Acta Pharmacologica Sinica*, *42*, 1201–1211. https://api.semanticscholar.org/CorpusID:224828595

Waters, A. M., & Der, C. J. (2018). KRAS: The Critical Driver and Therapeutic Target for Pancreatic Cancer. *Cold Spring Harbor Perspectives in Medicine*, *8 9*. https://api.semanticscholar.org/CorpusID:3299043

Wedegaertner, P. B. (2012). G Protein Trafficking. In D. J. Dupré, T. E. Hébert, & R. Jockers (Eds.), *GPCR Signalling Complexes -- Synthesis, Assembly, Trafficking and Specificity* (pp. 193–223). Springer Netherlands. https://doi.org/10.1007/978-94-007-4765-4_11

Weis, W. I., & Kobilka, B. K. (2018). The Molecular Basis of G Protein–Coupled Receptor Activation. *Annual Review of Biochemistry*, *87*(1), 897–919. https://doi.org/10.1146/annurev-biochem-060614-033910

Wennerberg, K., Rossman, K. L., & Der, C. J. (2005). The Ras superfamily at a glance. *Journal of Cell Science*, *118*(5), 843–846. https://doi.org/10.1242/jcs.01660

Wilson, T. (1995). The Role of the Pinhole in Confocal Imaging System. In J. B. Pawley (Ed.), *Handbook of Biological Confocal Microscopy* (pp. 167–182).

Springer US. https://doi.org/10.1007/978-1-4757-5348-6_11

Wu, D., Lee, C. H., Rhee, S. G., & Simon, M. I. (1992). Activation of phospholipase C by the alpha subunits of the Gq and G11 proteins in transfected Cos-7 cells. *The Journal of Biological Chemistry*, *267 3*, 1811–1817. https://api.semanticscholar.org/CorpusID:41185531

Wu, P. G., & Brand, L. (1994). Resonance Energy Transfer: Methods and Applications. *Analytical Biochemistry*, *218*(1), 1–13. https://doi.org/https://doi.org/10.1006/abio.1994.1134

Yanagida, K., Igarashi, H., Yasuda, D., Kobayashi, D., Ohto-Nakanishi, T., Akahoshi, N., Sekiba, A., Toyoda, T., Ishijima, T., Nakai, Y., Shojima, N., Kubota, N., Abe, K., Kadowaki, T., Ishii, S., & Shimizu, T. (2018). The Gα12/13-coupled receptor LPA4 limits proper adipose tissue expansion and remodeling in diet-induced obesity. *JCI Insight*, *3*(24). https://doi.org/10.1172/jci.insight.97293

Yang, J., Nie, J., Ma, X., Wei, Y., Peng, Y., & Wei, X. (2019). Targeting PI3K in cancer: mechanisms and advances in clinical trials. *Molecular Cancer*, *18*. https://api.semanticscholar.org/CorpusID:67752254

Yang, Y. M., Kuen, D.-S., Chung, Y., Kurose, H., & Kim, S. G. (2020). G$α$12/13 signaling in metabolic diseases. *Experimental \& Molecular Medicine*, *52*, 896–910. https://api.semanticscholar.org/CorpusID:219977199

Yoon, H. H., Tougeron, D., Shi, Q., Alberts, S. R., Mahoney, M. R., Nelson, G. D., Nair, S. G., Thibodeau, S. N., Goldberg, R. M., Sargent, D. J., Sinicrope, F. A., & for the Alliance for Clinical Trials in Oncology. (2014). KRAS Codon 12 and 13 Mutations in Relation to Disease-Free Survival in BRAF–Wild-Type Stage III Colon Cancers from an Adjuvant Chemotherapy Trial (N0147 Alliance). *Clinical Cancer Research*, *20*(11), 3033–3043. https://doi.org/10.1158/1078-0432.CCR-13-3140

Yuan, T. L., Amzallag, A., Bagni, R., Yi, M., Afghani, S., Burgan, W., Fer, N., Strathern, L. A., Powell, K. L., Smith, B., Waters, A. M., Drubin, D. G., Thomson, T. M., Liao, R., Greninger, P., Stein, G. T., Murchie, E., Cortez, E. C. M., Egan, R. K., … McCormick, F. (2018). Differential Effector Engagement by Oncogenic KRAS. *Cell Reports*, *22 7*, 1889–1902. https://api.semanticscholar.org/CorpusID:3293046

Zeissig, M. N., Ashwood, L. M., Kondrashova, O., & Sutherland, K. D. (2023). Next batter up! Targeting cancers with KRAS-G12D mutations. *Trends in Cancer*. https://api.semanticscholar.org/CorpusID:260938403

Zhu, Z., Xiao, S., Hao, H., Hou, Q., & Fu, X. (2019). Kirsten Rat Sarcoma Viral Oncogene Homologue（KRAS） mutations in the occurrence and treatment of pancreatic cancer. *Current Topics in Medicinal Chemistry*. https://api.semanticscholar.org/CorpusID:201655044

APPENDICES

A. Amino Acid Table and Properties

Table A.1: 20 amino acids and their properties

Amino Acid	**Single Letter Code**	**pI (25 °C)**	**DNA Codon**
Alanine	A	6.11	GCT, GCC, GCA, GCG
Arginine	R	10.76	CGT, CGC, CGA, CGG, AGA, AGG
Asparagine	N	5.43	AAT, AAC
Aspartic Acid	D	2.98	GAT, GAC
Cysteine	C	5.15	TGT, TGC
Glutamic Acid	E	3.08	GAA, GAG
Glutamine	Q	5.65	CAA, CAG
Glycine	G	6.06	GGT, GGC, GGA, GGG
Histidine	H	7.64	CAT, CAC
Isoleucine	I	6.04	ATT, ATC, ATA
Leucine	L	6.04	CTT, CTC, CTA, CTG, TTA, TTG
Lysine	K	9.47	AAA, AAG
Methionine	M	5.71	ATG
Phenylalanine	F	5.76	TTT, TTC
Proline	P	6.30	CCT, CCC, CCA, CCG
Serine	S	5.70	TCT, TCC, TCA, TCG, AGT, AGC
Threonine	T	5.60	ACT, ACC, ACA, ACG
Tryptophan	W	5.88	TGG
Tyrosine	Y	5.63	TAT, TAC
Valine	V	6.02	GTT, GTC, GTA, GTG

B. Buffer and Media Composition in Bacterial & Mammalian Cell Culture

Table B.1: Lysogeny Broth (LB) Composition

Tryptone	10 g/L
NaCl	5 g/L
Yeast Extract	5 g/L
	Dissolve up to 1 L, pH: 7.0, autoclave For LB Agar Plate 20 g/L Agar is added.

Table B.2: Transformation Buffer I (TFBI) Composition

	100 mL Stock	**Final Concentration**
RbCl	10 mL of 1M stock	100 mM
CH_3CO_2K	0.296 g	30 mM
$CaCl_2.H_2O$	1 mL of 1M stock	10 mM
$MnCl_2.H_2O$	0.630 g	50 mM
Glycerol	15 mL of 85% stock	15%
	Dissolve up to 100 mL, pH: 5.8 w/Glacial acetic acid 0.2 µm filter sterilization	

Table B.3: Transformation Buffer II (TFBII) Composition

	15 mL Stock	**Final Concentration**
RbCl	0.15 mL of 1M stock	10 mM
MOPS	0.05 g	10 mM
$CaCl_2.H_2O$	1.12 mL of 1M stock	75 mM
Glycerol	2.62 mL of 85% stock	15%
	Dissolve up to 15 mL, pH: 6.5 w/KOH 0.2 µm filter sterilization	

Table B.4: 50X Tris Base, Acetic acid, EDTA (TAE) Composition

		Final concentration
Tris base	242 g	2 M
Glacial acetic acid	57.1 mL	1 M
0.5 EDTA pH:8.0	100 mL	0.05 M
	Dissolve up to 1 L	

Table B.5: 10X Phosphate Buffer Saline **(**PBS) Composition

NaCI	80 g
KCI	2 g
Na_2HPO_4	14.4 g
KH_2PO_4	2.4 g
	Dissolve up to 1 L, pH: 7.4, autoclave

C. Buffer Composition used in Western Blot

Table C.1: Separating gel composition (%8)

dH_2O	2.7 ml
40 % Acry/Bisacryl (37:5:1)	1.76 ml
1.5 M, pH 8.8 Tris-HCl	1.7 ml
10% APS	67 µl
TEMED	6.7 µl

Table C.2: Stacking gel composition (%4)

dH_2O	2.1 ml
40 % Acry/Bisacryl (37:5:1)	433 µl
1.5 M, pH 8.8 Tris-HCl	833 µl
10% APS	33.3 µl
TEMED	3.3 µl

Table C.3: 10X Running buffer

Glycine (192 mM	144 g
Tris base (25 mM)	30.3 g
SDS (0.1%)	10 g
	Dissolve up to 1 L

Table C.4: 10X Transfer buffer

Glycine (192 mM	144 g
Tris base (25 mM)	30.3 g
	Dissolve up to 1 L

Table C.5: 20X Tris-buffered saline (TBS)

Tris base (0.4 M)	48.4 g
NaCl	160 g
	Dissolve up to 1 L

Table C.6: 1X Tris-buffered saline-Tween20 (TBS-T)

10% Tween-20	10 ml
20X TBS	50 ml
dH_2O	940 ml

Table C.7: Antibody dilutions

K-Ras antibody	1:1000
GAPDH antibody	1:4000